

Load and Deformation Measurements - Instrumentation of Transportation Structures

Dante Fratta, Ivy A. Harmon, and Maxiliano Garnier Villarreal

University of Wisconsin-Madison

WisDOT ID no. 0092-09-05

February 2016



RESEARCH & LIBRARY UNIT



WISCONSIN HIGHWAY RESEARCH PROGRAM

WISCONSIN DOT
PUTTING RESEARCH TO WORK

Technical Report Documentation Page

1. Report No. 0092-09-05	2. Government Accession No	3. Recipient's Catalog No	
4. Title and Subtitle Load and Deformation Measurements - Instrumentation of Transportation Structures		5. Report Date February 2016	
		6. Performing Organization Code University of Wisconsin-Madison	
7. Authors Dante Fratta, Ivy A. Harmon, and Maxiliano Garnier Villarreal		8. Performing Organization Report No.	
9. Performing Organization Name and Address 1415 Engineering Drive Madison, WI 53706		10. Work Unit No. (TRAIS)	
		11. Contract or Grant No.	
12. Sponsoring Agency Name and Address Wisconsin Department of Transportation Research & Library Unit 4802 Sheboygan Ave. Rm 104 Madison, WI 53707		13. Type of Report and Period Covered	
		14. Sponsoring Agency Code Wisconsin Highway Research Program	
15. Supplementary Notes			
<p>16. Abstract</p> <p>Prediction of foundation vertical and horizontal displacements due to dead and service loads is inexact and subject to assumptions and the quality models and input model parameters. A better understanding of the relationship between the loads a structure applies to the foundation and the interaction of the foundation with the subsurface may increase the accuracy and reduce the over-engineering of engineering designs. The intent of this research was to combine load, displacement, and geotechnical data to improve foundation settlement estimates.</p> <p>With this aim in mind, we instrumented and monitored bridges in Southern Wisconsin to collect load and settlement data during and after construction of bridges. Options to rapidly, accurately, and inexpensively measure the forces acting within the structures and the movements of the structures were evaluated and tested. Methods to install, use, and maintain the deployed instruments were developed. A program was developed to report collected data in a usable form, and preliminary analysis of the structural loads and movements was completed.</p> <p>Geotechnical information corresponding with the displacement and load data for each structure was limited. The subsurface information available for each project site was included in the construction documents. Most geotechnical reports or subsurface testing performed at the locations where the instruments were installed include Standard Penetration Test (SPT) values. These in situ test results, while commonly used in practice, are not of the quality required to performed robust numerical models nor could be used to establish strong correlations. An analysis of the predicted and actual settlement could not be reliably completed nor would it be transferrable to other design situations.</p> <p>While the research objective was to refine and publish design procedures for transportation structure foundations within the LRFD framework limitations in data collection and soil property determination prevented the completion of the main objective. For these reasons, this document focuses on the development of a methodology for the collection of loads and movements of transportation structures, on the development of recommendations for the measurement and selection of input parameters, on the assessment of analysis used on the performance of calculation of foundation movements, and on the interpretation of field measurements of foundation loads and movements of transportation projects in Southern Wisconsin.</p>			
17. Key Words		18. Distribution Statement No restriction. This document is available to the public through the National Technical Information Service 5285 Port Royal Road Springfield VA 22161	
18. Security Classif.(of this report) Unclassified	19. Security Classif. (of this page) Unclassified	20. No. of Pages 183	21. Price

DISCLAIMER

This research was funded through the Wisconsin Highway Research Program by the Wisconsin Department of Transportation and the Federal Highway Administration under Project 0092-09-05. The contents of this report reflect the views of the authors who are responsible for the facts and accuracy of the data presented herein. The contents do not necessarily reflect the official views of the Wisconsin Department of Transportation or the Federal Highway Administration at the time of publication.

This document is disseminated under the sponsorship of the Department of Transportation in the interest of information exchange. The United States Government assumes no liability for its contents or use thereof. This report does not constitute a standard, specification or regulation.

The United States Government does not endorse products or manufacturers. Trade and manufacturers' names appear in this report only because they are considered essential to the object of the document.

Table of Contents

Executive Summary	1
1. Introduction.....	3
1.1 AXIAL LOADING.....	4
1.2 QUALITY OF SETTLEMENT ESTIMATIONS	5
1.3 HORIZONTAL DEFORMATIONS.....	8
2. Foundation Structures	11
2.1 LOAD AND RESISTANCE FACTOR DESIGN (LRFD) METHODOLOGY.....	12
2.2 SETTLEMENTS.....	15
Foundation deformation limits.....	15
Settlement prediction	16
2.3 INSTRUMENTATION CHARACTERIZATION AND EVALUATION	20
Tilt measurements.....	23
Laboratory evaluation of tilt measurement instruments.....	28
Axis orientation testing.....	28
Long term stability and sensor resolution testing.....	32
Load measurement.....	42
Strainmeters	42
Modulus of elasticity of reinforced concrete.....	47
Modulus of elasticity as a function of compressive strength.....	48
Modulus of elasticity as a function of wave velocity.....	50
Test equipment and setup	52
Influence of reinforcement on concrete modulus of elasticity	53
Laboratory columns to evaluate method of load calculation.....	54
Laboratory column formwork and concrete	57
Modulus of elasticity of reinforced concrete evaluation.....	61
Compression load testing of laboratory columns.....	66

Minimum reinforcement column modulus of elasticity results	68
Minimum reinforcement column load cycle results	70
Maximum reinforcement column modulus of elasticity results	74
Maximum reinforcement column load cycle results	75
3. Wisconsin Structures.....	80
3.1 FIELD RESEARCH SITES' LOCATIONS	81
3.2 LOAD INSTRUMENTED BRIDGES	82
Layton Avenue Bridge	85
State Highway 164 Bridge.....	87
Lien Road Bridge	88
3.3 DEFORMATION MONITORED BRIDGES	90
Bridges on Highway 51 Deforest.....	90
3.4 FIELD RESEARCH SITES INSTRUMENTATION INSTALLATION	97
Layton Avenue Bridge Instrumentation	98
State Highway 164 Bridge Instrumentation	101
Lien Road Bridge Instrumentation	107
3.5 FIELD RESEARCH SITES' MODULUS OF ELASTICITY	110
3.6 FIELD RESEARCH SITES' COMPLICATIONS	112
3.7 LAYTON AVENUE BRIDGE RESULTS.....	115
Settlement results.....	115
Load results.....	115
Statistical Analysis.....	117
3.8 STATE HIGHWAY 164 BRIDGE RESULTS	119
Settlement results.....	119
Load results.....	120
3.9 LIEN ROAD BRIDGE RESULTS.....	125
Settlement results.....	125
Load results.....	125
3.10 HIGHWAY 51 BRIDGES - DEFORMATION RESULTS	129
Bear Tree Road Bridge.....	129

	iii
Windsor Road Bridge	138
Vinburn Road Bridge	147
4 Conclusions and Recommendations.....	156
References.....	160

List of Figures

Figure 1.1 Modeling drilled shaft behavior using elastic theory with (a) linear dilatometer stiffness (Mayne et al. 1999); and (b) non-linear stiffness (Mayne & Schneider 2001).	5
Figure 1.2 Results of shallow foundation in sand prediction symposium (a) distribution of predictions and field measurements at a load of 280 kN (b) level of over / under prediction as a function of foundation bearing stress (after Lehane et al. 2008).	6
Figure 1.3 Nonlinear soil stiffness behavior (a) in laboratory testing and design applications (Atkinson 2000); and (b) in situ testing and shallow foundation loading in a uniform sand (after Lehane et al. 2008).	8
Figure 2.1: Different type of piles and applications (Sources: URL: www.abuildersengineer.com)	12
Figure 2.2 Shallow foundation movements in two-dimensional plane: settlement, horizontal deformation, and rotation.	16
Figure 2.3 Scale drawings of shallow foundations evaluated for settlement by Lehane et al. (2008)	17
Figure 2.4 Foundation size 1.5 m by 1.5 m by 1 m: predicted and actual vertical settlement (Lehane et al. 2008)	18
Figure 2.5 Foundation size 1 m by 1 m by 1 m: predicted and actual vertical settlement (Lehane et al. 2008)	18
Figure 2.6 Foundation size 1 m by 1 m by 0.5 m: predicted and actual vertical settlement (Lehane et al. 2008)	19
Figure 2.7 Foundation size 0.67 m by 0.67 m by 1 m: predicted and actual vertical settlement (Lehane et al. 2008)	19
Figure 2.8 MTS 400 mote and its dimensions	25
Figure 2.9 The maximum range of the radio signal between the base station and motes	26

Figure 2.10 Indirect signal transfer, when data packets are relayed between motes, extends the range of the mote placement	26
Figure 2.11 Motes were within 30 m of the base station and the base station was hardwired to a dedicated computer during laboratory testing.....	26
Figure 2.12 Initial orientation of motes and arbitrary assigned axes	29
Figure 2.13 Position 1, initial and final orientation of both motes	30
Figure 2.14 Position 2	30
Figure 2.15 Position 3.....	30
Figure 2.16 Position 4.....	31
Figure 2.17 Measured acceleration change in the x-axis with time	31
Figure 2.18 Measured acceleration change in y-axis with time.....	32
Figure 2.19 Profile view of long-term mote stability test setup	33
Figure 2.20 Mote layout of long-term test setup and dimensions of planar surface	33
Figure 2.21 Battery power of the motes decays at a non-linear rate.....	35
Figure 2.22 The reported change in acceleration increases over time	36
Figure 2.23 Similar to x-axis behaviour, the acceleration measured by the motes varies with time.	36
Figure 2.24 Acceleration change in the x-axis compared to the change in battery voltage	37
Figure 2.25 Y-axis change in acceleration compared to the change in battery voltage	37
Figure 2.26 Mote 4921 change in acceleration compared to the change in voltage	38
Figure 2.27 Mote 4921 acceleration noise does not vary with elapsed time nor battery voltage.....	39
Figure 2.28 Foundation movement survey schematic, profile view	40
Figure 2.29 Foundation movement survey schematic, plan view.....	40
Figure 2.30 Reflective survey target.....	41
Figure 2.31 Schematic of Geokon vibrating wire strain meter and reinforment (Geokon 4911-2009)	43
Figure 2.32 Schematic of the sister bar strain meter reinforcement in concrete (Geokon 4911-2009)	43

Figure 2.33 Manufacturer's calibration report for sister bar strain meter ID 4643	44
Figure 2.34 The modulus of elasticity may be evaluated several ways using the stress vs. strain diagrams	47
Figure 2.35 Comparison of the predicted and measured modulus of elasticity (Mirza et al. 1979)	50
Figure 2.36 Ultrasonic wave transmission through concrete specimen	53
Figure 2.37 Reinforcement cage design of laboratory test columns (minimum reinforcement pictured on left, maximum reinforcement pictured on right).....	56
Figure 2.38 Completed cage of maximum reinforcement column placed into formwork	56
Figure 2.39 Completed formwork with reinforcement chairs, before the reinforcement cage is in place.....	58
Figure 2.40 Exterior of column formwork shows supports along the length and width and connections in shear	58
Figure 2.41 Minimum and maximum reinforcement columns' dimensions, grid, and reinforcement orientation.....	60
Figure 2.42 Ultrasonic wave transit time, direction of wave propagation is parallel to reinforcement.....	62
Figure 2.43 Ultrasonic wave transit time, direction of wave propagation is perpendicular to reinforcement.....	62
Figure 2.44 0.2% reinforcement column projection of modulus of elasticity.....	63
Figure 2.45 6% reinforcement column projection of modulus of elasticity	63
Figure 2.46 Modulus of elasticity at each point on the surface grid of the minimum (0.2%) reinforcement column	64
Figure 2.47 Modulus of elasticity at each point on the surface grid of the maximum (6%) reinforcement column.....	65
Figure 2.48 Column configuration during compressive loading of instrumented columns.....	66
Figure 2.49 Minimum reinforcement column, modulus of elasticity variations with applied load.....	69

Figure 2.50 Minimum reinforcement column, modulus of elasticity variation during small load and unload cycle.....	69
Figure 2.51 Minimum reinforcement column, modulus of elasticity variation during large load and unload cycle.....	70
Figure 2.52 All compressive loads applied to the minimum reinforcement column	72
Figure 2.53 Small loads applied to the minimum reinforcement column	72
Figure 2.54 Large loads applied to the minimum reinforcement column	73
Figure 2.55 Loading and unloading the minimum reinforcement column.....	73
Figure 2.56 Maximum reinforcement column, modulus of elasticity variations with all applied loads.....	74
Figure 2.57 Maximum reinforcement column, modulus of elasticity variation during small load and unload cycle.....	75
Figure 2.58 Maximum reinforcement column, modulus of elasticity variation during large load and unload cycle.....	75
Figure 2.59 All compressive loads applied to the maximum reinforcement column	76
Figure 2.60 Small loads applied to the maximum reinforcement column.....	78
Figure 2.61 Large loads applied to the maximum reinforcement column.....	79
Figure 2.62 Loading and unloading the maximum reinforcement column	79
Figure 3.1 Location of the seven research site locations in Southern Wisconsin.	81
Figure 3.2 Detailed location of the deep foundation bridges on Highway 51. The red circle indicates the location of the bridges.	92
Figure 3.3 Pictures of the finished bridges on USH51. Bridge over Bear Tree Road (Top). Bridge over Windsor Road (Middle). Bridge over Vinburn Road (Bottom).....	94
Figure 3.4 Surveying target and Surveying set up use to measure the deformation of the Highway 51 bridges.....	95
Figure 3.5: Location of the surveying points at Bear Tree Road and Windsor Road Bridges (top) and Vinburn Road Bridges (bottom).....	96
Figure 3.6 Cross section of instrumented column at the Layton Avenue Bridge, including strainmeter locations.	99

Figure 3.7 Ultrasonic wave transit time measurements through the column at the Layton Avenue Bridge.....	100
Figure 3.8 Ultrasonic wave paths used to determine modulus of elasticity at the Layton Avenue Bridge.....	100
Figure 3.9 Plan view of survey locations at the Layton Avenue Bridge	101
Figure 3.10 Cross section of instrumented column at the STH 164 Bridge Pier, including strainmeter locations	102
Figure 3.11 Ultrasonic wave paths used to determine modulus of elasticity E_c at the STH 164 Bridge Pier	103
Figure 3.12 Cross section of STH-164 Abutment, including strainmeter locations....	104
Figure 3.13 Plan view of survey locations at STH-164 Bridge Pier	105
Figure 3.14 Plan view of survey locations at STH-164 Bridge Abutment.....	106
Figure 3.15 Cross section of the Lien Road Bridge column, including strainmeter locations	107
Figure 3.16 Ultrasonic wave paths used to determine modulus of elasticity at the Lien Road Bridge research site.....	108
Figure 3.17 Plan view of survey locations at Lien Road Bridge.....	109
Figure 3.18 Modulus of elasticity calculated at each research site, compared to the travel distance of the ultrasonic waves.....	110
Figure 3.19 Modulus of elasticity calculated at each field site within one standard deviation.....	111
Figure 3.20 Load experienced by the Layton Avenue bridge structure over time	117
Figure 3.21 Load sensed by the STH 164 Bridge pier over time	123
Figure 3.22 Load experienced by the STH 164 Bridge abutment over time.....	124
Figure 3.23 Load experienced by the the Lien Road Bridge column over time.....	127
Figure 3.24 Subsurface exploration data for the bridge over Bear Tree Road.	131
Figure 3.25 Relative vertical deformation on the abutment walls. Positive values correspond to upward movement.	132
Figure 3.26 Relative vertical deformation on the bridge deck. Positive values correspond to upward movement.	132

Figure 3.27 Relative vertical deformation on the north approaching road. Positive values correspond to upward movement.	133
Figure 3.28 Relative vertical deformation on the south approaching road. Positive values correspond to upward movement.	133
Figure 3.29 Relative lateral deformation on the abutment wall with respect to the reference point.....	135
Figure 3.30 Relative lateral deformation on the abutment wall with respect to the NC surveying point.....	135
Figure 3.31: Bear Tree Road Bridge. Comparison of relative settlement of NE abutment wall and deck versus temperature (at the time of measurement and daily average) and rain fall (one month cumulative and daily total).....	136
Figure 3.32: Bear Tree Road Bridge. Comparison of relative settlement of NW abutment wall and deck versus temperature (at the time of measurement and daily average) and rain fall (one month cumulative and daily total)	137
Figure 3.33: Bear Tree Road Bridge. Comparison of relative settlement of NE deck and approaching road versus temperature (at the time of measurement and daily average) and rain fall (one month cumulative and daily total).	137
Figure 3.34: Bear Tree Road Bridge. Comparison of relative settlement of NW deck and approaching road versus temperature (at the time of measurement and daily average) and rain fall (one month cumulative and daily total).	138
Figure 3.35 Subsurface exploration data for the bridge over Windsor Road.....	139
Figure 3.36 Relative vertical deformation on the abutment walls. Positive values correspond to upward movement.	141
Figure 3.37 Relative vertical deformation on the bridge deck. Positive values correspond to upward movement.	141
Figure 3.38 Relative vertical deformation on the north approaching road. Positive values correspond to upward movement.	142
Figure 3.39 Relative vertical deformation on the south approaching road. Positive values correspond to upward movement.	142

Figure 3.40 Relative lateral deformation on the abutment wall with respect to the reference point..... 143

Figure 3.41 Relative lateral deformation on the abutment wall with respect to the NC surveying point..... 144

Figure 3.42: Windsor Road Bridge. Comparison of relative settlement of NE abutment wall and deck versus temperature (at the time of measurement and daily average) and rain fall (one month cumulative and daily total)..... 145

Figure 3.43: Windsor Road Bridge. Comparison of relative settlement of NW abutment wall and deck versus temperature (at the time of measurement and daily average) and rain fall (one month cumulative and daily total)..... 145

Figure 3.44: Windsor Road Bridge. Comparison of relative settlement of NE deck and road approach versus temperature (at the time of measurement and daily average) and rain fall (one month cumulative and daily total). 146

Figure 3.45: Windsor Road Bridge. Comparison of relative settlement of NW deck and road approach versus temperature (at the time of measurement and daily average) and rain fall (one month cumulative and daily total)..... 146

Figure 3.46: Subsurface exploration data for the bridge over Vinburn Road. 148

Figure 3.47: Relative vertical deformation on the abutment walls. Positive values correspond to upward movement. 149

Figure 3.48: Relative vertical deformation on the bridge deck. Positive values correspond to upward movement. 149

Figure 3.49: Relative vertical deformation on the north approaching road. Positive values correspond to upward movement. 150

Figure 3.50: Relative vertical deformation on the south approaching road. Positive values correspond to upward movement. 150

Figure 3.51: Relative lateral deformation on the abutment wall with respect to the reference point..... 152

Figure 3.52: Relative lateral deformation on the abutment wall with respect to the NC surveying point..... 152

- Figure 3.53:** Vinburn Road Bridge. Comparison of relative settlement of NE abutment wall and deck versus temperature (at the time of measurement and daily average) and rain fall (one month cumulative and daily total)..... 153
- Figure 3.54:** Vinburn Road Bridge. Comparison of relative settlement of NW abutment wall and deck versus temperature (at the time of measurement and daily average) and rain fall (one month cumulative and daily total)..... 154
- Figure 3.55:** Vinburn Road Bridge. Comparison of relative settlement of NE deck and approach road versus temperature (at the time of measurement and daily average) and rain fall (one month cumulative and daily total)..... 154
- Figure 3.56:** Vinburn Road Bridge. Comparison of relative settlement of NW deck and approach road versus temperature (at the time of measurement and daily average) and rain fall (one month cumulative and daily total)..... 155

List of Tables

Table 2.1 Shallow foundation types and usage suggestions (after Salgado 2008).....	11
Table 2.2: Load Factors for Geotechnical Structures (FHWA 2001; Budhu 2007 and Salgado 2008 after AASHTO 2004).....	13
Table 2.3: Resistance Factors for Bearing Capacity Calculations (After FHWA 2001, Budhu 2010).....	14
Table 2.4 Relative characterization of some types of instrumentation for load and deformation measurement.....	21
Table 2.5 Studies reviewed for instrumentation and monitoring techniques	22
Table 2.6 Reference test mote position	29
Table 2.7 Long-term mote test termination data.....	35
Table 2.8 Thermal coefficients used to calculate strain in sister bar strain meters (Geokon 4911-2009).....	45
Table 2.9 Information needed to calculate load and footing stress using strain meter output.....	48
Table 2.10 Constants used to evaluate modulus of elasticity of test columns (ASTM C597-2009)	54
Table 2.11 Laboratory test column design details	55
Table 2.12 Strainmeter identification and grid location in test columns.....	61
Table 2.13 Load schedule for compressive loading of the instrumented columns	68
Table 2.14 Minimum reinforcement column load test results	71
Table 2.15 Maximum reinforcement column load test results	77
Table 3.1 Research site locations and design information provided by WisDOT	83
Table 3.2 Research site construction data provided by WisDOT	84
Table 3.3 Subsurface exploration details for each research site included in construction documents	85
Table 3.4 Design conditions and temperature averages for the studied bridges.....	93
Table 3.5 Research site instrumentation location and identification.....	97

Table 3.6 Comparison of reinforcement ratios in research sites to laboratory columns	98
Table 3.7 Modulus of elasticity E_c at each research site.....	111
Table 3.8 Layton Avenue Bridge structural load calculation input information	116
Table 3.9 STH-164 Pier settlement results along with the location of reference point, level, and marker on the bridge. Their locations are presented in Figure 3.13. (Negative values indicate settlements).....	119
Table 3.10 STH-164 Abutment settlement results along with the location of reference point, level, and marker on the bridge. Their locations are presented in Figure 3.14. (Negative values indicate settlements).....	120
Table 3.11 STH-164 Bridge Pier structural load calculation input information	121
Table 3.12 STH-164 Bridge abutment structural load calculation input information	122
Table 3.13 Lien Road Bridge settlement results. (Negative values indicate settlements).	125
Table 3.14 Lien Road Bridge structural load calculation input information	126
Table 3.15 Summary of relative vertical deformations for the Highway 51 Bridge over Bear Tree Road. Positive values indicate upward movement.	134
Table 3.16 Summary of relative lateral deformations on the abutment wall with respect to the reference point.....	134
Table 3.17 Summary of relative lateral deformations on the abutment wall with respect to the NC surveying point.	134
Table 3.18 Summary of relative vertical deformations for the Windsor road bridge. Positive values indicate upward movement.	140
Table 3.19 Summary of relative lateral deformations on the abutment wall with respect to the reference point.....	140
Table 3.20 Summary of relative lateral deformations on the abutment wall with respect to the NC surveying point.	141

Table 3.21 Summary of relative vertical deformations for the Vinburn Road Bridge. Positive values indicate upward movement. 151

Table 3.22 Summary of relative lateral deformations on the abutment wall with respect to the reference point..... 151

Table 3.23 Summary of relative lateral deformations on the abutment wall with respect to the NC surveying point. 151

Executive Summary

Prediction of foundation vertical and horizontal displacements due to dead and service loads is inexact and subject to assumptions and the quality models and input model parameters. A better understanding of the relationship between the loads a structure applies to the foundation and the interaction of the foundation with the subsurface may increase the accuracy and reduce the over-engineering of engineering designs. The intent of this research was to combine load, displacement, and geotechnical data to improve foundation settlement estimates.

With this aim in mind, we instrumented and monitored bridges in Southern Wisconsin to collect load and settlement data during and after construction of bridges. Options to rapidly, accurately, and inexpensively measure the forces acting within the structures and the movements of the structures were evaluated and tested. Methods to install, use, and maintain the deployed instruments were developed. A program was developed to report collected data in a usable form, and preliminary analysis of the structural loads and movements was completed.

Geotechnical information corresponding with the displacement and load data for each structure was limited. The subsurface information available for each project site was included in the construction documents. Most geotechnical reports or subsurface testing performed at the locations where the instruments were installed include Standard Penetration Test (SPT) values. These in situ test results, while commonly used in practice, are not of the quality required to performed robust numerical models nor could be used to establish strong correlations. An analysis of the predicted and actual

settlement could not be reliably completed nor would it be transferrable to other design situations.

While the research objective was to refine and publish design procedures for transportation structure foundations within the LRFD framework limitations in data collection and soil property determination prevented the completion of the main objective. For these reasons, this document focuses on the development of a methodology for the collection of loads and movements of transportation structures, on the development of recommendations for the measurement and selection of input parameters, on the assessment of analysis used on the performance of calculation of foundation movements, and on the interpretation of field measurements of foundation loads and movements of transportation projects in Southern Wisconsin.

1. Introduction

Wisconsin DOT engineers use the AASHTO Design Code for the design of foundations for transportation structures. The AASHTO Design Code is based on the Load and Resistance Factor Design (LRFD) methods. While the LRFD method specifies that in addition to satisfying the requirement of global stability, the AASHTO Design Code also requires that the structure must fulfill horizontal and vertical serviceability displacement requirements.

Historically, foundations structures were designed using the Allowable Stress Design (ASD) approach with high factor of safeties. Under this approach, the large factor of safety was assumed to yield small vertical and horizontal deformations. In the LRFD method, the movements of the foundations are assumed to be small when the load factors are large (e.g., FHWA 2001, Salgado 2008, Sargand and Hazen 1999, Wang et al. 2007). Assuming zero foundation movement is not consistent with observable behavior of structures in the field (e.g. Briaud and Gibbens 1999, Mayne and Poulos 1999, Sargand and Hazen 1999, Sargand et al. 2003). Foundations for transportation structures, such as bridges or retaining walls do move due to the applied load, changes in temperature, and creep of foundation and structural elements. Therefore, assessing the assumptions of displacement in the LRFD method would improve the design of structural foundations (Sargand and Hazen 1999). A better foundation design should improve safety of the structure as well as to reduce cost by limiting the extra capacity designed into the foundation. Refinement of the LRFD method will be based on the soil information below the foundations, field measurements of foundations' loads and movements for

transportation structures in Wisconsin should validate and calibrated design procedures and input parameters. Therefore design assumptions related to foundation movements must be refined to be better assess if they indeed fulfil the AASHTO Design Code requirements.

1.1 Axial Loading

Settlements (δ_v) due to vertical loading of deep and shallow foundations are typically modeled using elastic theory by providing an appropriate 'operational' stiffness (E) and influence factors (I_p). For deep foundation systems, vertical settlement equation is:

$$\delta_v = I_p \frac{P}{D \cdot E} \quad 1.1$$

where P is the applied load at the pile head and D is the foundation diameter. Differences in the analysis of deep foundation vertical displacements using linear and non-linear stiffness methods are shown in Figure 1.1.

Figure 1.1a shows that the use of a constant modulus may provide a reasonable average prediction. However the use of a more appropriate nonlinear soil modulus better matches the foundation settlement behavior from working loads to failure (Figure 1.1b).

For shallow foundation structures, the vertical settlement equation is:

$$\delta_v = I \frac{q \cdot B}{E} \quad 1.2$$

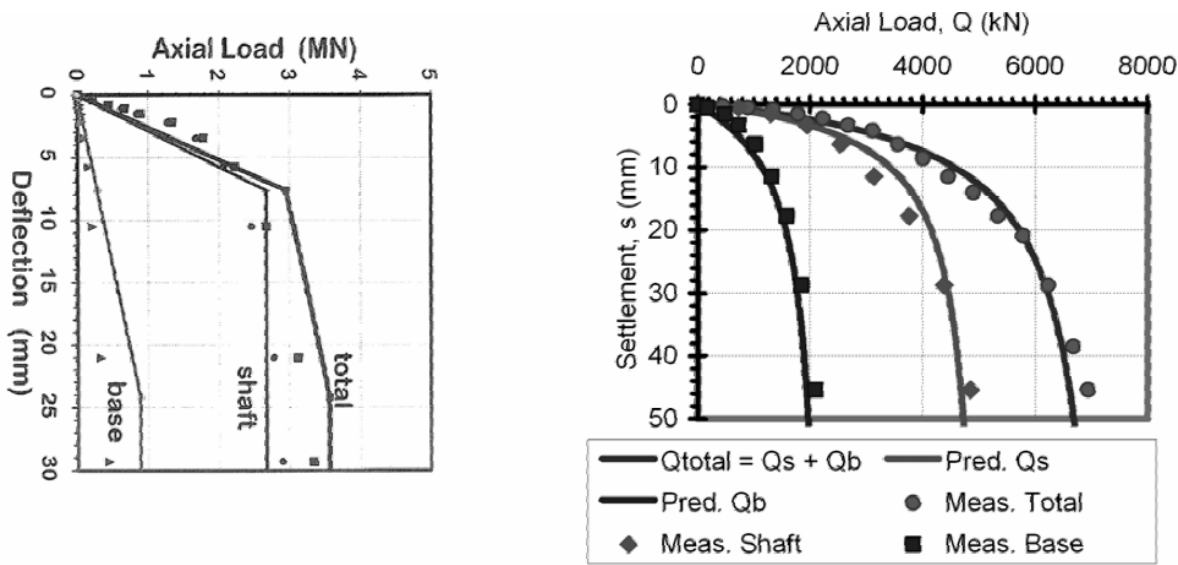


Figure 1.1: Modeling drilled shaft behavior using elastic theory with (a) linear dilatometer stiffness (Mayne et al. 1999); and (b) non-linear stiffness (Mayne & Schneider 2001).

where I is the influence factor, q is the applied stress, B is the foundation width, and E is the Young's modulus. Influence factors for both types of foundation systems are affected by foundation and soil stiffness, foundation geometry, and soil layering. For typical soils and foundation systems, the value of influence factor has been tabulated (e.g., Banerjee 1978, Randolph and Wroth 1979, Poulos 1987, Poulos 1989, Mayne and Poulos 1999).

1.2 Quality of settlement estimations

Equations 1.1 and 1.2 are simple formulations used in the estimation of settlements in foundation systems. However, there is a significant level of uncertainty in the application of the equations in practice. There are problems in the estimation of the “operational” stiffness in soils. The operation stiffness in soils depends on the effective

stresses (that changes with the induced loading and the strain level caused by the structure) and the strain level caused by the foundation system.

For example, shallow foundation settlement prediction symposiums have systematically shown that majority of participants significantly err in assessing footing settlements for shallow foundations (e.g., Tan and Duncan 1991). In 2008, Lehane et al. (2008) presented the results of a settlement prediction competition of four footings in Perth, Australia. Of 26 written submissions, the average level of under prediction of settlements was by more than a factor of two, with some predictions being unconservative by a factor of over ten. The footing widths were 0.67 m, 1 m, and 1.5 m, and comparison of the distribution of predictions to the measured settlement for a load of 280 kN are summarized in Figure 1.2a.

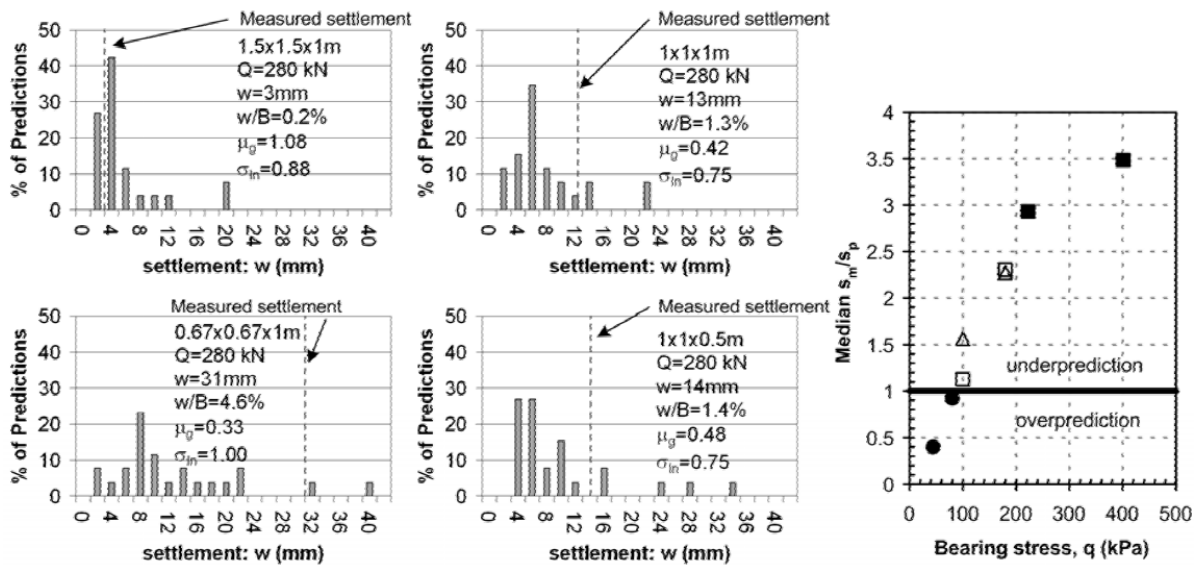


Figure 1.2: Results of shallow foundation in sand prediction symposium (a) distribution of predictions and field measurements at a load of 280 kN (b) level of over / under prediction as a function of foundation bearing stress (after Lehane et al. 2008).

While the average predictions were reasonable for a footing width of 1.5 m and bearing pressure $q=125$ kPa, the Coefficient of Variation (CoV) was very large (from 75 to 100% for each footing size) and the level of under prediction of settlement increased with stress level (Figure 1.2b). This large uncertainty comes from several sources, including the large number of different predictive methods used (i.e., 15) and the significant uncertainty in selection of the 'operational' level of stiffness.

In footing settlement prediction competition reported by Lehae et al. (2008), most engineers used the simple Schmertmann (1970)'s method to estimate vertical settlement. The main problem was that the primary input parameter (i.e., E/q_c) used in this method varied within an order of magnitude (between 2 and 24!). Furthermore, the use of a constant linear modulus, or modulus which does not degrade in an appropriate manner with strain distribution nor it increases with effective stress distribution within the foundation soil, caused the trend in the ratio of measured to predicted settlements (δ_{vm}/δ_{vp} - Figure 1.2b).

The non-linear decrease in operational stiffness with strain level results in the degradation of soil stiffness as shown in Figure 1.3b. This non-linearity in soil stiffness is not typically captured in laboratory testing, the resolution of laboratory measurements of stiffness, as well as disturbance induced during soil sampling all lead to uncertainty in selection of an appropriate stiffness value and influence the high levels of uncertainty in calculation of foundation movements illustrated in Figure 1.2.

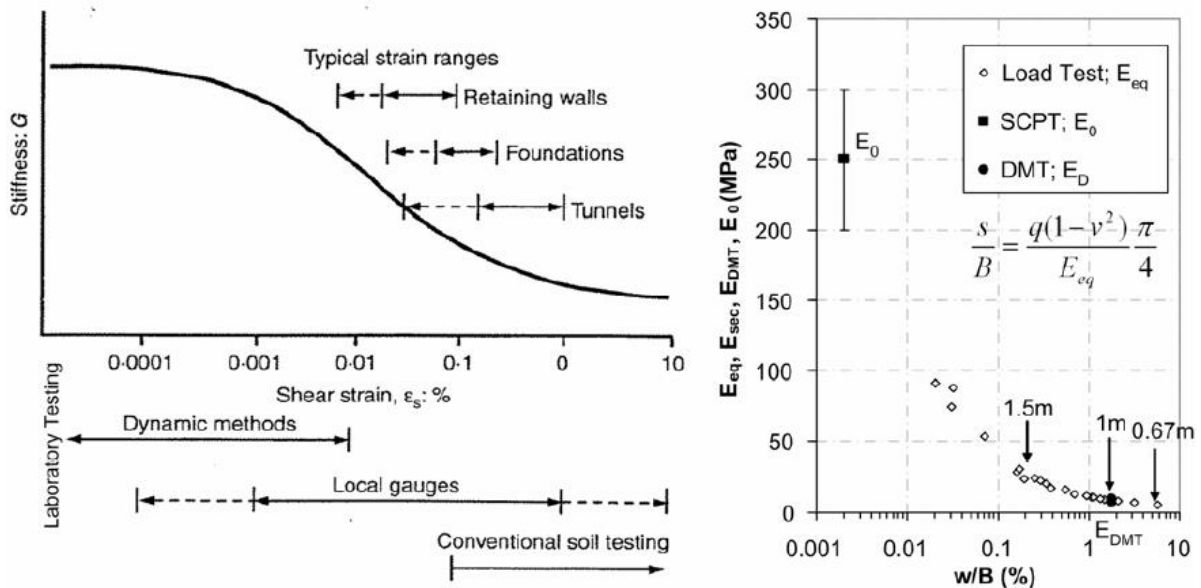


Figure 1.3: Nonlinear soil stiffness behavior (a) in laboratory testing and design applications (Atkinson 2000); and (b) in situ testing and shallow foundation loading in a uniform sand (after Lehane et al. 2008).

1.3 Horizontal deformations

The analysis and prediction of horizontal deformations of deep foundations, many Departments of Transportation (DOTs) engineers use the software program LPILE (ENSOFT 2015). The LPILE code is based on the Winker's beam over spring model using input p-y curves (i.e., load vs. deformation curves) as definition for the reaction springs. A number of p-y curves have become standards for "common" soil types within the program, however there is significant uncertainty in the value of the input parameters for these curves. Most commonly, these parameters are based on data obtained from laboratory testing. Furthermore, these uncertainties become larger for the levels of deformation expected under working conditions as the calculated parameters are strongly influenced by the 'initial' stiffness (e.g., Robertson et al. 1989, Ashford and Juirnarongrit 2003). This initial stiffness cannot be measured accurately using

conventional laboratory tests (e.g., Atkinson 2000). Field measurements of stiffness are more reliable for working loads, although, the conversion of in situ test data to p-y curves typically uses local correlations that have not been calibrated for soils typically found in Wisconsin transportation construction practices with the exception of the work by Farouz et al. (2005). These researchers presented results from the Marquette Interchange project in Milwaukee, WI and developed p-y curves based on dilatometer and pressurimeter tests. None of these tests were available on the studied structures.

To properly assess assumptions and performance of these empirical correlations need to be compared to larger databases of load test results with adjacent in situ test data, analyzed so that the influence of design method formulation can be quantified, and validated with field measurements of foundation performance in Wisconsin soil conditions.

To validate the assumptions, deformation analyses in relation to loading requires additional information, including (Lutenegger and DeGroot 1995):

- *Selection of soil stiffness for input to models.* The selection of soil stiffness in foundation soils is complicated by the nonlinear increase of stiffness with effective stresses and the decrease of stiffness with increasing strain levels. This problem is compounded with the redistribution of effective stresses and strains caused by the forces carried by the foundation structure.
- *Evaluation of the influence of foundation type and construction methodology.* The effect of foundation type (i.e., shallow foundation, driven pile, bored pile),

foundation geometry, foundation structure stiffness, soil type, and soil layering on stresses transferred to the soil must be incorporated to deformation analyses.

The main problem is with the *Selection of soil stiffness for input to models* as most Department of Transportations do not used a systematic testing methodology to assess design soil parameters. Most Departments of Transportation still use Standard Penetration Tests (SPT) and correlations to determine geotechnical engineering design parameters. These practices add to the unreliability of settlements and displacement calculations.

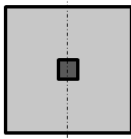
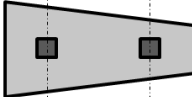
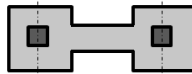
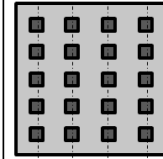
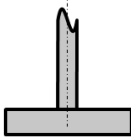
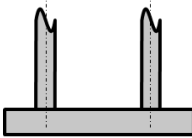
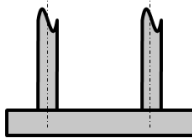
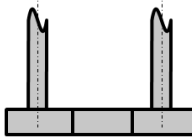
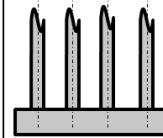
The overall research objective was to refine and publish design procedures for transportation structure foundations within the LRFD framework. The original goal of this research program was to analyze the relationship between the loads applied to the foundations and the movements of the foundations. Using this deformation we have originally intended to develop, refine, and publish modified LRFD procedures. However, due to measurement limitations faced during the field evaluation, we focused this document on the development of a methodology to the collection of load and movement of transportation structures, on the draft of recommendations for the measurement and selection of input parameters for those design procedures, on the assessment of analysis used on the performance of existing methods for the calculation of foundation movements, and on the interpretation of field measurements of foundation loads and movements from transportation projects in Wisconsin for validation.

2. Foundation Structures

Foundations elements are designed to support the structure while minimizing the movement of the structure. Foundation behavior can be understood by combining information about the soil at the foundation location, the loads that the foundation supports, and the movement of the foundation. Foundation types that may be used to support transportation structures include shallow, deep, and piled rafts foundations. Shallow foundations are those which are located less than 2 m below the soil and transmit the structural loads means of vertical pressure at the bottom surface of the foundation element (Salgado 2008; Day 2010). Salgado (2008) compiled

to illustrate several shallow foundation geometries. Deep foundations, including piles, are installed at much greater depths and transmit the structural loads by means of vertical pressure and side friction (AASHTO 2007; Salgado 2008; Day 2010). Deep foundation can be driven or drilled. They can also be made of very different materials, including concrete, steel, wood, composite, etc. (Figure 2.1 - Coduto et al. 2016).

Table 2.1 Shallow foundation types and usage suggestions (after Salgado 2008)

Foundation type	Isolated footing	Combined footing		Strap footing	Mat foundation
		Rectangular	Trapezoidal		
Plan view					
Profile view					
Applicability	Relatively high ratio of soil resistance to structural loads	Columns too closely spaced; support of column too close to obstruction/ property line (column spacing $< \sim 7$ m)		Support too close to obstruction/ property line (column spacing $> \sim 7$ m)	Relatively low ratio of soil resistance to structural loads

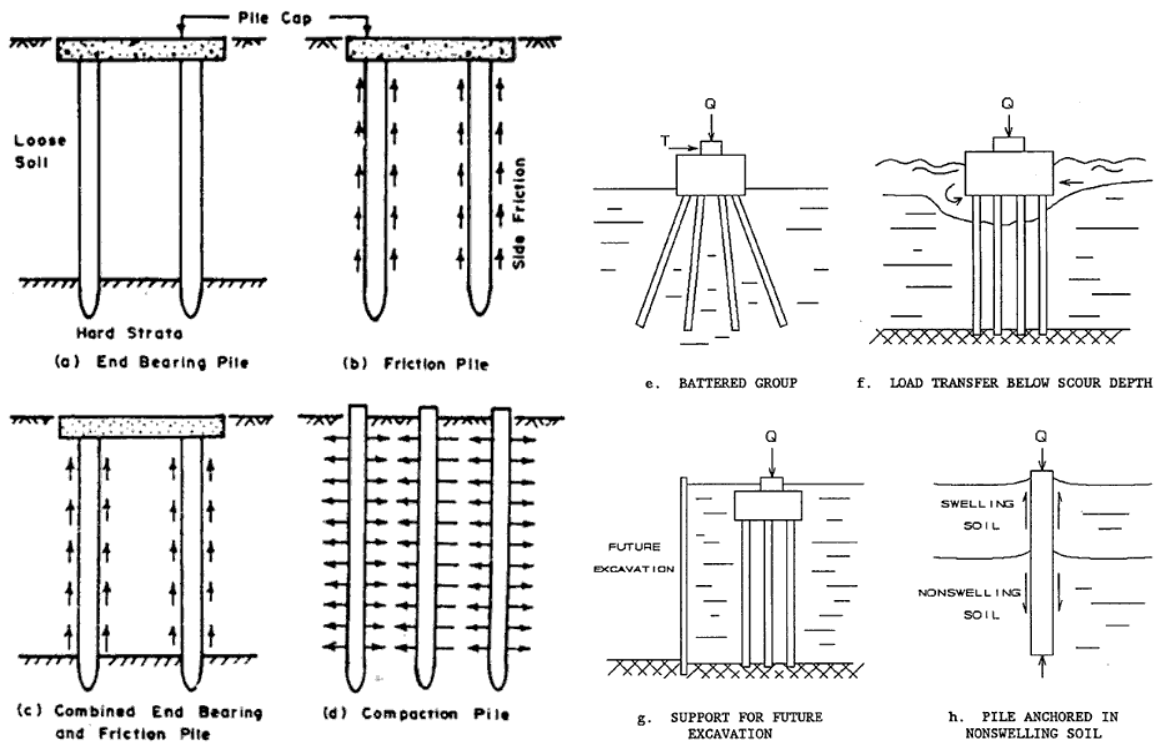


Figure 2.1: Different type of piles and applications (Sources: URL: www.abuildersengineer.com)

2.1 Load and Resistance Factor Design (LRFD) Methodology

Load and Resistance Factor Design (LRFD) is a “reliability based design methodology in which force effects caused by factored loads are not permitted to exceed the factored resistance of the components” (AASHTO 2007).

Load and resistance factors were developed based on statistical probabilities of loads combining and acting on the structure and account for structural and material variability (FHWA 2001):

$$Q \leq R \quad 2.1$$

$$Q = \sum(Q_{ni} \cdot \phi_i) \quad 2.2$$

$$R = R_n \cdot \phi$$

2.3

The combination of factored loads Q and factored resistances R represents the limit states which form the design inequality (2.1). Loads (Q_{ni}), including dead load (Q_{DL}), live load (Q_{LL}), and snow load (Q_{SL}), are multiplied by load factors ϕ_i and summed to calculate Q for each limit state. Table 2.2 summarizes the loads factors for bridge design. These AASHTO factors consider ductility, redundancies and importance of the load and element in assigning the weigh to the load factors (Budhu 2007).

Table 2.2: Load Factors for Geotechnical Structures (FHWA 2001; Budhu 2007 and Salgado 2008 after AASHTO 2004)

Load Types	Load Factors	
	Minimum	Maximum
Live Load (Q_L)	1.35	1.75
Component and structural loads (Q_{DL})	0.90	1.25
Downdrag (Q_{DD})	0.45	1.80
Wearing Surfaces and Utilities (Q_{WD})	0.65	1.50
Horizontal Earth Pressure (Q_{EL})		
Active	0.9	1.50
At rest	0.9	1.35
Vertica Earth Pressure (Q_{EV})		
Retaining Structure	1.00	1.35
Rigid Buried Structure	0.90	1.30
Rigid Frame	0.90	1.35
Flexible Buried Structure	0.90	1.95
Flexible Metal Box Culverts	0.90	1.50
Earth Surcharge (Q_{ES})	0.75	1.50
Wind (Q_{WL})		1.40
Seismic (Q_{EQ})		1.00

The resistance R of each limit state is the product of the nominal structural resistance R_n and the resistance factor Φ (2.3). Table 2.3 presents a summary of resistance factors used in Geotechnical Engineering design. The summarized resistance factors grade the quality of parameters used in geotechnical engineering design. Please note the low factor of the resistance factor obtained for Standard Penetration Testing (SPT) parameters and how high is the value of the resistance factor when the critical state friction angle is obtained from laboratory testing. These results seem to indicate the importance of a cost-benefit analysis before simply deciding the use of SPT in site characterization for obtaining design parameters in soils.

The serviceability limit state is reached when the structure ceases to perform as designed without the loss of safety and the structure remains usable. When the structure becomes potentially unsafe and may collapse, the ultimate limit state has been attained.

Table 2.3: Resistance Factors for Bearing Capacity Calculations (After FHWA 2001, Budhu 2010)

Bearing Capacity Parameter		Resistance Factor Φ
<i>Effective Stress Analysis: Coarse-grained soils</i>		
Friction angle	Critical State (from Laboratory Testing)	0.95
	Peak (from Laboratory Testing)	0.8
	Peak (from Standard Penetration Test)	0.35
	Peak (from Cone Penetration Test)	0.45
N-value (from Standard Penetration Test)		0.45
q_t (from Cone Penetration Test)		0.55
Plate Load Test		0.55
Pile Driving Analysis (for pile design formulations)		0.75
<i>Total Stress Analysis: Saturated fine-grained soils</i>		
Undrained shear strength	UU (from Laboratory Testing)	0.60
	Vane shear (from Laboratory Testing)	0.60
	(from Cone Penetration Testing)	0.50
	Vane shear (from Field Testing)	0.60
	(from Plate Load Test)	0.55

2.2 Settlements

Settlement are a function of the magnitude and geometry of the force applied to the subsurface and the properties of the subsurface soil. Displacements of foundations are limited to reduce potential damage to the supported structure and to maintain serviceability conditions. For these reasons, the prediction of the foundation displacements must be refined. Calculation refinement can only be achieved by the proper definition of the structure geometry and response, and by calibration of models using measurements of settlements and settlement-induced loads. The measurements of settlements and loads can be accomplished through several different instrumentation schemes.

Foundation deformation limits

Foundation movements are in the vertical, horizontal, and rotational directions, seen in Figure 2.2. Deformations of structures are limited for safety, aesthetics, user experience, and cost of future repairs (AASHTO 2007). The maximum allowable movement that a bridge may experience at the top of the foundation is 100 mm vertical settlement (w_y), 50 mm horizontal settlement (w_x), and 0.229 degrees rotation (AASHTO 2007).

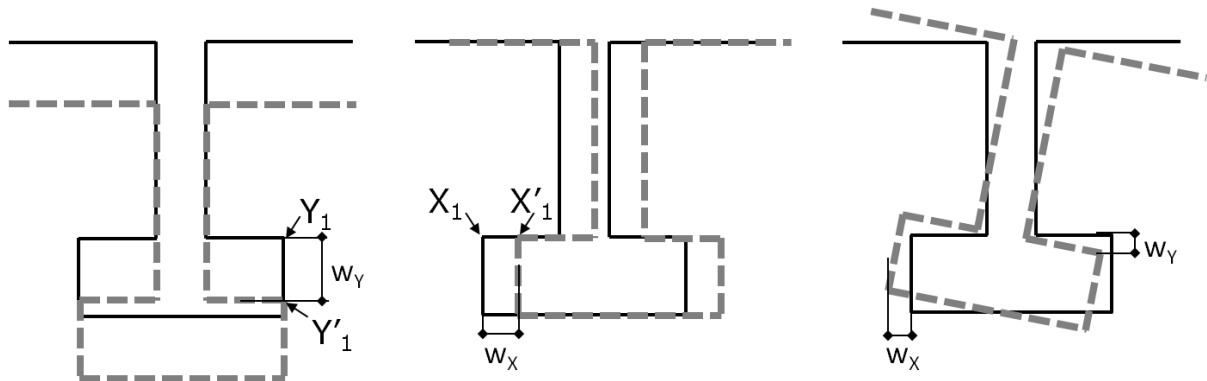


Figure 2.2 Shallow foundation movements in two-dimensional plane: settlement, horizontal deformation, and rotation.

Settlement prediction

Displacements of shallow foundations are frequently underestimated, even when the foundation geometry, applied load, and subsurface conditions are known (Briaud and Gibbens 1999, Cai et al. 1999, Mayne and Poulos 1999, Sargand et al. 2003). Attendees of an industry foundation design conference demonstrated this uncertainty when they were asked to submit vertical settlement estimates of four shallow foundations given information including the dimensions of the foundations, the soil underlying the foundations, and the load applied to the foundations (Lehane et al. 2008). Foundations were of varying size: 1.5 m by 1.5 m by 1.0 m; 1.0 m by 1.0 m by 1.0 m; 1.0 m by 1.0 m by 0.5 m; and 0.67 m by 0.67 m by 1.0 m (Figure 2.3). All of these foundation elements were loaded to 280 kN. The foundations were constructed in a sand test pit compacted to the same density preceding each test. The settlement of each foundation was measured once load was applied, and measured settlements were compared to those predicted by the industry practitioners (Lehane et al. 2008).

The predictions and the actual settlement are compared in Figures 2.4 through 2.7. The settlement of the largest foundation was conservatively predicted by 75% of the respondents. In every other case the settlements of the foundations were under-predicted by the majority of the participants. The decrease in the cross sectional area of the foundation was mirrored in the decrease of conservative settlement predictions. The settlement of the 0.67 m by 0.67 m by 1.0 m foundation was conservatively predicted by only 4% of the study participants.

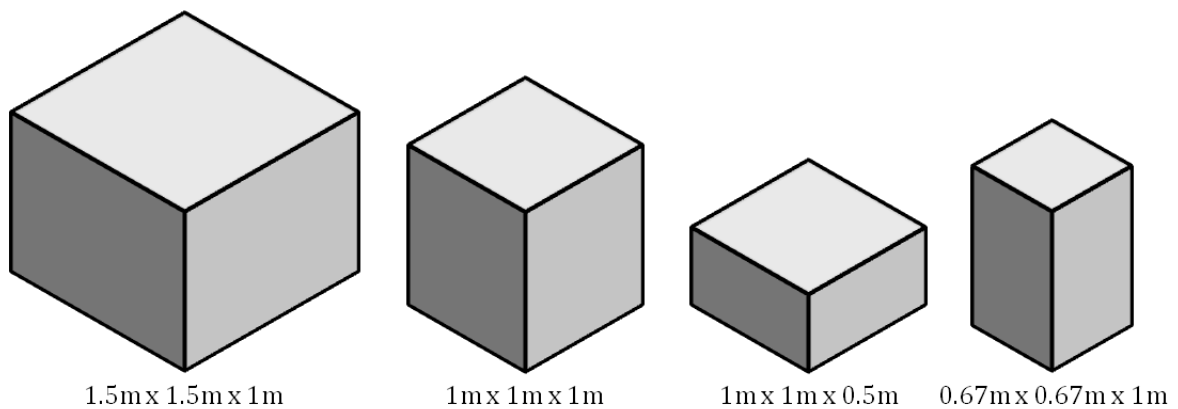


Figure 2.3 Scale drawings of shallow foundations evaluated for settlement by Lehane et al. (2008)

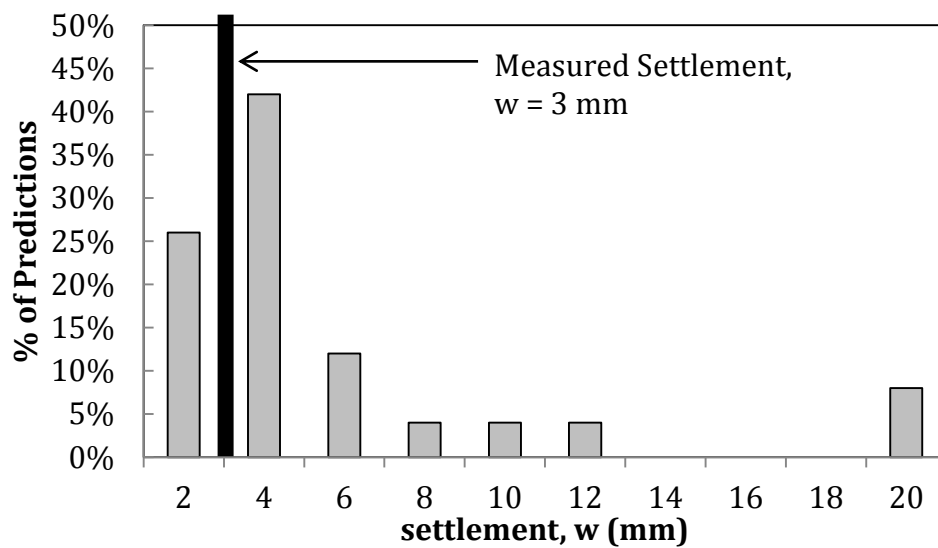


Figure 2.4 Foundation size 1.5 m by 1.5 m by 1 m: predicted and actual vertical settlement (Lehane et al. 2008)

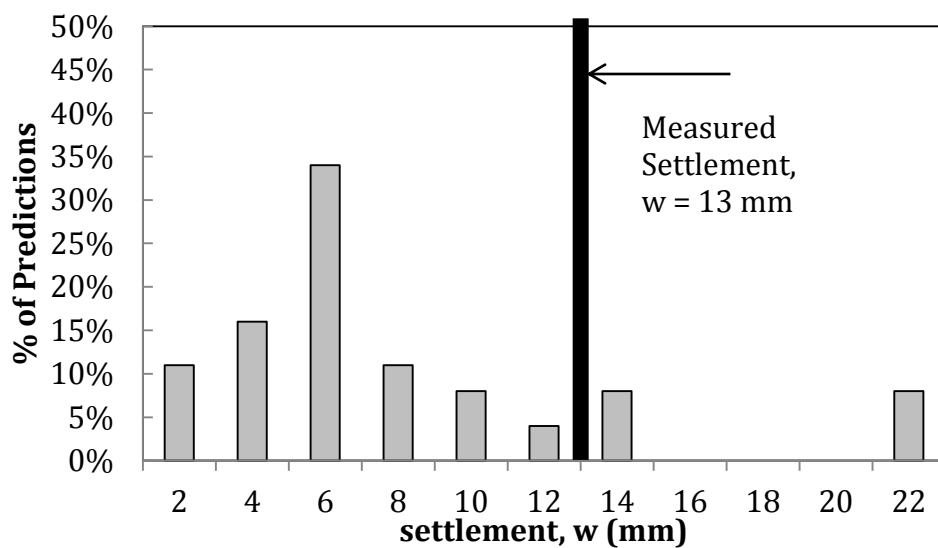


Figure 2.5 Foundation size 1 m by 1 m by 1 m: predicted and actual vertical settlement (Lehane et al. 2008)

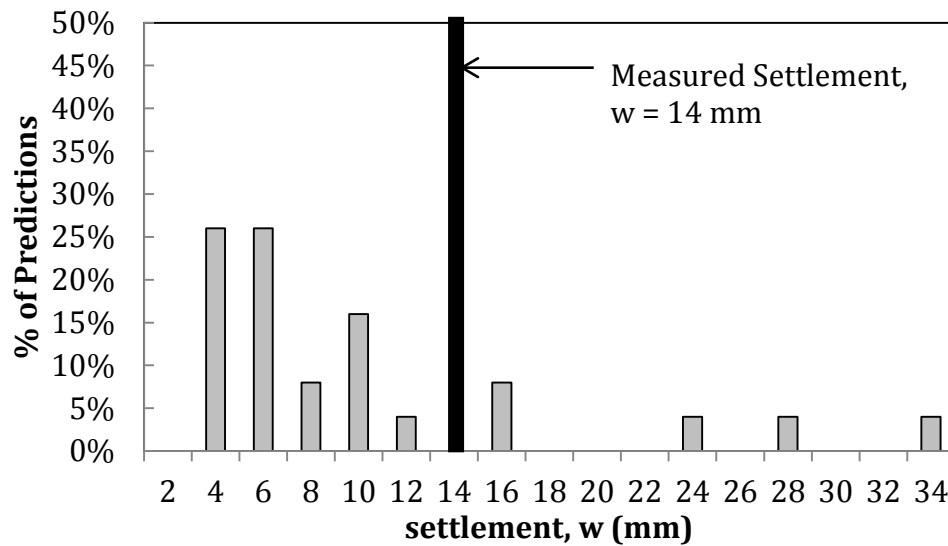


Figure 2.6 Foundation size 1 m by 1 m by 0.5 m: predicted and actual vertical settlement (Lehane et al. 2008)

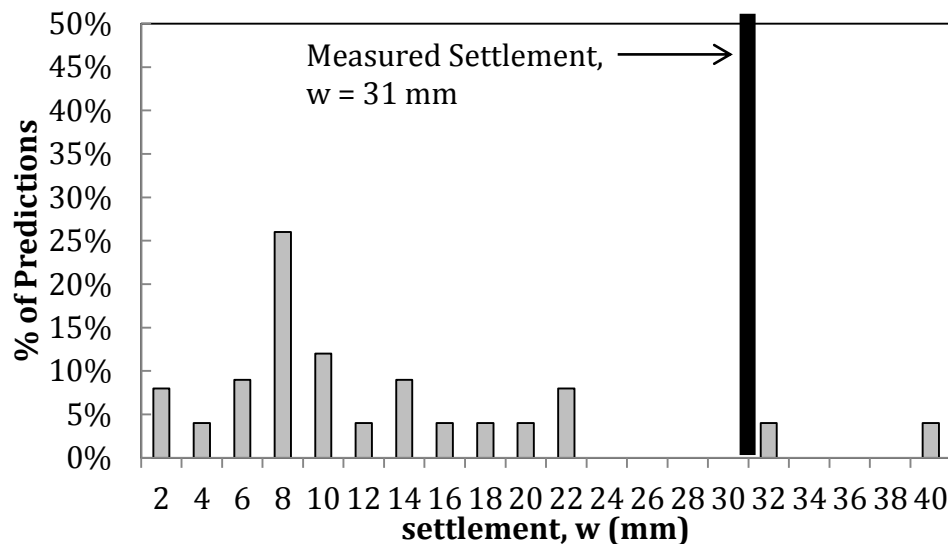


Figure 2.7 Foundation size 0.67 m by 0.67 m by 1 m: predicted and actual vertical settlement (Lehane et al. 2008)

Lehane et al. (2008)'s study showed that the reliability of foundation settlement predictions were low even when all information about factors influencing the movement were known. When the subsurface conditions and loading are not well known, settlement

is even more difficult to conservatively estimate (Lehane et al. 2008). Then, the study of actual structures' settlements along with a proper evaluation mechanical parameters of foundation soil should increase the accuracy of the settlement prediction methods and models. However, it is important to note that WisDOT engineers estimate that in their evaluation of design practices they have observed an overprediction rather than an underprediction in settlement calculations (R. Arndorfer 2015 - Personal Communication).

Finally, a comprehensive study on coarse grain soil in 1995 already recommended (Luttenegeer and deGroot 1995) that "...lack of a complete site investigation to provide sufficient test results on the nature and variability of granular deposits at a particular site" and "... the use of simplistic, empirical and generally outdated methods of analysis which tend to give erratic results which are not of a sufficiently general nature and generally do not recognize the important factors contributing to the deformation characteristics of granular soils...". That is, better site characterization and methods of analysis would be required for the proper assessment of deformation of transportation structures.

2.3 Instrumentation characterization and evaluation

The instrumentation of the foundations to record movements and loads was designed to meet several specific criteria. The instrumentation to be used at potential structures had to be long-term, non-invasive, rapid to install, redundant, robust, and sensitive (Greenwood and Herrick 1990). Each of the first four monitored structures was assigned a budget for instrumentation of \$2000. (Four other structures were later

monitored using a total station). Several types of instrumentation and monitoring techniques were considered (Table 2.4). Previous studies of foundation movements have been conducted using varied instrumentation and survey methods. Table 2.5 summarizes the studies that were reviewed.

Table 2.4 Relative characterization of some types of instrumentation for load and deformation measurement

Sensor/ Technique	Application	Cost	Precision	Measurement Frequency	Interference
Traditional optical surveying	Surface movement	Medium-Low	Medium – High	Low	Low
Automated optical surveying system	Surface movement	High	Medium-High	High	Low
Deep benchmarks with optical surveying	Movement at depth	Very High	Medium-High	Low	Medium
LVDT ¹ displacement transducers	Surface movement	High	High	High	Very High
Photogrametry, PIV ²	Surface movement	Low	Medium-High	Medium/ High	Low/ Medium
Local Differential GPS ³ Network	Surface movement	High	Medium-High	High	Low
Inclinometers	Rotation	Low	Low-Medium	Low	High
Tiltmeters, Accelerometers	Rotation	High-Medium	Low-Medium	High	Low
Assessment of construction schedule	Load at top of foundation	Low	Low-Medium	High	Low
Electrical resistance strain gage load cell	Load at top of foundation	High	High	High	Low
Electrical resistance strain gage for axial load	Vertical deformation	High	High	High	Low
Electrical resistance strain gages for bending	Horizontal deformation	High	High	High	Low
Piezometers	Consolidation settlement	High	High	High	Low

Notes: ¹ Linear Variable Differential Transformer

² Particle Image Velocimetry

³ Global Positioning System

Table 2.5 Studies reviewed for instrumentation and monitoring techniques

Study	Type of Structure	Type of Foundation	Measurements	Instruments		Load Tests?
				Total Quantity	Type	
Bentler et al. (2008)	Bridge	piles and spread footings	lateral movement settlement and vertical movement rotation	12	inclinometers earth pressure cells tiltmeters total station survey	No
Briaud & Gibbens (1999)	Isolated test foundations	spread footings	vertical movement lateral movement creep	40	inclinometers tell-tales LVDTs	Yes
DeJong et al. (2002)	Integrated Abutment Bridge	H-piles	lateral movement earth pressures settlement rotation	89	earth pressure cells joint meters tilt meters temperature gages strain gages thermistors	No
Inaudi et al. (1999)	Bridge	piles	internal vertical displacements internal horizontal displacements	110	mechanical dial gages fiber optic deformation sensors pairs	Yes
Lawver et al. (2000)	Integrated Abutment Bridge	H-piles	horizontal movement rotation of the abutments strains in abutment piles strains in pier piles earth pressures girder displacements settlement, vertical movement strains in prestressed girders strains in concrete deck strains in steel reinforcement	180	extensometers tiltmeters pile gages total station survey	Yes

The movement of the structure and the loads the foundation supports must be measured to understand the behavior of the structure. Deformation and load measurements were collected by separate instruments to minimize cost. Measurements of structural movement were planned to be by direct survey of the structure and installed accelerometers to measure tilt. Instrumentation to measure loads directly exceeded the budget per instrumented structure. Strain measurements in a structure are less expensive to instrument and better in reliability, robustness, and expected lifespan. Measurement of strain in the structure can be converted to load when characteristics of the material are known.

Tilt measurements

Measuring displacements of geotechnical installations, including dams, retaining structures, and foundations has been achieved through several methods (e.g., Bentler et al. 2009, Briaud and Gibbens 1999, Inaudi et al. 1999). The instruments to measure tilt are typically large, bulky, wired through the structure and subject to disturbance during construction (Inaudi et al. 1999, Sargand and Hazen 1999, Sargand and Khoury 1999). Tilt measurements also typically require installation of a reference pile to anchor the gages at an additional expense and added complication at the construction site (Greenwood and Herrick 1990). Small, easily protected, wireless sensors were proposed for tilt measurements at each structure to be monitored for the WisDOT structures in this study. The sensitivity of the proposed system's monitoring devices to the structural

deformations and the long-term reliability of the devices had to be established prior to field installation.

Motes, small wireless sensors capable of measuring tilt, are an alternative method of instrumenting structures. A mote, also referred to as a sensor node, has self-contained sensors, a communication system, and a power supply. The remote access available with the built-in wireless communication options may also eliminate the need to survey structures to measure tilts. The motes considered for potential installation at the field sites were model MTS 400 manufactured by CrossBow Technology, Inc. The manufacture's literature suggests that the MTS 400 is appropriate for agricultural monitoring, environmental monitoring, and art preservation. The MTS 400 is encased in a plastic box with dimensions of 35 mm by 63 mm, a 43 mm antenna that extends 20 mm above the body of the mote as seen in Figure 2.8. Two AA batteries power each mote. Total mass of each mote is 47.4 g (95.8 g including the weight of the installed batteries). The sensors installed on the MTS 400 measure ambient light, relative humidity, temperature, barometric pressure, and 2-axis acceleration.

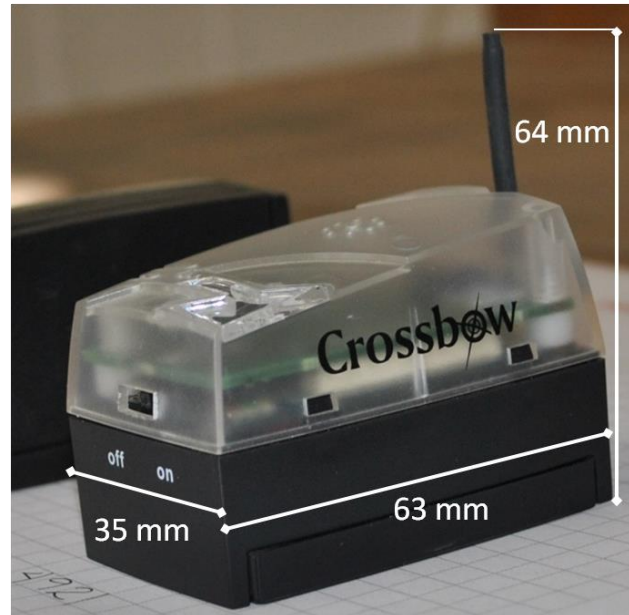


Figure 2.8 MTS 400 mote and its dimensions

The two-axis accelerometer installed on the surface of the Micro Electro-Mechanical Systems (MEMS) sensors is an Analog Devices ADXL202JE and is appropriate for tilt detection, movement, vibration and/or seismic measurements. The sensor's range is ± 2 g (± 19.62 m/s²). The sensitivity of the sensor is 167 mV/g or $\pm 17\%$ and the resolution of the sensor is 0.002 g.

Motes do not have onboard data storage and must relay sensor output stored. The motes send and receive data packets containing sensor outputs and programming between other motes and a gateway. The gateway, or base station, is a microprocessor able to send and receive information packets from the deployed motes, store and aggregate data, and transfer data to a standard dedicated computer or server. The motes and gateway have a 30 m direct signal range (Figure 2.9 - CrossBow Catalogue 2007). Indirect signal transfer (daisy-chain) of data packets allows the motes to be deployed beyond the 30 m signal range (Figure 2.10). During laboratory testing, the base station

was hardwired to a dedicated laptop and the motes were all within range of the gateway to directly transfer information packets (Figure 2.11).

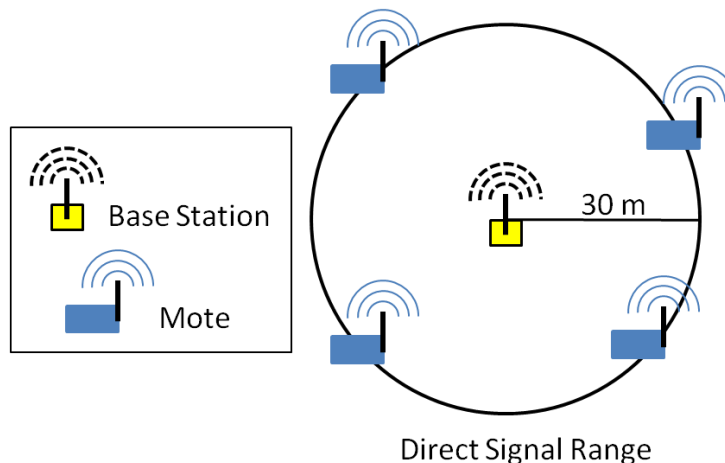


Figure 2.9 The maximum range of the radio signal between the base station and motes

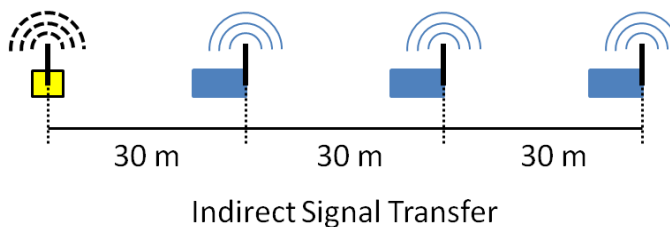


Figure 2.10 Indirect signal transfer, when data packets are relayed between motes, extends the range of the mote placement

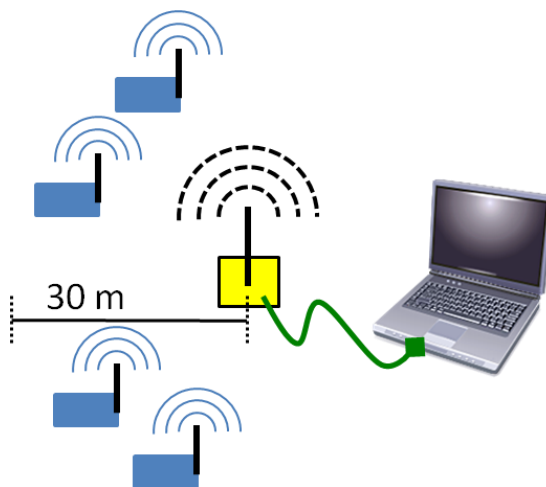


Figure 2.11 Motes were within 30 m of the base station and the base station was hardwired to a dedicated computer during laboratory testing

Measurement of a structure's tilt may be used to calculate the deformation of the structure in all directions. Accelerometers on each mote measure the force of gravity acting on the device in the x-axis and y-axis. Perpendicular orienting the accelerometer axes provides benefits of:

1. The minimum sensitivity of each axis does not occur at the same orientation;
2. An accurate tilt can be measured even when the mote is rotated about the third axis, z; and
3. Angles can be measured as the mote rotates 360 degrees, rather than being restricted to inclination change maximum 180 degrees.

The accelerations were measured in units of gravity (g). The relationship between accelerometer output (A, equal to A_{xi} or A_{yi}) and the tilt, or angle of inclination (θ) in presented in Equation 2.4. Equation 2.5 expresses the tilt angle (θ) in radians as a function of A. Equation 2.6 achieves a more accurate calculation of the tilt angle when acceleration is measured in x-axis and y-axis directions. The change in angle is calculated using Equation 2.7 and the inclination change ($\Delta\theta = \theta_2 - \theta_1$).

$$A_x = g \cdot \sin \theta \quad 2.4$$

$$\theta = \sin^{-1} \left[\frac{A}{g \cdot \sin\left(\frac{\pi}{2}\right)} \right] \quad 2.5$$

$$\theta = \tan^{-1} \left(\frac{A_x}{A_y} \right) \quad 2.6$$

$$\Delta A = (A_2 - A_1) = g \cdot \sin(\Delta\theta) \quad 2.7$$

Laboratory evaluation of tilt measurement instruments

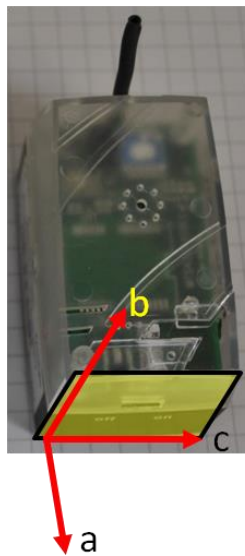
Two reference tests were conducted to establish the usability of the MTS 400 motes. The first test examined the orientation of the motes' accelerometer axes using two motes, one as a control, and the other to establish the change in acceleration recorded during rotation. The second test examined the long term stability of the all five motes' sensor readings and checked the sensors' resolution.

Axis orientation testing

Two motes were placed on a smooth, level surface, resting on their bases. The control mote remained in this orientation throughout the testing, while the experimental mote was rotated in 90 degree-increments about its axes. The experimental mote was placed in different orientations for a minimum of 40 readings of the sensors. Sensor readings were not recorded during the repositioning of the mote for each orientation. It was necessary to assign an orientation system to the motes until the orientation of the accelerometers' axes was established. The base of the mote is in the a-c plane, the antenna is parallel to the b-axis, and the nose of the mote is in the b-c plane and highlighted in Figure 2.12. The orientation of the experimental mote and the comparison to the control mote are presented in Table 2.6.

Table 2.6 Reference test mote position

Position	Rotation of experimental mote from control mote position	Reference Faces	Figure
1, Initial	0 degrees rotation about any axis	Nose in b-c plane, base in a-c plane	2.12
2	90 degree clockwise rotation about c-axis.	Nose in a-c plane, base in b-c plane	2.13
3	90 degree counter-clockwise rotation about c-axis.	Nose in a-c plane, base in b-c plane	Figure 2.14
4	90 degree counter-clockwise rotation about a-axis	Nose in b-c plane, base in a-b plane	2.15
5	Same orientation as position 1	Nose in b-c plane, base in a-c plane	2.16

**Figure 2.12** Initial orientation of motes and arbitrary assigned axes

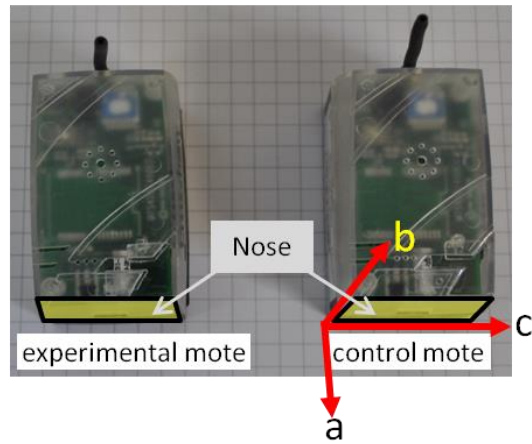


Figure 2.13 Position 1, initial and final orientation of both motes

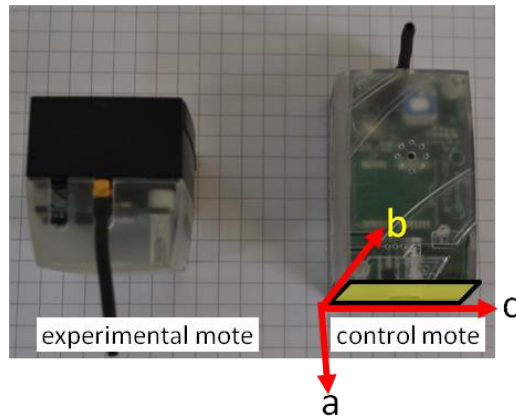


Figure 2.14 Position 2

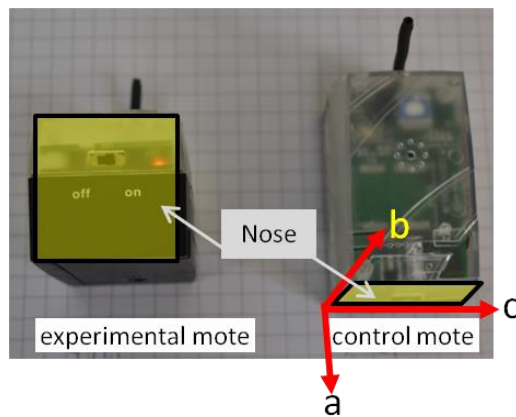


Figure 2.15 Position 3

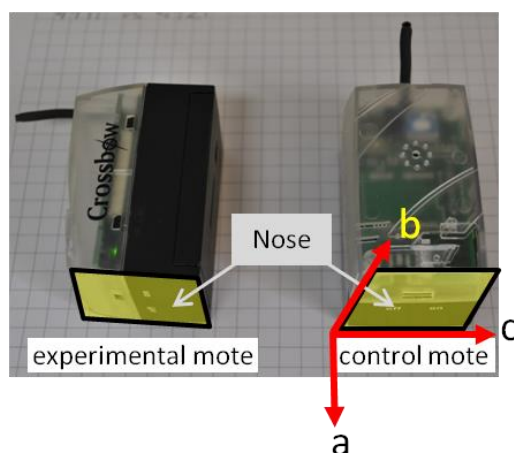


Figure 2.16 Position 4

Graphs were made of the acceleration changes with elapsed time (Figures 2.17 and 2.18). The acceleration in the y-axis occurs when the mote was rotated about the arbitrarily assigned c-axis. Acceleration in the x-axis was only recorded when the mote was in positioned in position 4 (see Figure 2.16). The x-axis acceleration corresponded with the generally assigned a-axis.

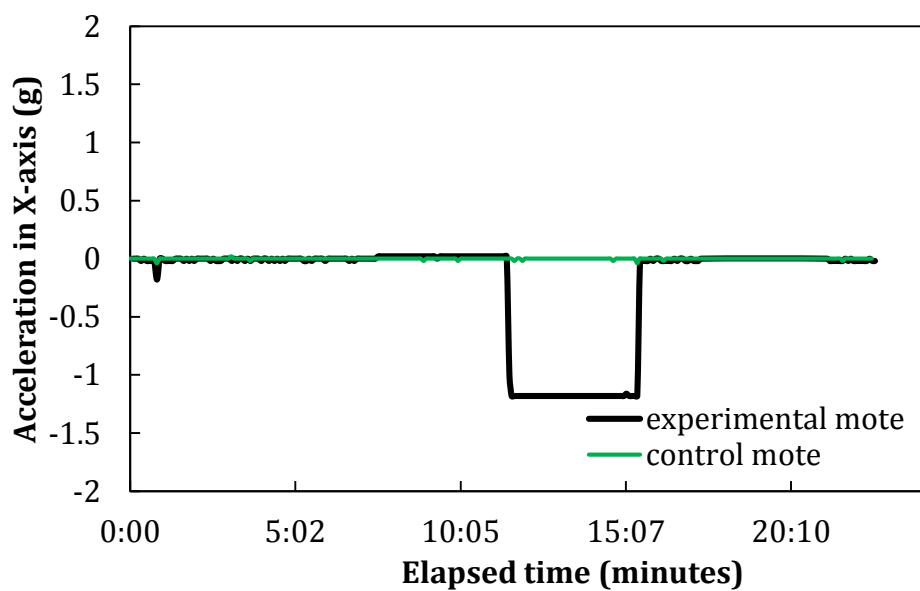


Figure 2.17 Measured acceleration change in the x-axis with time

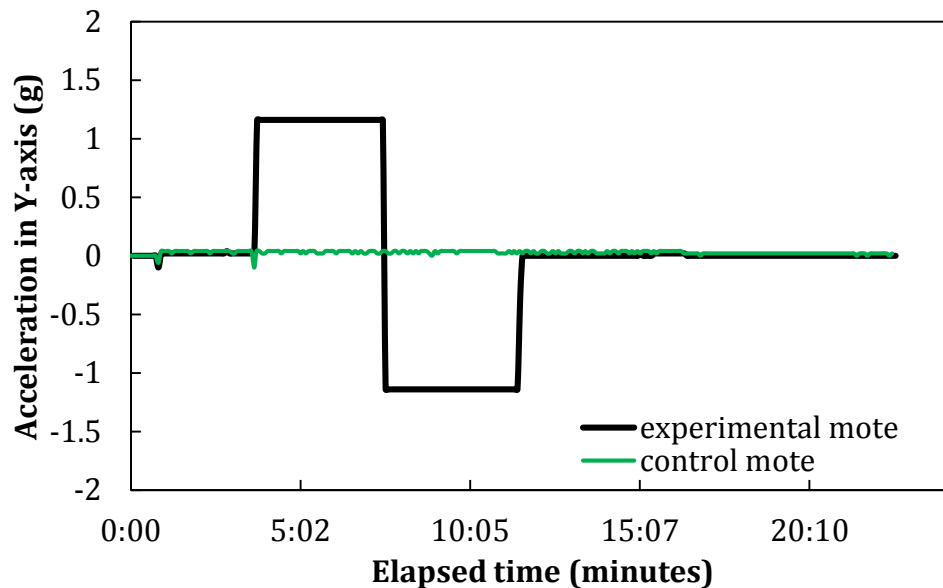


Figure 2.18 Measured acceleration change in y-axis with time

Long term stability and sensor resolution testing

The stability of the accelerometers over time was investigated by positioning the motes and collecting accelerometer readings until the batteries were exhausted. Results indicate that the change in acceleration reported by the motes is not directly related to the battery voltage. The variation of the accelerometers' measurements reduces the precision of the results, too.

The long-term stability test was performed using a 1.24 m by 1.82 m planar surface to which the motes were attached. The planar surface was compressed wood particle board 20 mm thick reinforced by diagonal boards to reduce deformation under its own weight. A hinge was attached to the edge of the board, and the hinge then connected to a board anchored to the laboratory floor. The planar surface was held upright in place by a chain linked through the board to an eye-anchor mounted into the cinderblock wall. Motes were mounted flush to the board face and oriented to detect

acceleration change in the y-axis. Dimensions of the planar surface and layout of the motes are shown in Figure 2.19 and 2.20.

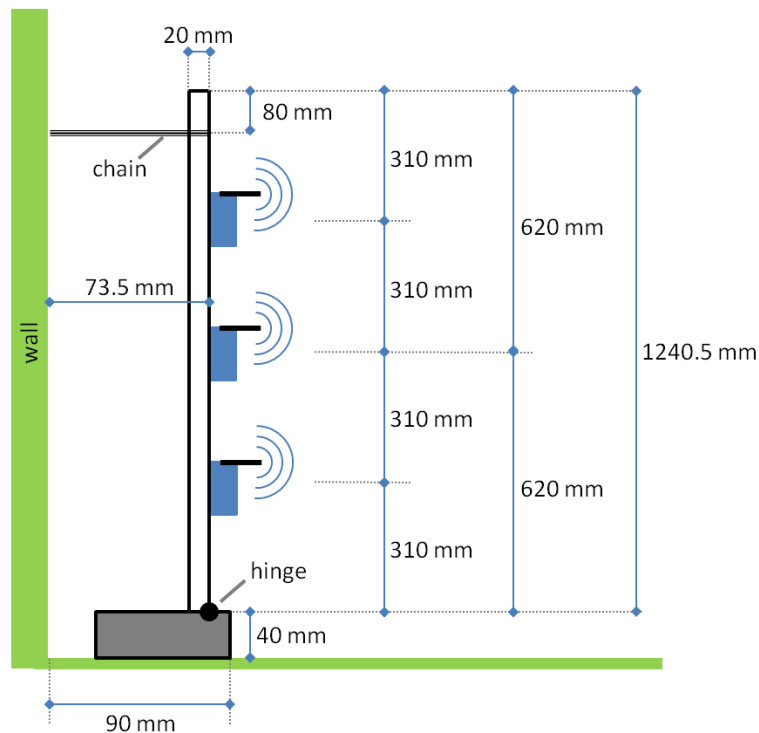


Figure 2.19 Profile view of long-term mote stability test setup

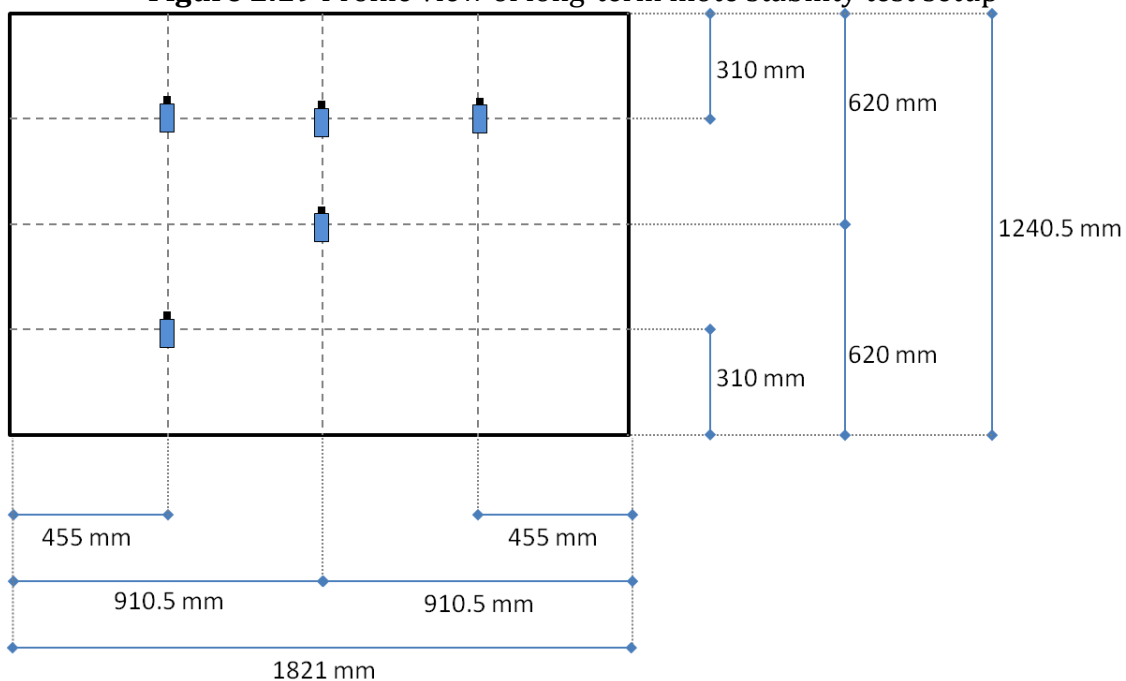


Figure 2.20 Mote layout of long-term test setup and dimensions of planar surface

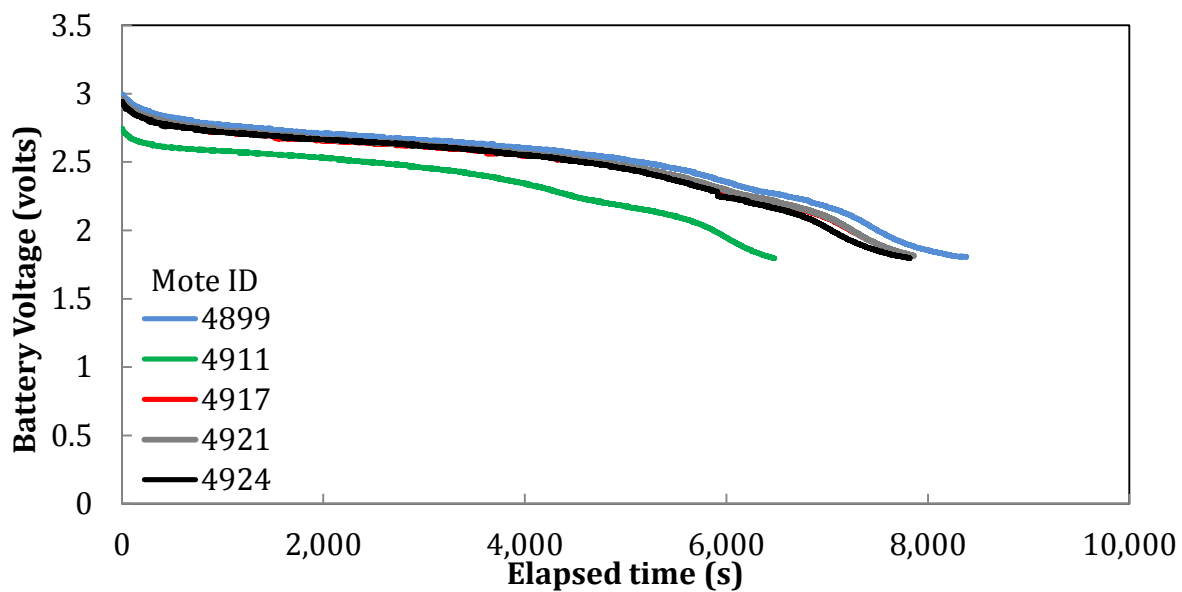
Motes measured acceleration in the x-axis and y-axis once every 60 seconds until the batteries were exhausted. The long term testing ended after different elapsed times and at different battery power (Table 2.7). The decay of battery voltage with time is shown in Figure 2.21.

The change in measured acceleration is presented for the x-axis (Figure 3.22) and the y-axis (Figure 2.23) and was not constant. This result implies that the sensors were experiencing tilt and the rate of the tilt was variable. Bryson et al. (2008) reported a similar phenomenon and explained it as being the result of gravity deforming the planar surface. The reinforcement to the planar surface used for the long-term test increased the rigidity of the surface and decreased the likelihood of the surface deforming while this test was being completed.

Another potential explanation of the variation of measured acceleration with elapsed time was the influence of the decaying battery voltage on the reading of acceleration. Figure 2.24 and 2.25 compare the change in voltage to the change in acceleration. The change in y-axis acceleration with the change in voltage appears to be more linear than the change in the x-axis acceleration. The greater correlation may be a result of the orientation of the motes, which were positioned to detect y-axis acceleration. A predictable relationship was not found between the acceleration and the battery voltage.

Table 2.7 Long-term mote test termination data

Mote ID (number)	Total elapsed time (hh:mm:ss)	Total elapsed time (seconds)	Initial voltage (volts)	Final voltage (volts)	Number of Readings
4899	135:02:08	8384	2.9961	1.8071	8384
4911	105:13:18	6479	2.7464	1.7968	6479
4917	123:32:16	7600	2.9537	1.872	7600
4921	127:52:43	7861	2.9606	1.815	7861
4924	127:15:52	7823	2.9398	1.7968	7823

**Figure 2.21** Battery power of the motes decays at a non-linear rate

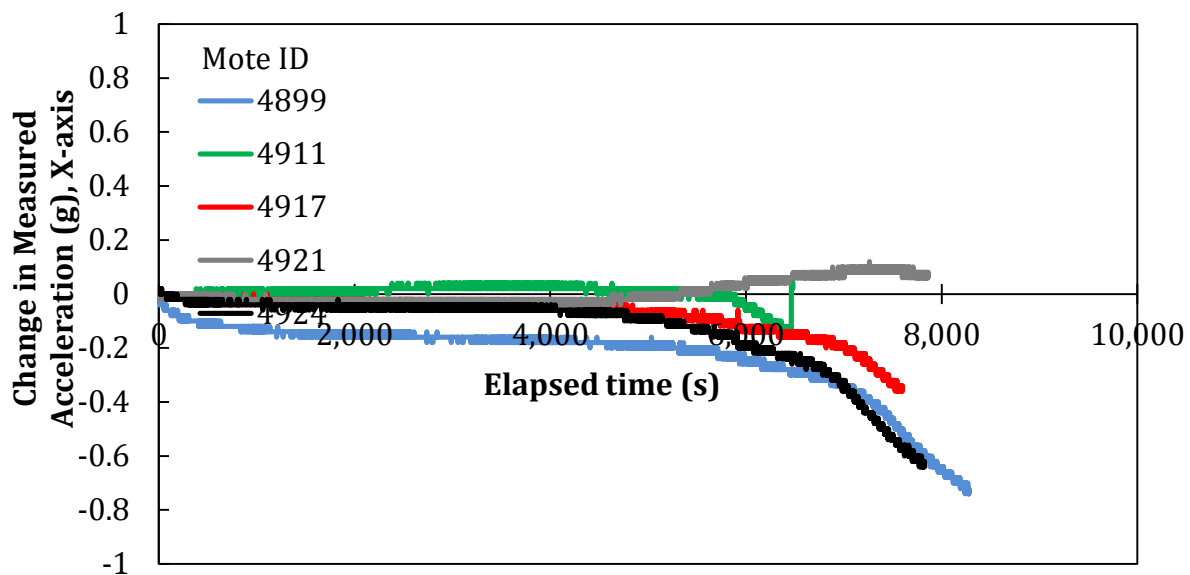


Figure 2.22 The reported change in acceleration increases over time

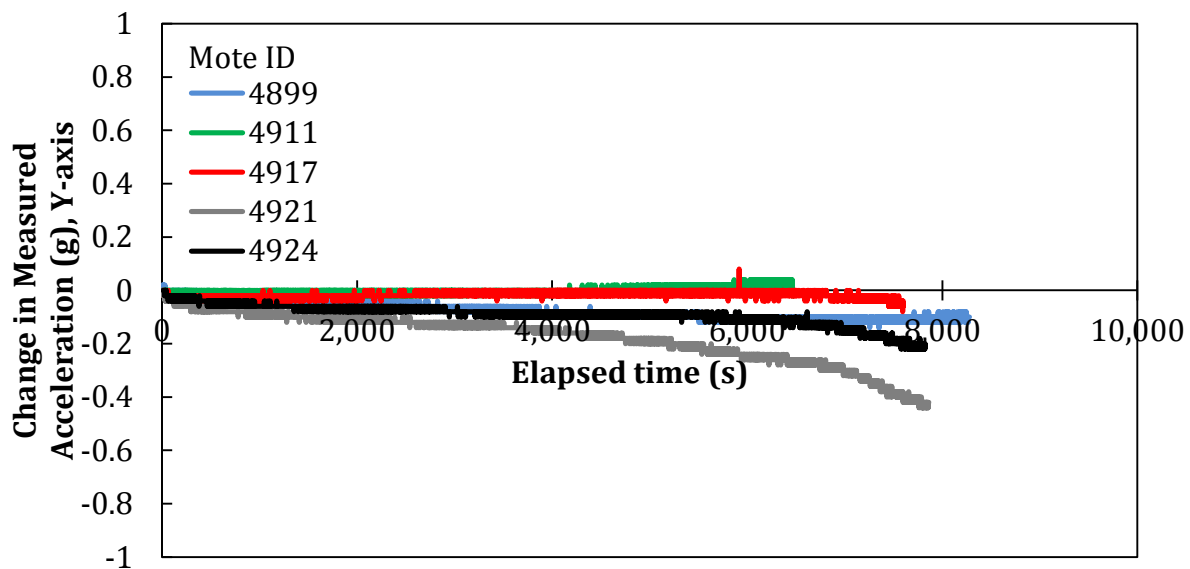


Figure 2.23 Similar to x-axis behaviour, the acceleration measured by the motes varies with time.

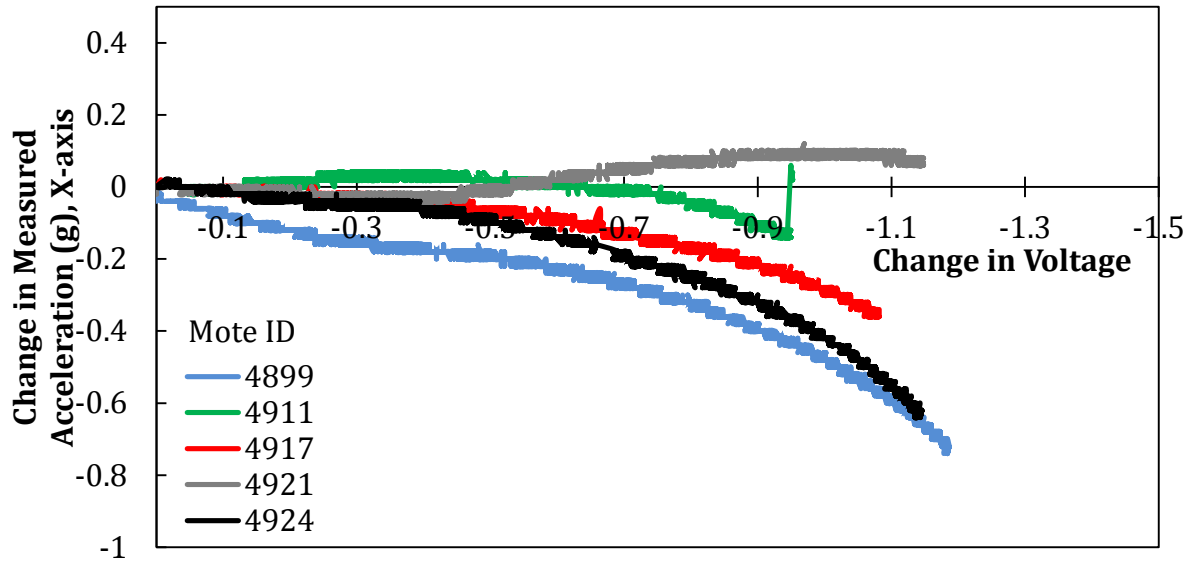


Figure 2.24 Acceleration change in the x-axis compared to the change in battery voltage

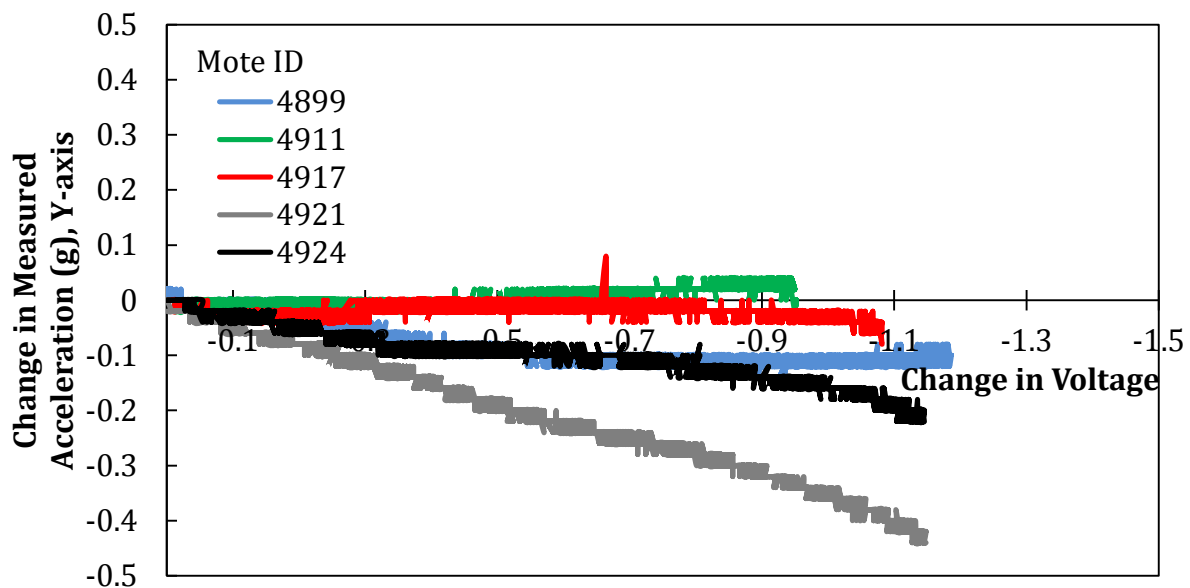


Figure 2.25 Y-axis change in acceleration compared to the change in battery voltage

The variation in the measured acceleration can be easily seen when looking more closely at the change in the acceleration with the change in voltage or the change in time. Figures 2.26 and 2.27 show the level of noise the accelerometers report. The change in

acceleration and the change in voltage appear linearly related across a small time scale (Figure 2.28). The minimum variation in the change in acceleration measured by the motes is ± 0.02 g, or 1.15 degrees tilt, although the manufacturer's literature states the minimum acceleration detectable is 0.002 g. The testing demonstrated that the motes were not able to detect tilt with enough precision, 0.114 degrees or less, to be able to provide useful information about structural movements, where the maximum allowable is tilt is 0.229 degrees.

The mote testing demonstrated the orientation of the accelerometers, the influence of the battery voltage, and captured the noise level in the acceleration measurements. The noise level of the accelerometers was too great to measure tilt of transportation structures.

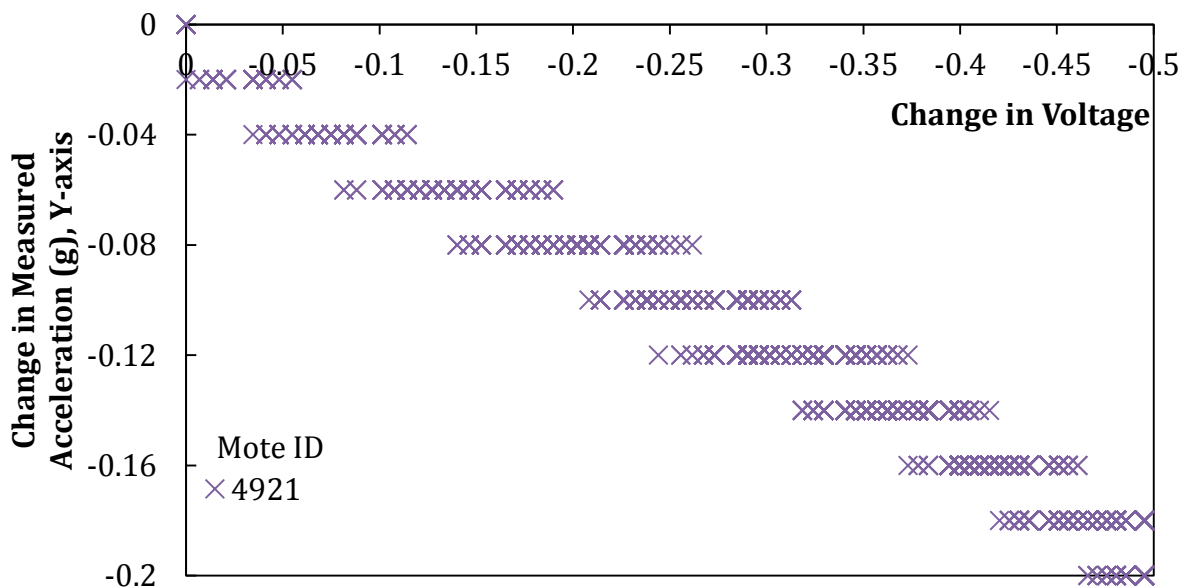


Figure 2.26 Mote 4921 change in acceleration compared to the change in voltage

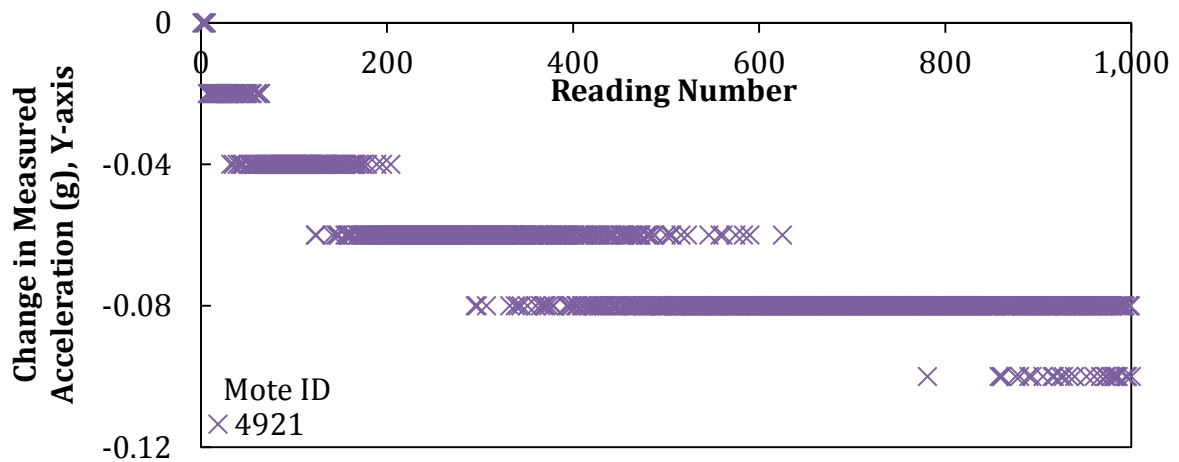


Figure 2.27 Mote 4921 acceleration noise does not vary with elapsed time nor battery voltage.

Settlement survey

Vertical and horizontal displacements of the structures measured by survey were expected to supplement the motes' tilt measurement. The motes were not finally used because testing demonstrated the noise level recorded by the accelerometers was too great, and an alternative method to study the structural movements was developed.

Survey methods to measure the deformation of a structure were discussed in Lawver et al. (2000) and Bentler et al. (2008). These cases used a fixed survey marker at a known elevation and fixed survey points on the structure. The method designed for this research attached a stainless steel scale to different faces of the structure (Figure 2.28). A plan view of the installation of the survey markers, fixed point location, and sight level location is shown in Figure 2.29. The steel survey markers were permanently installed, and a level was used to sight between the markers and at least one fixed point on the construction site. A benefit to this method of settlement measurement is that the sight

level does not have to be located in the same position each time the survey is performed as long as the fixed point and survey marker are unmoving and used consistently.

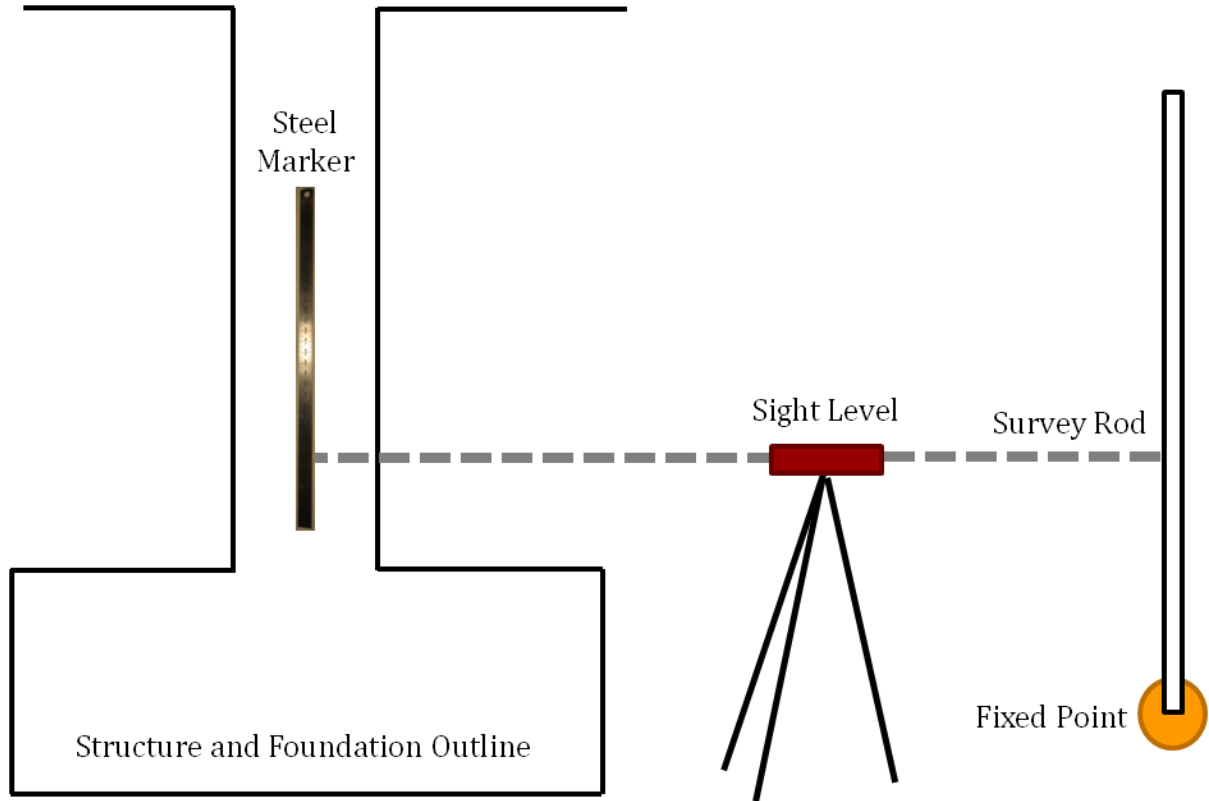


Figure 2.28 Foundation movement survey schematic, profile view

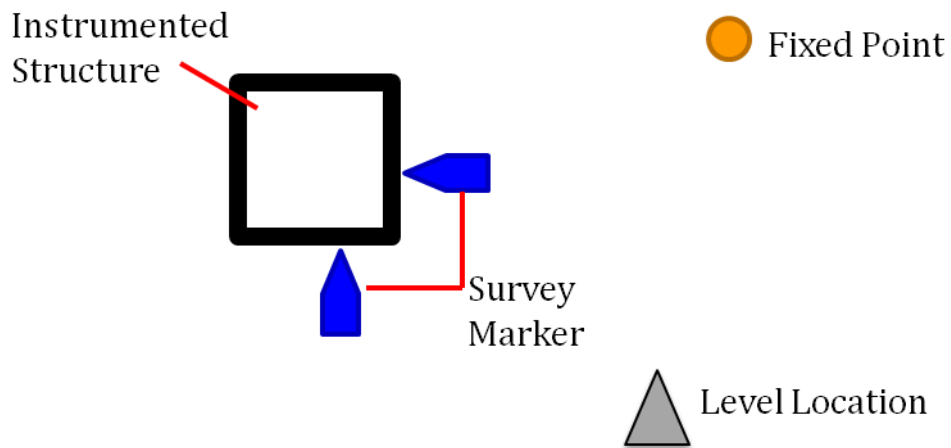


Figure 2.29 Foundation movement survey schematic, plan view

An improved survey marker was used for later displacement measurements once the gradation on the scale proved very difficult to measure using the optical level initially available. A reflective survey target (Figure 2.30) could be attached to a known location of the structure and then removed, eliminating the need to permanently install the larger steel survey marker. The reflective survey target has the additional advantage of being readable by a Total Station. The distance between the Total Station and the survey target should be between 10 and 30 meters, outside of this range the accuracy of the Total Station measurement of angle of incline and distance is decreased. The Total Station replaced the locations of the sight level during later surveys.

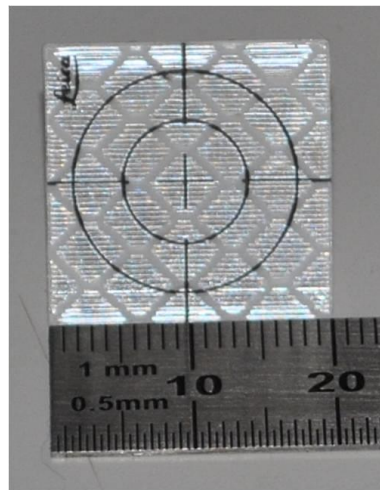


Figure 2.30 Reflective survey target

Load measurement

Direct measurement of the load transferred to the soil by pressuremeters was too expensive and are not known to be highly reliable following construction activities at the structure (Herrero et al. 2008, Rutz and Rens 2008, Sargand and Khoury 1999). Load experienced by the soil may be indirectly determined by measuring the load applied to the foundation by the structure. Measuring the strain in the structure, the dimensions of the structure, and the material properties of the structure where the strain measurements are conducted allows calculation of the load transferred by the structure into the foundation and supporting soils.

Strainmeters

Instruments selected to measure the strain were Geokon Vibrating Wire Strain Meters. The strain meters met the criteria established for field instrumentation: strain meters and associated hardware were within the \$2000 per site budget, rapid to install, and expected to perform reliably for a long period of time. The strain meter are attached to a rod of reinforcing steel placed as a “sister bar” in the column rebar cage prior to framing and pouring the concrete (Figure 2.31 and Figure 2.32). The Geokon Vibrating Wire Strain Meter also measures the temperature through a thermistor to allow temperature correction in the strain reading. A data logger is connected to the instrument cable to collect and store the captured data.

Variables used in the calculation of the strain experienced by the strainmeters are provided by the calibration sheets from the manufacturer. An example of a calibration

sheet is shown in Figure 2.33. The last four digits of the strainmeters' serial numbers identifying each instrument allow easy reference to the appropriate calibration reports.

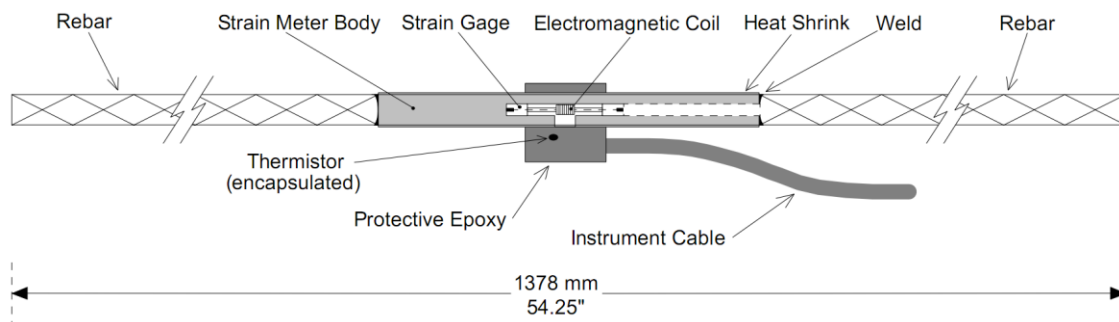


Figure 2.31 Schematic of Geokon vibrating wire strain meter and rebarment (Geokon 4911-2009)

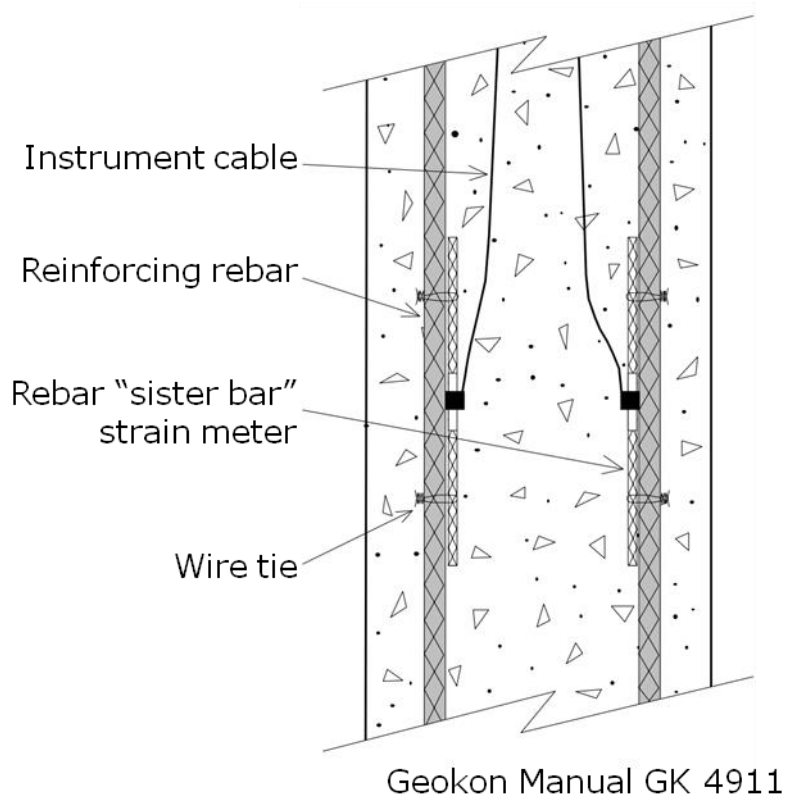


Figure 2.32 Schematic of the sister bar strain meter reinforcement in concrete (Geokon 4911-2009)

GEOKON 48 Spencer St. Lebanon, N.H. 03766 USA

Sister Bar Calibration Report

Model Number : 4911-4 Date of Calibration: March 8, 2010
 Serial Number: 1004643 Cable Length: 20 ft.
 Prestress: 35,000 psi Factory Zero Reading: 6761
 Temperature: 21.2 °C Regression Zero: 6786
 Calibration Instruction: CI-VW Rebar Technician: *Elise*

Applied Load: (pounds)	Readings				Linearity % Max.Load
	Cycle #1	Cycle #2	Average	Change	
100	6844	6841	6843		
1,500	7507	7508	7508	665	-0.22
3,000	8237	8236	8237	729	-0.18
4,500	8974	8972	8973	737	0.12
6,000	9700	9700	9700	727	0.09
100	6841				

For conversion factor, load to strain, refer to table C-2 of the Installation Manual.

Gage Factor: 0.348 microstrain/ digit (GK-401 Pos. "B")

Calculated Strain = Gage Factor(Current Reading - Zero Reading)

Note: The above calibration uses the linear regression method.

Users are advised to establish their own zero conditions.

Linearity: $((\text{Calculated Load}-\text{Applied Load})/\text{Max.Applied Load}) \times 100$ percent

The above instrument was found to be In Tolerance in all operating ranges.

The above named instrument has been calibrated by comparison with standards traceable to the NIST, in compliance with ANSI Z540-1.

This report shall not be reproduced except in full without written permission of Geokon Inc.

Figure 2.33 Manufacturer's calibration report for sister bar strain meter ID 4643

The variables input into the data logger are the gage factor (GF), gage offset (GO), zero reading (ZR), and temperature at the time of the zero reading (T_0). The data logger detects the current reading of the strain meter (R_1) and the current temperature (T_1) then calculates the apparent microstrain, $\mu\epsilon_{\text{apparent}}$, in the strain meter based on the programming inputs according to Equation 2.8 The equation which reflects the tension and compression of the structure ($\epsilon < 0$ is compression) is Equation 2.9.

$$\mu\epsilon_{\text{apparent}} = GF \cdot (ZR - R_1) + GO \quad 2.8$$

$$\mu\epsilon_{\text{apparent}} = GF \cdot (R_1 - ZR) + GO \quad 2.9$$

Microstrain calculated by Equation 2.8 was changed to reflect the sign convention in Equation 2.9 and averaged over 24-hours. To determine the actual and load related strain of the structure, the thermal coefficient of the steel, the concrete, and the composite are provided by the strain meter manufacturer (Table 2.8 - Geokon 4911-2009). The apparent strain is used in calculations to find the actual strain (Equation 2.10) and the load related strain (Equation 2.11).

Table 2.8 Thermal coefficients used to calculate strain in sister bar strain meters (Geokon 4911-2009)

	Variable	ppm/degrees Celsius
Thermal Coefficient of Concrete	K_{concrete}	10.0
Thermal Coefficient of Steel	K_{steel}	12.2
Thermal Coefficient Differential	$K = K_{\text{steel}} - K_{\text{concrete}}$	2.2

$$\mu\varepsilon_{actual} = GF * (R_1 - ZR) + K_{steel} * (T_1 - T_0) \quad 2.10$$

$$\mu\varepsilon_{load\ related} = GF * (R_1 - ZR) + K * (T_1 - T_0) \quad 2.11$$

The load experienced in the column (Q) is calculated by using the measured strain, the dimensions of the column, and the elastic modulus of the column. The information that is needed for this calculation is summarized in Table 2.9. Load experienced by the column is calculated by Equation 2.11. The stress experienced in the footing of the column due to the applied load measured by the strain meters is calculated by Equation 2.13.

Table 2.9 Information needed to calculate load and footing stress using strain meter output

	Variable	Units
Length	L	Meter
Width	W	Meter
Elastic Modulus of Concrete	E_c	meter/meter
Load	Q	Newtons
Footing Stress	q	Pascal

$$Q = \varepsilon_{load\ related} * E_C * L_{column} * W_{column} \quad 2.12$$

$$q = \frac{Q}{L_{footing} * W_{footing}} \quad 2.13$$

Modulus of elasticity of reinforced concrete

The modulus of elasticity of concrete, E_c , is the modulus of linear deformation and reflects the ability of concrete to deform under load. The modulus of elasticity is the slope of the stress-strain curve and varies significantly between different types of concrete mixtures (Galan 1990, Reinhardt et al. 1996, 2004). E_c is influenced by the strength of the cement, age of concrete, aggregate type, rate of loading, aggregate size distribution, etc. (Galan 1990, Ohtsu et al. 2003). Various moduli of elasticity are determined using the stress-strain curve (Figure 2.34). The secant modulus of elasticity of concrete is the slope of the line through the origin point and a point on the stress-strain curve at a percentage of the ultimate strength of the tested specimen. The initial tangent modulus and the tangent modulus are occasionally used as elastic modulus in design. The secant modulus of a concrete compression stress-strain curve is usually considered the modulus of elasticity of the specimen and used for structural design.

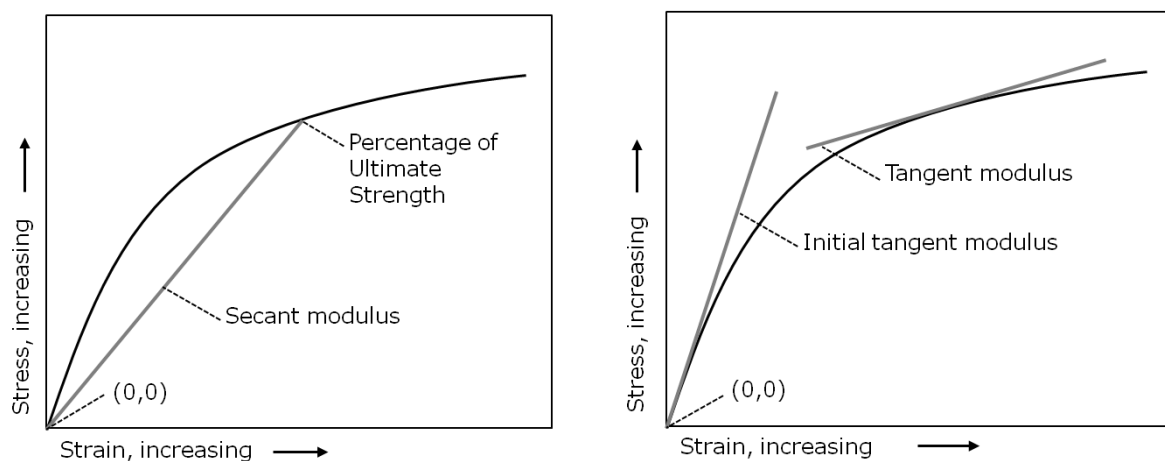


Figure 2.34 The modulus of elasticity may be evaluated several ways using the stress vs. strain diagrams

The modulus of elasticity E_c may be determined by include destructive and non-destructive methods. Destructive testing to determine E_c is standardized in ASTM-C469-10 Standard Test Method for Static Modulus of Elasticity and Poisson's Ratio of Concrete in Compression (2010). The compressive strength of the concrete is determined through destructive testing according to ASTM-C39-11 Standard Test Method for Compressive Strength of Cylindrical Concrete Specimens (2011) and AASHTO (2007, 2008) provides a method to predict the modulus of elasticity knowing the compressive strength of the concrete. Destructive testing requires compression of concrete samples to failure. Non-destructive testing may be performed on an instrumented structure in the laboratory or in field conditions itself. Non-destructive testing methods measure the properties of the concrete based on the elastic deformation of the concrete as the velocity of ultrasonic pulses (Na et al. 2001, Ohtsu et al. 2003, Pascale and DiLeo 1984, Popovics et al. 1997, Pucinotti et al. 2007).

Modulus of elasticity as a function of compressive strength

AASHTO (2007) recommend estimating E_c in a concrete as a function of the compressive strength of concrete, f'_c . Density of normal cast-in-place concrete, ρ_c , may be assumed to be 2320 kg/m³, so AASHTO (2007) predicts E_c according to Equation 2.14:

$$E_c = 4800 \text{ MPa} \sqrt{\frac{f'_c}{1 \text{ MPa}}} \quad \mathbf{2.14}$$

This equation is valid for concrete densities that vary between 1450 kg/m³ and 2450 kg/m³ and for compressive strength less than 40 MPa. ACI suggests small variation of this equation (AASHTO 2007, Al-Omaishi et al. 2009, Popovics et al. 1997):

$$E_c = 4700 \text{ MPa} \sqrt{\frac{f_{r_c}}{1 \text{ MPa}}} \quad 2.15$$

The difference between Equations 2.14 and 2.15 does not greatly influence the calculation of E_c . However, the correlation between the compressive strength is not an ideal fit. The first challenge in this correlation is the variability of concrete compression testing. ASTM C39 (2011) allows a 2.4% coefficient of variation when the concrete cylinders are cast and cured under laboratory conditions from the same batch. Mirza et al. (1979) compared the calculated and directly measured moduli of elasticity of concrete samples (Figure 2.35). The scatter of concrete specimen compressive strength and elastic modulus tests demonstrates the degree of variation encountered. The initial tangent E_c calculated based on the compressive strength of concrete cylinders and the initial tangent E_c measured directly were analyzed and Mirza et al. (1979) determined that the coefficient of variation for the 139 sample study was 7%. When the initial tangent E_c was compared to the measured secant E_c at 30% maximum stress, the coefficient of variation increased to 12%. The large coefficient of variation increases uncertainty in the calculations that depend including E_c . Loads calculated including E_c may differ as much as a factor of 2 from the actual loads, which in an unacceptably large range.

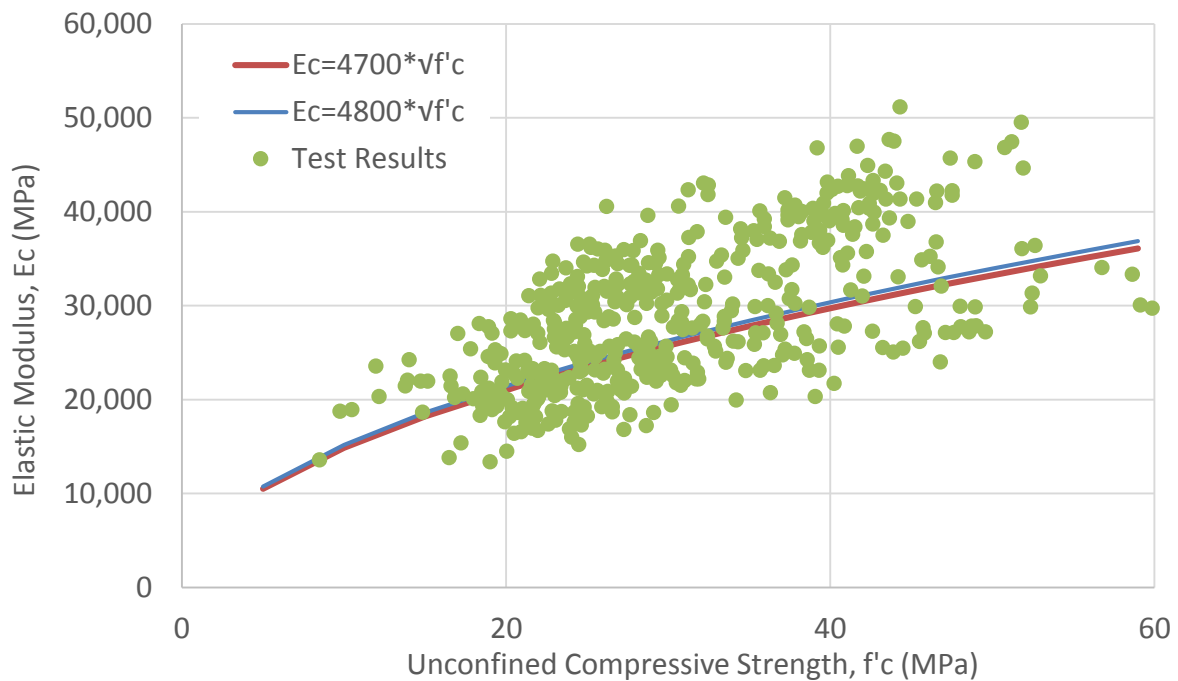


Figure 2.35 Comparison of the predicted and measured modulus of elasticity (Mirza et al. 1979)

Modulus of elasticity as a function of wave velocity

The modulus of elasticity may be determined through compression wave analysis. The velocity of the ultrasonic compression wave measures the physical properties of the medium through which it is transmitted. The ultrasonic wave velocity is influenced by the physical properties of the concrete, including concrete hardening time, water-cement ratio, aggregate content and reinforcement concentration.

The standard for conducting this test is presented in ASTM C597 Standard Test Method for Pulse Velocity through Concrete (2009). The propagation velocity is a function of the material properties, and is not influenced by the stress applied to the material (Galan 1990, Grosse and Reinhardt 2001). The wave propagation velocity (V) is

calculated as the ratio between the distance between the sensors that the stress wave traveled (x) and the transit time of the stress wave (t).

$$V = \frac{x}{t} = \sqrt{\frac{M_c}{\rho}} \quad 2.16$$

The constrained modulus M_c is then determined by solving Equation 2.16 by squaring the wave velocity V and multiplying it by the density of the concrete ρ :

$$M_c = V^2 \cdot \rho \quad 2.17$$

Finally, if the Poisson's ratio ν is known, modulus of elasticity E_c is calculated as (ASTM C597-2009, Galan 1990):

$$E_c = \frac{V^2 \rho (1 + \nu)(1 - 2\nu)}{(1 - \nu)} \quad 2.18$$

AASHTO LRFD Bridge Design Specifications (2007) state that the Poisson's ratio in concrete is assumed to be 0.25 unless otherwise determined through testing. The reinforcement within the concrete structures must be included in the evaluation of the properties of the concrete. The modulus of elasticity of steel, E_s , within the concrete is 200,000 MPa.

In a specimen made of ideal, homogeneous material, the waves generated at a point source will propagate in a radial, hemispherical shaped field away from the source (Galan 1990). The heterogeneity of concrete causes the waves to decay differently depending on the internal friction between particles, friction between the aggregate and cement, diffraction of waves at cracks, cavities, and other irregularities in the concrete

matrix. The decay, or attenuation, of the waves through concrete may be decreased by selection of an appropriate wave frequency (Galan 1990).

Frequencies of ultrasonic waves through concrete typically range from 20 kHz to 5 MHz (Galan 1990, Reinhardt et al. 2004). The range of frequencies suggested by ASTM C597 is 20 kHz to 100 kHz. The fronts of the wave pulses are not easily detected at frequencies greater than 1 MHz because the waves attenuate more rapidly than at lower frequencies due to signal scattering (ASTM C597 2009, Galan 1990). Galan (1990) states that unreinforced plain concrete and typical concrete structures “frequencies on the order of 50 kHz are adequate... [for] a good possibility of recording the fronts of the ultrasonic pulses.”

Test equipment and setup

Ultrasonic wave travel times were measured through the concrete test columns and concrete cylinders during curing, before load testing, and during load testing. Ultrasonic testing followed ASTM C597 Standard Test Method for Pulse Velocity through Concrete.

Ultrasonic waves were transmitted and received by a CNS Farnell Pundit Plus. This device measured transit times with a resolution of 0.1 μ s, which was sufficient sensitivity for evaluating the E_c . Sensors used to transmit and receive the waves had a contact surface of 50 mm diameter and frequency of 54 kHz. Coupling between sensors and concrete specimens was improved by a water-based jelly applied to the surfaces. Ultrasonic waves were transmitted through the concrete specimens, and the transit time

between the transmitter and receiver were recorded. A schematic representation of the test setup is presented in Figure 2.36.

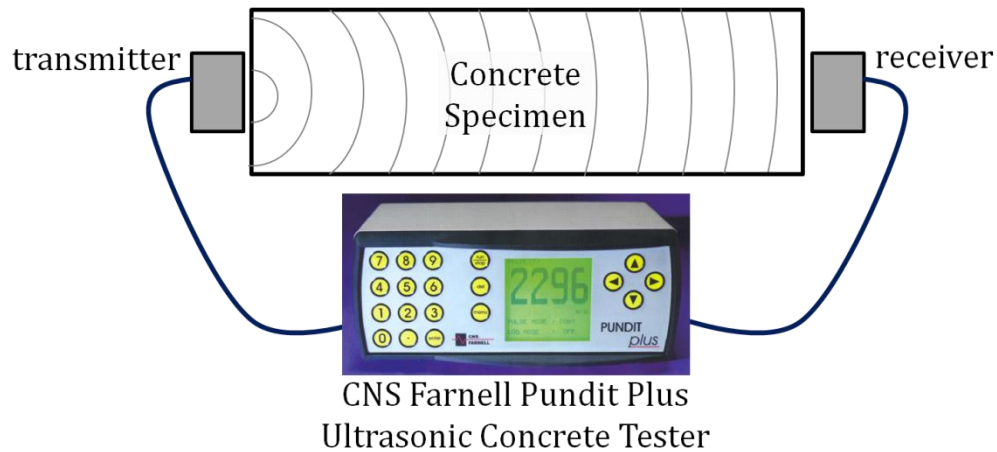


Figure 2.36 Ultrasonic wave transmission through concrete specimen

Influence of reinforcement on concrete modulus of elasticity

Steel reinforcement in concrete specimens may affect the measured compression wave velocity. The velocity of ultrasonic waves in steel may be twice the velocity of ultrasonic waves in concrete (ASTM C597 2009). ASTM C597 (2009) does not offer a methodology for correcting the ultrasonic velocity when steel cannot be avoided. Popovics et al. (1995) examined several methods measuring ultrasonic wave velocity through concrete with reinforcement and Galan (1990) presented his own test results.

Reinforcement orientation relative to the ultrasonic wave path influences the transit time of the waves through the concrete. The reinforcement has greatest effect on the wave velocity when the steel bars are parallel to the propagation direction of the ultrasonic waves. When the steel is perpendicular to the wave path, the effect of the steel

bars may be neglected if the concentration of steel is below 0.1 (ratio of reinforcing bar diameter over path length - Popovics et al. 1995).

Laboratory columns to evaluate method of load calculation

Concrete columns were designed with varying concentrations of reinforcement to evaluate the effect of steel on the modulus of elasticity. An accurate measurement of E_c is required for conversion of the strain meter measurements to load. Constants used when evaluating the test results are summarized in Table 2.10.

Table 2.10 Constants used to evaluate modulus of elasticity of test columns (ASTM C597-2009)

Test Setup, Constants		
Density, ρ	kg/m ³	2320
Poisson's Ratio, ν	unitless	0.25

The test columns were designed with a range of reinforcement to represent the extremes anticipated in practice. Column designs conformed to AASHTO specifications for reinforced concrete structures (AASHTO 2008) and the AASHTO LRFD Bridge Design specifications (AASHTO 2007). The columns met the sister bar strain meter manufacturer's development length recommendations. The final design of the two columns to be tested in the laboratory is summarized in Table 2.11. One column contained four instrumented strain meters without additional parallel reinforcement. The approximate ratio of reinforcement to gross cross sectional area of the column for the minimally reinforced column was 0.2%. The second column contained twelve

bundles of 2 #10 reinforcement as well as the instrumentation and achieved a 6% reinforcement ratio. Two stirrups of #4 reinforcement were used in both columns, and each column had four loops of #4 reinforcement to be used as lifting points for the reinforcement cage and the concrete column. The stirrups and lifting loops were not included in the calculation of the reinforcement ratio.

Table 2.11 Laboratory test column design details

Column Name		Laboratory Column Minimum Reinforcement	Laboratory Column Maximum Reinforcement
Cross sectional area of column	cm ²	2787.1	2787.1
Minimum concrete cover of reinforcement	Cm	5	5
#4 sister bar strain meter reinforcement	quantity	4	4
#10 reinforcement	quantity	0	24
Length of Steel	Cm	66	66
Cross sectional area of steel	cm ²	5.16	169.03
Reinforcement Ratio	%	0.19%	6.06%

The reinforcement cages for the columns were constructed and then the sister bar strainmeters were installed. This order of operations allowed the installation of the strainmeters to be practiced in a controlled setting. Each strainmeter was attached to the reinforcement cage at two points. Figure 2.37 is a diagram of the designed cross section of the columns, including the name of each of the strainmeters installed in the columns. The completed reinforcement cage was lifted by the loops and placed in the formwork (Figure 2.38).

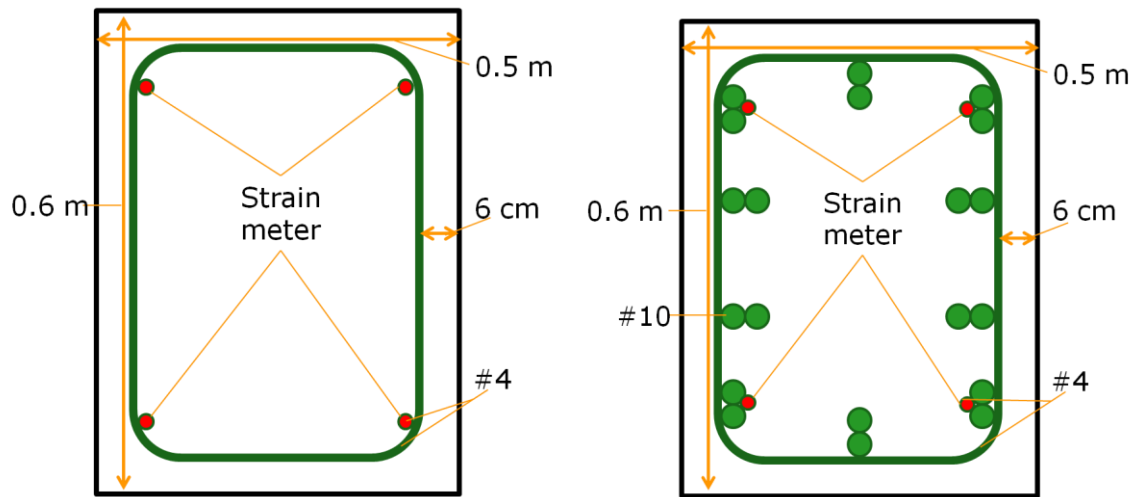


Figure 2.37 Reinforcement cage design of laboratory test columns (minimum reinforcement pictured on left, maximum reinforcement pictured on right)



Figure 2.38 Completed cage of maximum reinforcement column placed into formwork

Laboratory column formwork and concrete

Concrete formwork for the columns was designed to be efficient, compact and reduce labor. To reduce the material needed for construction of the column formwork, two column forms were constructed end to end. The connected form reduced the footprint of the formwork and provided easy access to the form for the ready-mix concrete truck driver for delivery of the wet concrete. Reduction of the lateral loads experienced by the formwork was achieved by orienting the column on edge during the pour and curing. This orientation used the formwork to create the surfaces of the column that would be loaded to significantly reduce the finishing labor needed and better controls the final shape of the columns.

The wooden formwork was constructed with 1.2 cm thick plywood and 2"x4" lumber studs. The plywood formed the sides and bottom of the form, and also created the barrier that separated the columns end to end (Figures 2.39 and 2.40). Reinforcement of the plywood was achieved using 2"x4" boards along the edges and at the corners of the formwork. To further increase the stability of the formwork, 2"x4" boards were placed on the sides of the formwork at six even intervals along the length and 2 even intervals along the width. Blocking was attached at four even intervals at the top of the form to provide stability during pouring and for use in stabilizing the rebar cage and lifting handles prior to the concrete curing. The sides and bottom of the form were initially connected using nails, and the reinforcing lumber studs were connected using wood screws. Additional reinforcement was installed at locations expected to be in shear.



Figure 2.39 Completed formwork with reinforcement chairs, before the reinforcement cage is in place



Figure 2.40 Exterior of column formwork shows supports along the length and width and connections in shear

The completed formwork was caulked to prevent any seeping of wet concrete. A high gloss latex paint was applied to the inside of the form to seal the plywood and ease the form release oil application. The plywood barrier between the columns was placed into the form after painting, and was held in place using angle brackets. The completed formwork was transported to the designated laboratory space before inserting the rebar cages and pouring concrete. The formwork was placed on top of a heavy plastic sheet to protect the laboratory and to enclose the concrete in plastic during curing.

Concrete was ordered from a local ready-mix supplier. An electric, hand held concrete vibrator was used during concrete placement to improve consolidation and eliminate irregularities in the concrete around the reinforcement. The concrete mix design was performed by the ready-mix supplier to conform to the AASHTO (2008) concrete mix specifications for concrete transportation structure columns.

Testing was conducted on the concrete during placement. Six concrete cylinders were cast according to ASTM C31 (2010). A slump test and an air content test were performed according to standards, as well. Once the concrete was placed, the entire form was wrapped in heavy plastic and the concrete columns were undisturbed for 28 days.

After curing, the concrete columns were removed from the formwork. The exposed columns were measured and a grid was drawn over the columns' faces (Figure 2.41). The grid lines were spaced at intervals of 10.16 cm. The location of the reinforcement within the finished columns can be approximated by the grid coordinates on the top face of the column (Table 2.12).

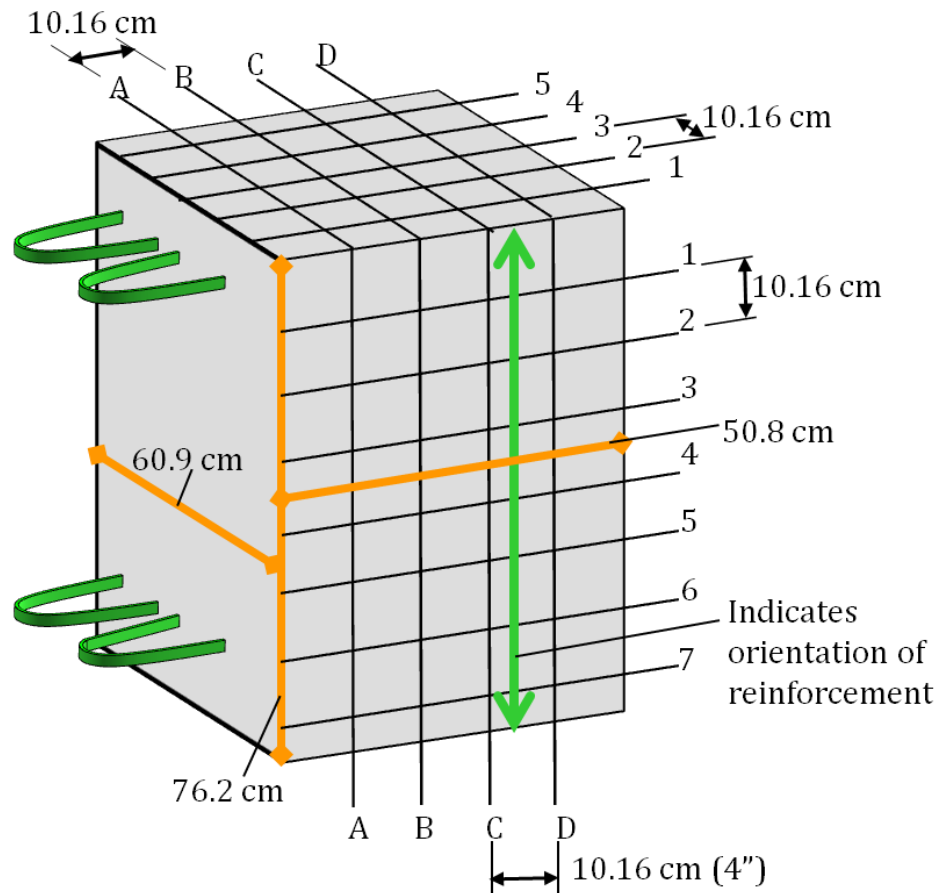


Figure 2.41 Minimum and maximum reinforcement columns' dimensions, grid, and reinforcement orientation

Table 2.12 Strainmeter identification and grid location in test columns

Minimum Reinforcement	
Strainmeter ID	Location
1539	D, 5
1542	A, 5
1545	A, 1
1546	D, 1
Maximum Reinforcement	
Strainmeter ID	Location
1541	D, 5
1543	A, 5
1544	D, 1
5863	A, 1

Modulus of elasticity of reinforced concrete evaluation

Ultrasonic velocity measurements were taken parallel and perpendicular to the reinforcement of the columns (Figures 2.42 and 2.43). Measurements were taken with the transmitter at the same coordinate location as the receiver on the opposite face. E_c was calculated at each point of the grid. A projection of the modulus of elasticity values is shown on each column with minimum (0.2%) reinforcement (Figures 2.44 and 2.45) and maximum (6%) reinforcement (Figures 2.46 and 2.46).

The elastic modulus E_c perpendicular to the reinforcement was 35,000 MPa to 40,000 MPa in both columns. The variation at grid location (A, 7) in the minimum reinforcement and maximum reinforcement columns may have resulted from reduced finishing at the corner or nearness of reinforcement stirrups to the surface. The elastic modulus E_c of the minimum reinforcement column did not vary outside the 35,000 MPa to 40,000 MPa range when it was evaluated parallel to the reinforcement. The maximum reinforcement column's E_c ranged from 25,000 MPa to 50,000 MPa when E_c was evaluated by ultrasonic waves parallel to the reinforcement. The average E_c perpendicular to the reinforcement for the minimally reinforced column was 37069 MPa and 38,055 MPa for the maximum reinforcement column.

The elastic modulus E_c measured perpendicular to the reinforcement appears uninfluenced by the reinforcement. E_c testing was completed prior to relocating the columns to the loading machine. During loading, E_c measurements were taken at (A, 4), (B, 4), (C, 4), and (D, 4) perpendicular to the reinforcement.

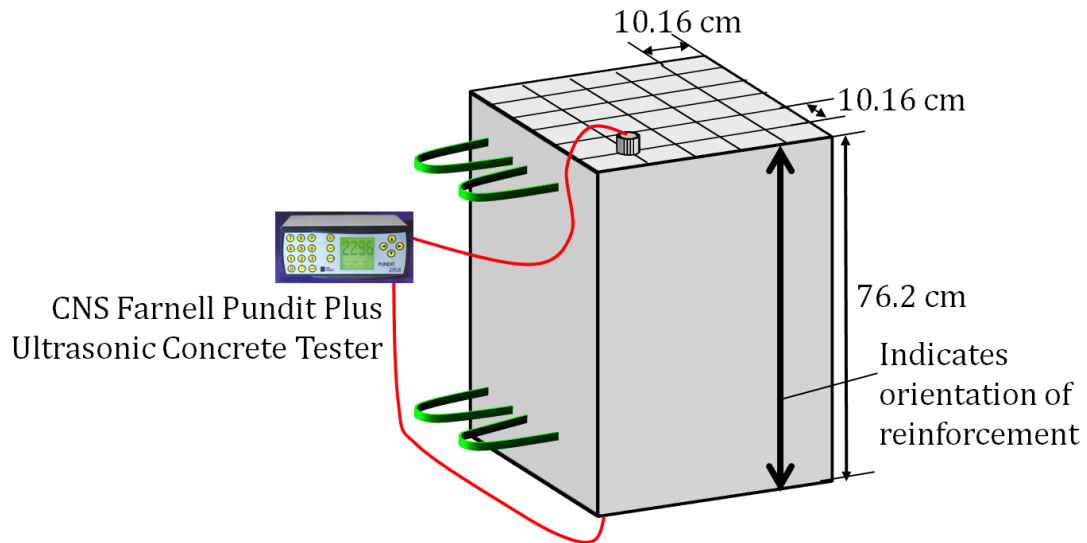


Figure 2.42 Ultrasonic wave transit time, direction of wave propagation is parallel to reinforcement

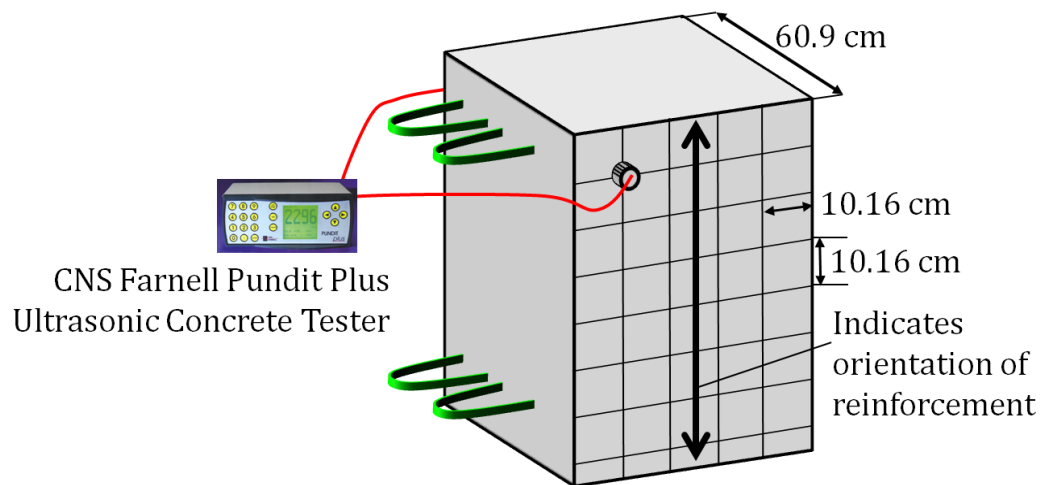


Figure 2.43 Ultrasonic wave transit time, direction of wave propagation is perpendicular to reinforcement

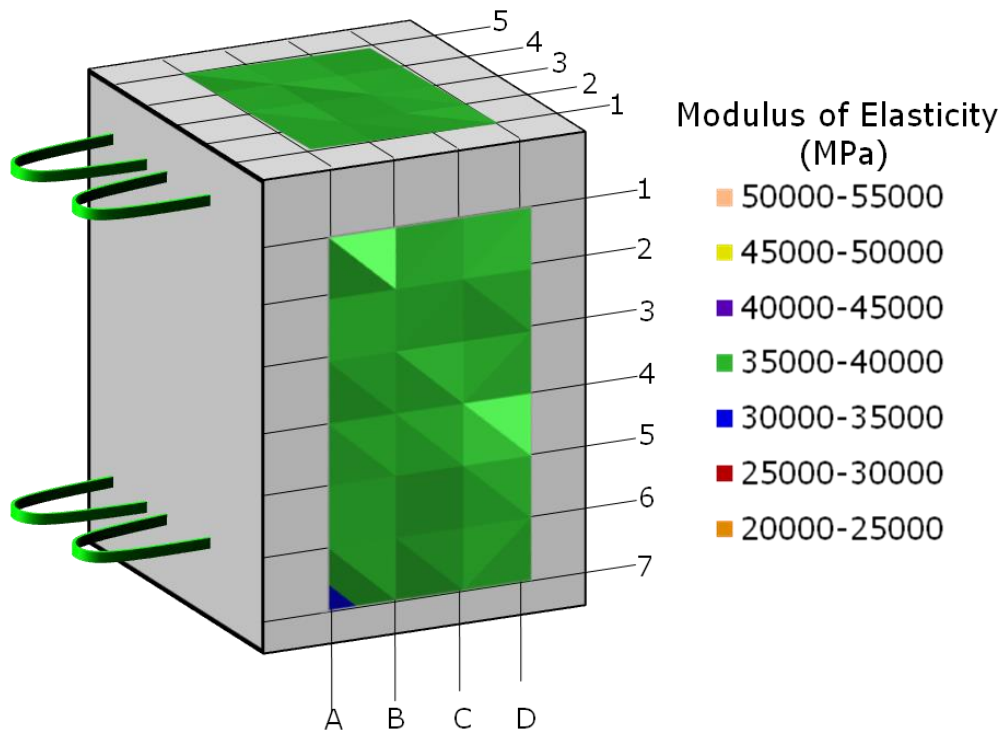


Figure 2.44 0.2% reinforcement column projection of modulus of elasticity

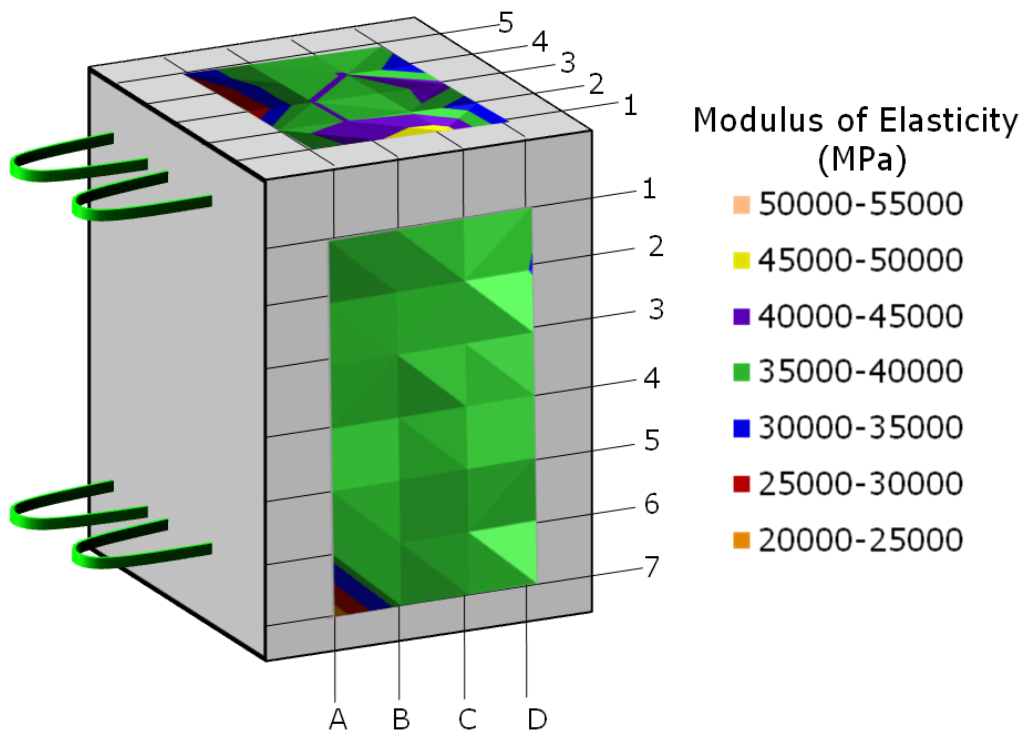


Figure 2.45 6% reinforcement column projection of modulus of elasticity

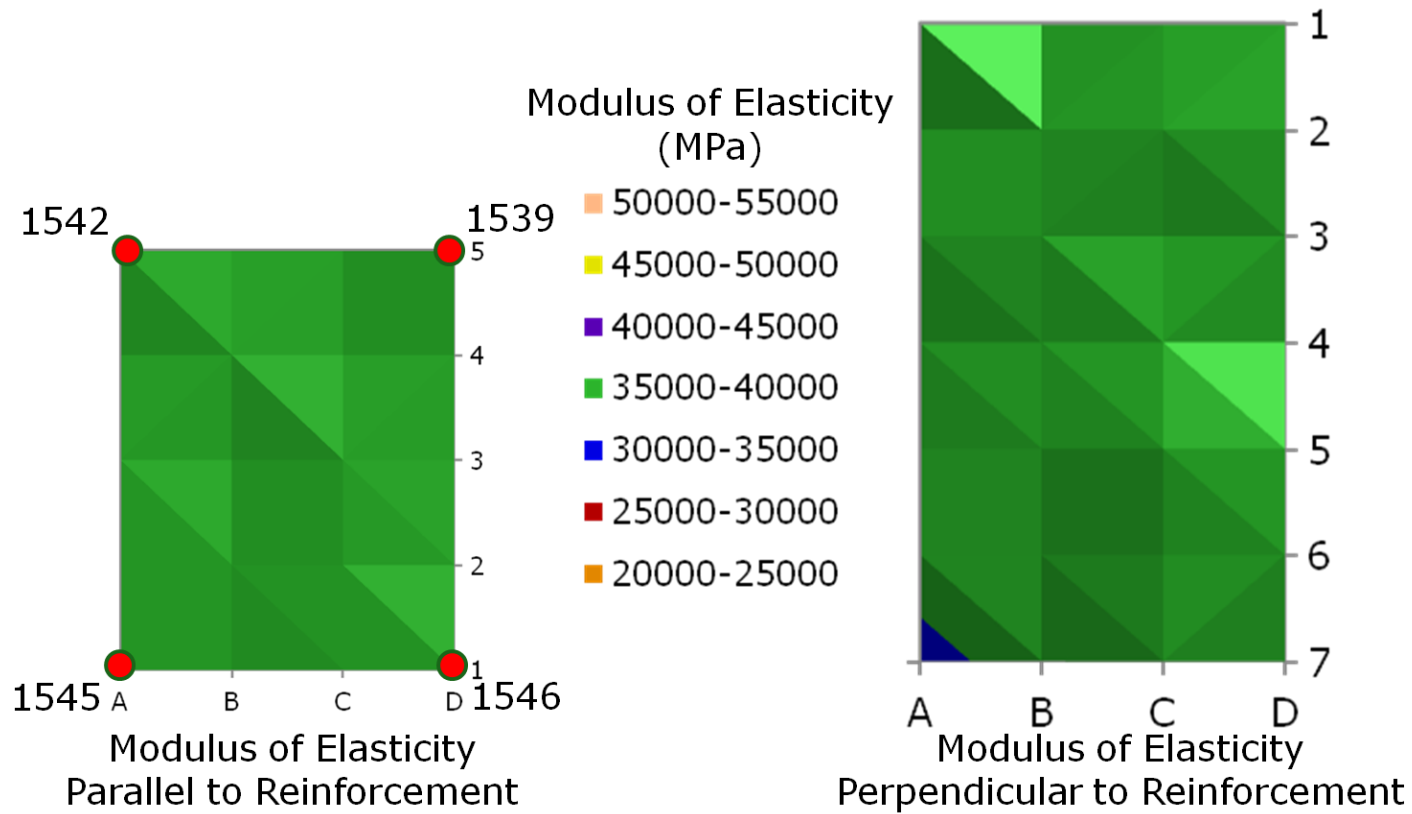


Figure 2.46 Modulus of elasticity at each point on the surface grid of the minimum (0.2%) reinforcement column

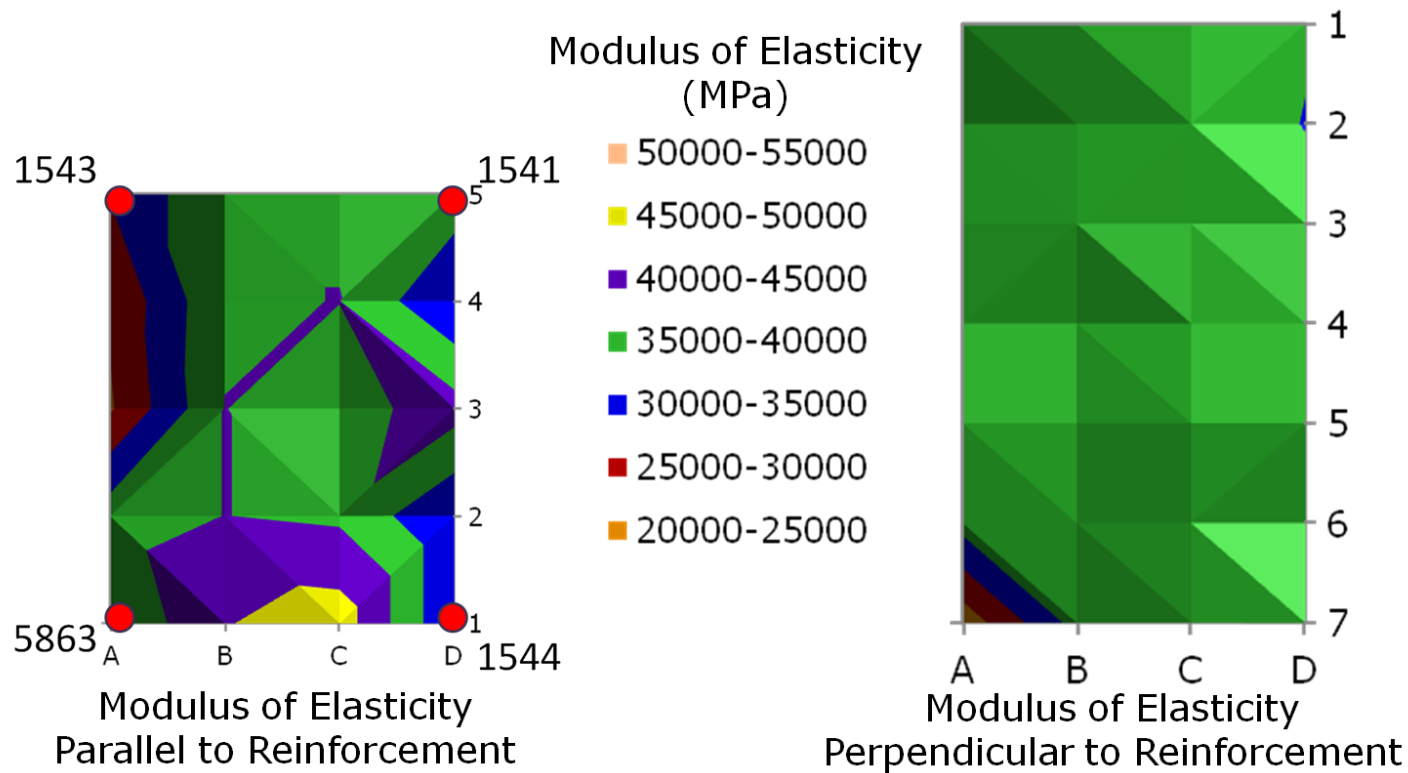


Figure 2.47 Modulus of elasticity at each point on the surface grid of the maximum (6%) reinforcement column

Compression load testing of laboratory columns

The instrumented columns were loaded in compression by the MTS Corp. 1000TE “One Million Pound” machine. The load cell was calibrated to 4,448,221 N (1,000 kip.) The area of the top load cell of this machine was less than the area of the instrumented columns’ faces to be loaded. An un-instrumented concrete block of the same dimensions as the column was placed between the load cell and the instrumented column to distribute the load evenly across the instrumented column’s face. No object was placed between the load distribution column and the instrumented column. This set up was used for both columns. Figure 2.48 is a schematic of the set up for load application.

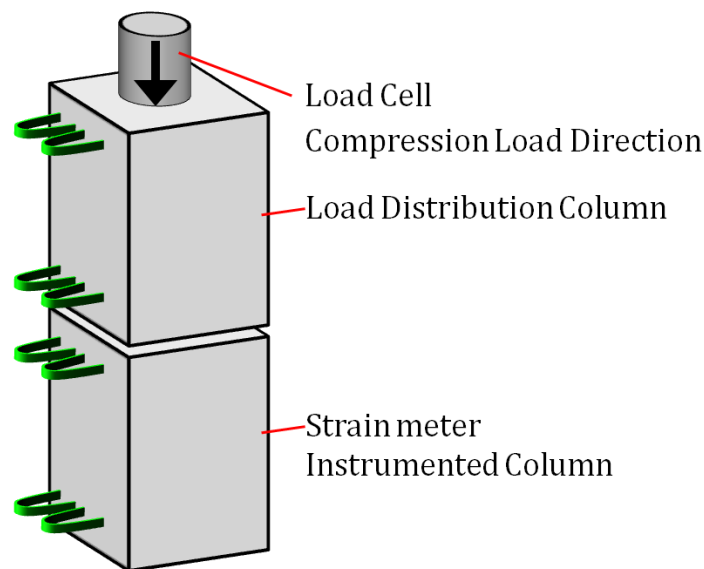


Figure 2.48 Column configuration during compressive loading of instrumented columns

The compressive load schedule testing the columns included two loading and unloading cycles. The first loading and unloading cycle measured the sensitivity of the strainmeters to small loads. The second loading and unloading cycle applied large loads

(greater than 124,550 N) to the column. The strainmeters measured the strain in the concrete columns once every 10 seconds during loading and unloading in the laboratory. Each load step was held for 3 minutes once the load cell readings stabilized. The load calculated using the strainmeters does not include the additional weight of the load distribution column. The minimum reinforcement column was load tested 45 days after concrete placement, and the maximum reinforcement column was load tested at 49 days after concrete placement.

E_c was evaluated at each scheduled load step. The ultrasonic wave velocity through the column was measured perpendicular to the reinforcement at (A, 4), (B, 4), (C, 4), and (D, 4). Equation 2.18 was used to calculate the modulus of elasticity at each location. Table 2.13 provides the scheduled load for the columns, and the actual load applied to the columns. Variations from the schedule arose due to the difficulty of controlling the amount load applied below 125,000 N.

Table 2.13 Load schedule for compressive loading of the instrumented columns

Scheduled Load	Applied Load, Measured by Load Cell, Minimum Reinforcement Column	Applied Load, Measured by Load Cell, Maximum Reinforcement Column
<i>N</i>	<i>N</i>	<i>N</i>
0	0	0
2224	2278	2031
4448	4481	4337
8896	9261	8571
17793	17913	17330
31138	31658	30761
62275	62856	63066
124550	118915	123360
62275	NA ¹	62890
31138	36956	30738
17793	20257	17762
8896	8895	8898
4448	5472	4513
2224	2289	2313
0	0	0
124550	124550	124550
266893	266893	266893
533787	533787	533787
1067573	1067573	1067573
533787	533787	533787
266893	266893	266893
124550	124550	124550
0	0	0

NA¹ Load was not constant during this load step.

Minimum reinforcement column modulus of elasticity results

E_c at each load step of the 0.2% reinforcement column is shown in Figure 2.49. A change in the modulus of elasticity is more distinct when the values are separated by small or large loading cycle and designated as having been obtained during loading or unloading of the column (Figure 2.50 and 2.51). The modulus of elasticity E_c is greatest during loading, but a maximum E_c did not occur during application of the greatest load.

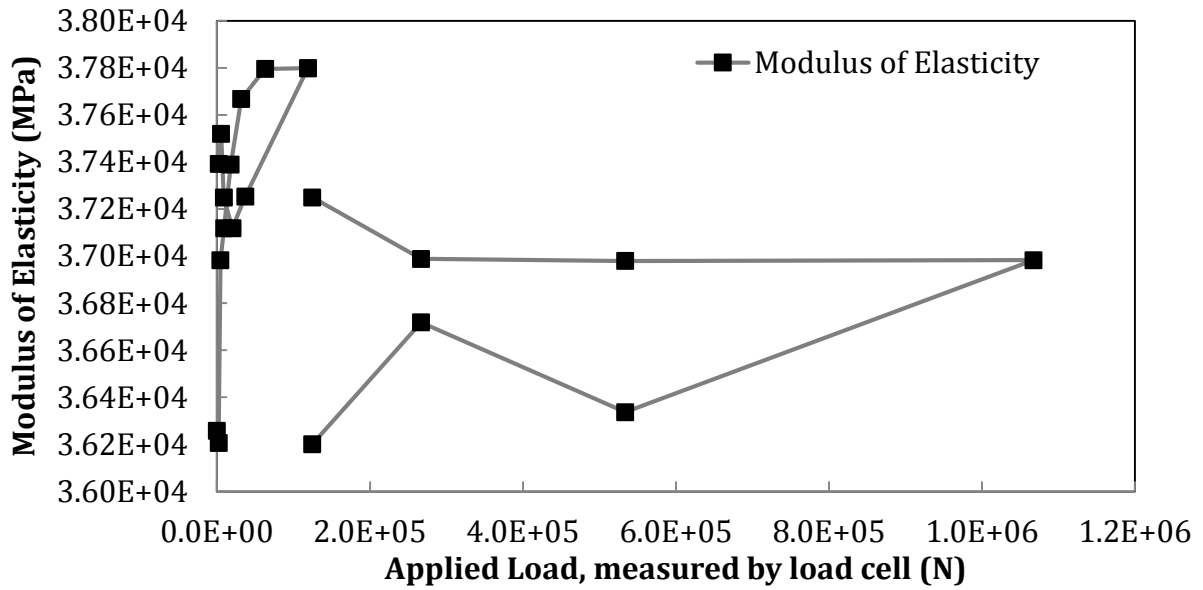


Figure 2.49 Minimum reinforcement column, modulus of elasticity variations with applied load

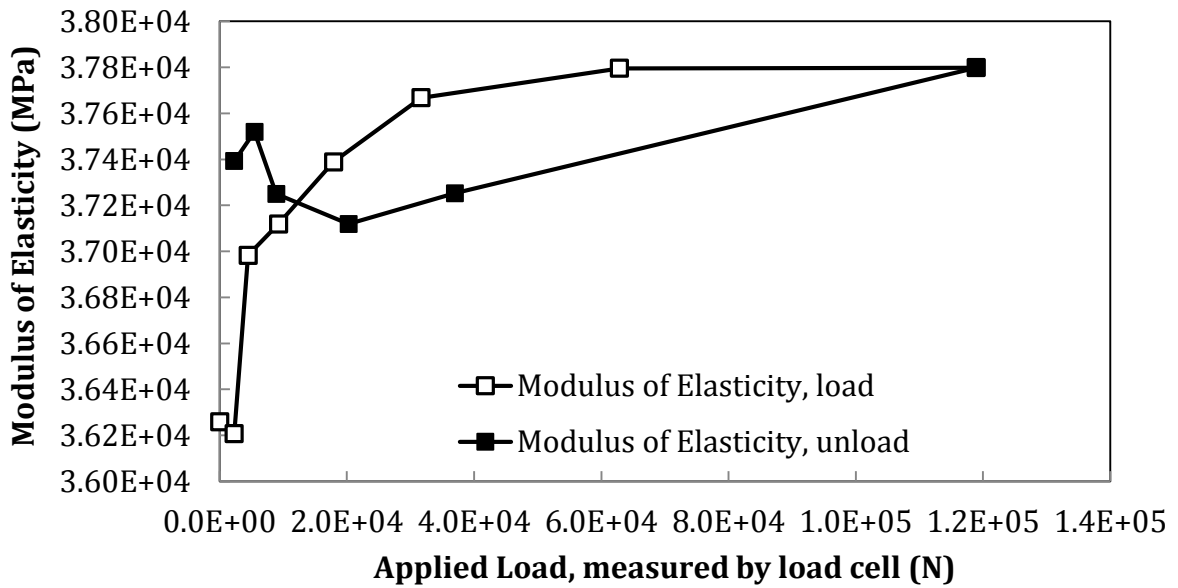


Figure 2.50 Minimum reinforcement column, modulus of elasticity variation during small load and unload cycle

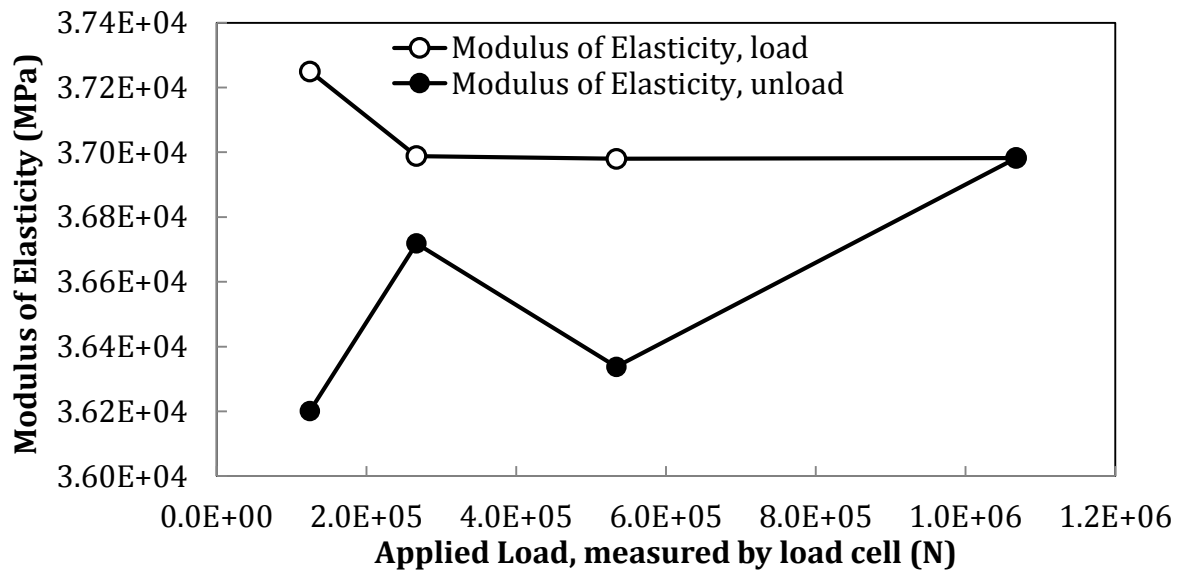


Figure 2.51 Minimum reinforcement column, modulus of elasticity variation during large load and unload cycle

Minimum reinforcement column load cycle results

The load test results of the minimum reinforcement column are presented in Table 2.14. E_c used to calculate the load recorded by the strainmeters is the average E_c before compression loading and not the E_c at that load step. The increase and decrease of the loads of each strainmeter through the loading and unloading cycles are compared to the applied load reported by the load cell in Figure 2.52. An ideal relationship between the strainmeter and load cell would agree 1:1, and the graph would track along the applied load line in Figure 2.52. The load cycle of small loads, less than 124.6 kN, shows a greater deviation from the 1:1 ideal than the large loads (Figure 2.53 and 2.54). Figure 2.55 shows the variation between loading and unloading behavior observed over 124,550 N. Each strainmeter recorded a greater load during unloading than during loading for the same actual, load cell measured, applied load. Three sensors, 1539, 1545,

and 1546, under-predicted the load applied to the column. Strainmeter 1542 under-predicted the load during load increase, but over-predicted the applied load as the column was unloaded.

Table 2.14 Minimum reinforcement column load test results

Scheduled Load	Applied Load, Measured by Load Cell	Applied load measured by strainmeters*				Average Modulus of Elasticity
		Strainmeter Number				
		1539	1542	1545	1546	
<i>N</i>	<i>N</i>	<i>N</i>	<i>N</i>	<i>N</i>	<i>N</i>	<i>MPa</i>
0	0	0	0	0	0	36258
2224	2278	3379	3866	1690	3051	36207
4448	4481	5326	5730	3467	5105	36983
8896	9261	7370	6210	3841	8005	37119
17793	17913	12905	11686	7908	13434	37389
31138	31658	22869	22950	17690	22017	37668
62275	62856	36937	43403	32341	33507	37795
124550	118915	67360	90465	68870	62868	37798
62275	NA ¹	NA ¹	NA ¹	NA ¹	NA ¹	NA ²
31138	36956	28045	32604	24976	23879	37252
17793	20257	18024	18965	19246	17146	37119
8896	8895	15213	12754	14668	12458	37250
4448	5472	13990	10197	13089	11102	37520
2224	2289	12112	9131	12001	8632	37392
0	0	12061	10394	12149	7982	NA ²
124550	124550	78620	111996	81460	60001	37250
266893	266893	159041	241101	168795	131312	36988
533787	533787	301693	480979	363008	289048	36980
1067573	1067573	610864	1014023	753343	631292	36983
533787	533787	342673	576432	423540	338000	36337
266893	266893	205498	344717	247054	185411	36718
124550	124550	135531	215330	151220	117868	36201
0	0	50757	95056	77864	65327	NA ²

NA¹ Load was not constant during this load step.

NA² Ultrasonic wave velocity was not measured during the application of load.

* E_c used to calculate each strainmeter load is the E_c average perpendicular to the reinforcement calculated prior to loading. E_c = 37069 MPa

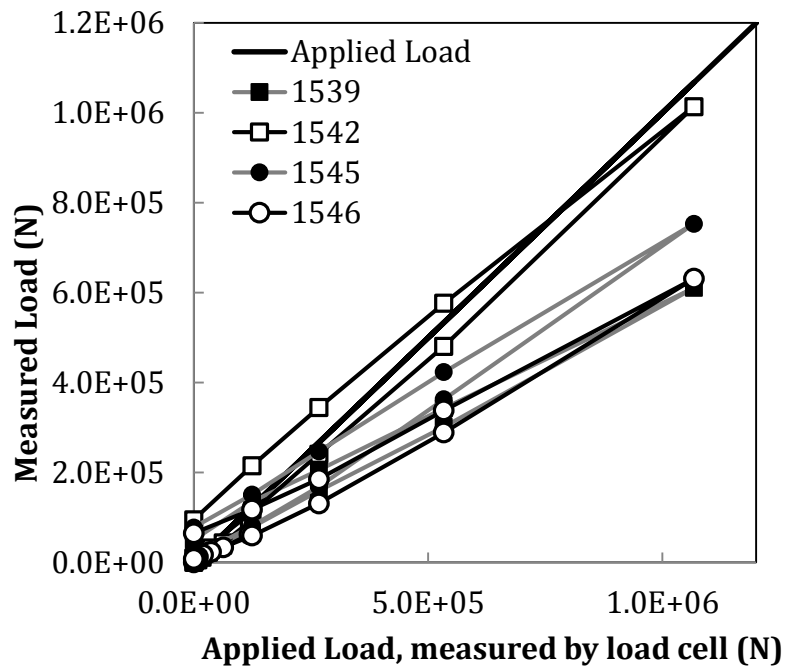


Figure 2.52 All compressive loads applied to the minimum reinforcement column

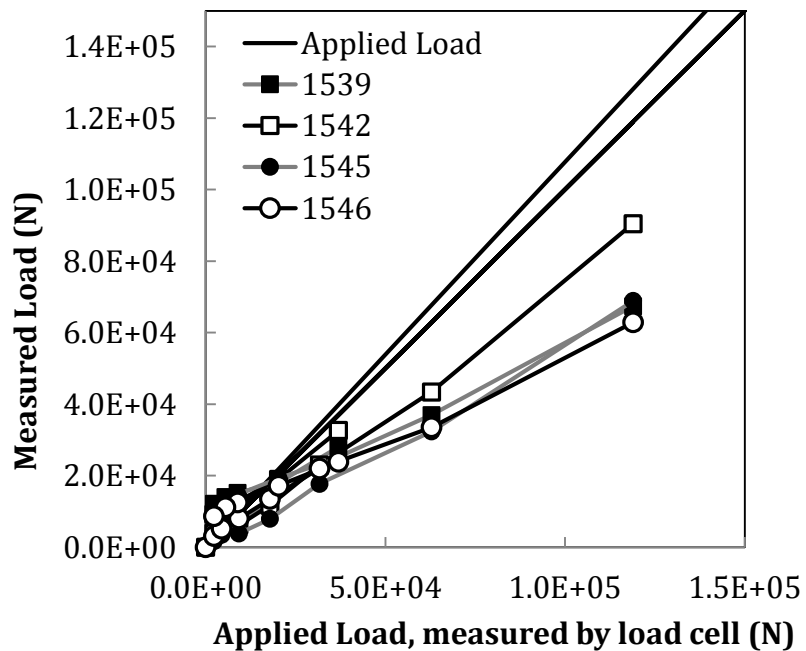


Figure 2.53 Small loads applied to the minimum reinforcement column

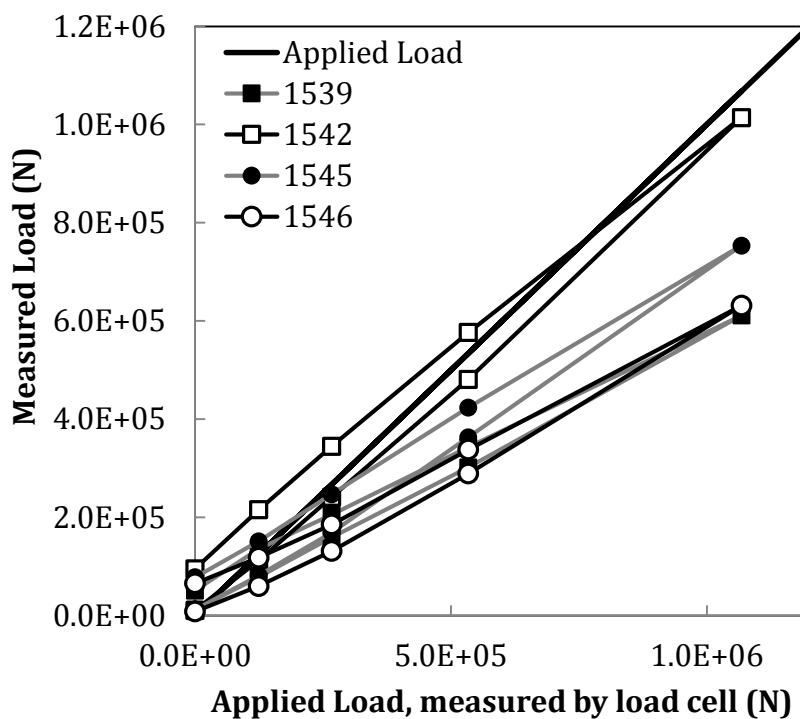


Figure 2.54 Large loads applied to the minimum reinforcement column

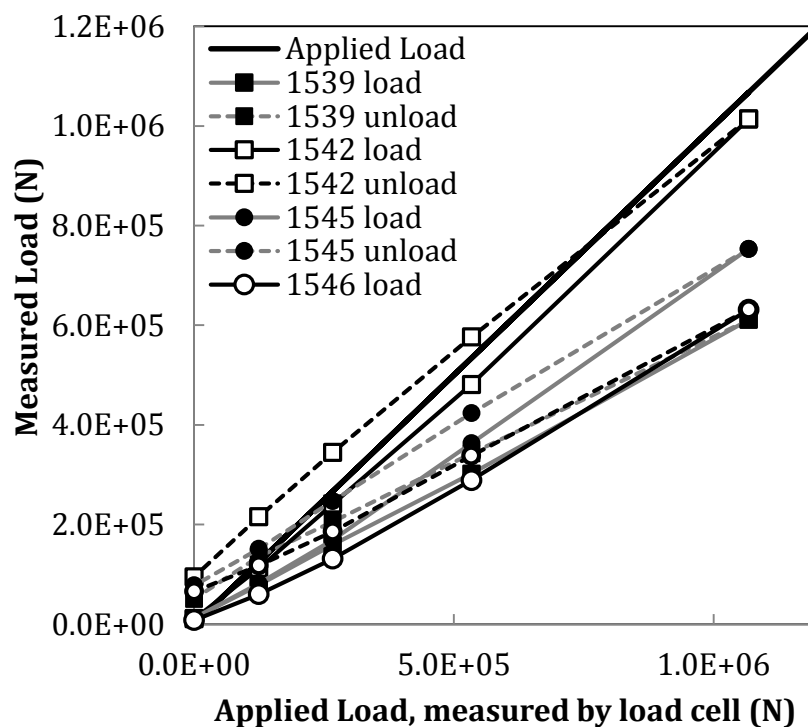


Figure 2.55 Loading and unloading the minimum reinforcement column

The discrepancies between each of the strainmeters and the load cell may be explained by hysteresis. The change may be occurring in the concrete and steel, as indicated by the variation of the modulus of elasticity E_c , or may be occurring in the load cell itself. The load recorded by the strainmeters may also vary due to the imperfect contact between the load distribution column and the instrumented column.

Maximum reinforcement column modulus of elasticity results

The modulus of elasticity E_c at each load step of the 6% reinforcement column is shown in Figure 2.56. A change in the E_c is more distinct when the values are separated by loading cycle and designated as having been obtained during loading or unloading of the column (Figures 2.57 and 2.58). The modulus of elasticity E_c is greatest during unloading. A greater variation in the E_c occurred during the small load cycle than during the large load cycle, and the maximum E_c occurred during small load cycle unloading.

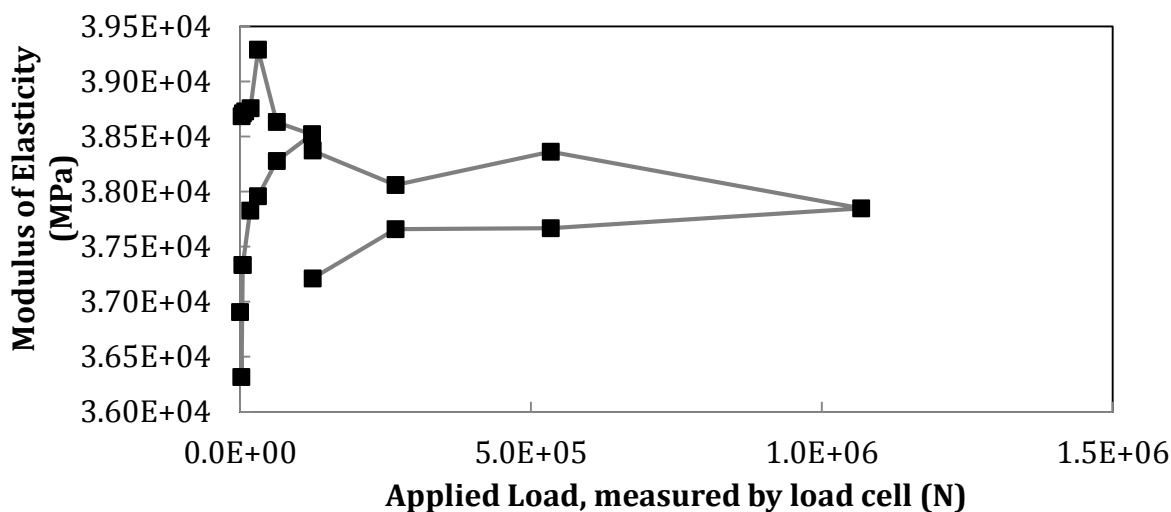


Figure 2.56 Maximum reinforcement column, modulus of elasticity variations with all applied loads

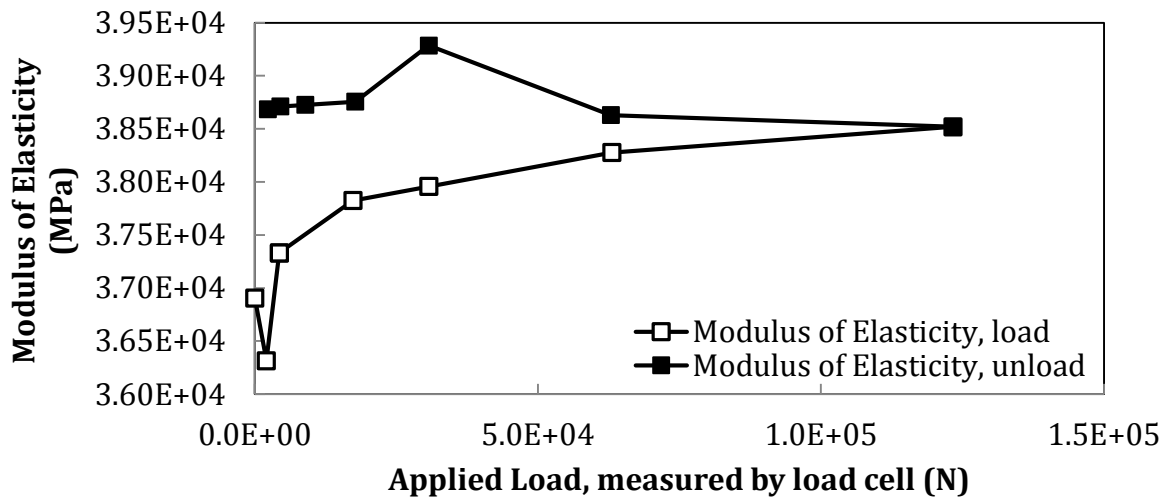


Figure 2.57 Maximum reinforcement column, modulus of elasticity variation during small load and unload cycle

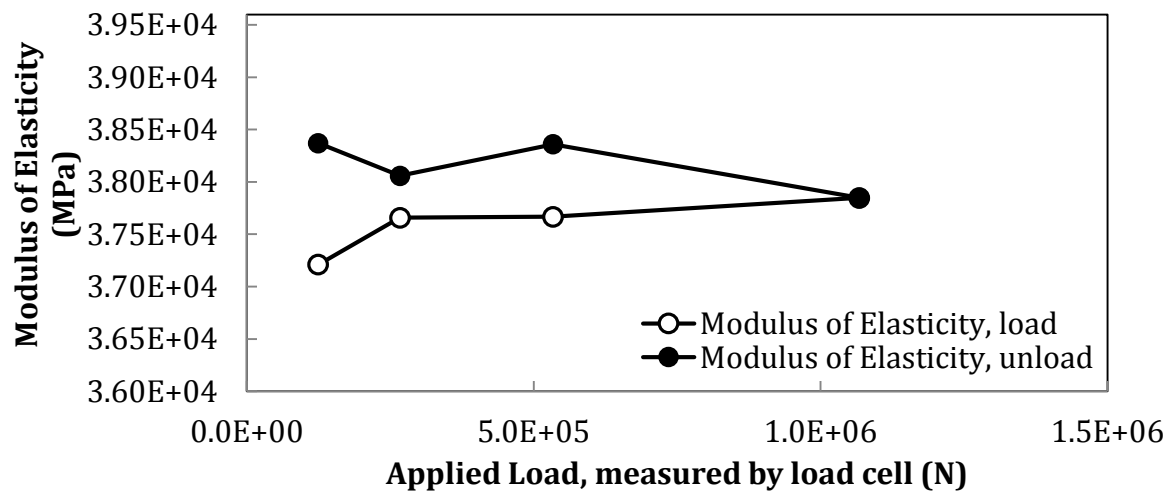


Figure 2.58 Maximum reinforcement column, modulus of elasticity variation during large load and unload cycle

Maximum reinforcement column load cycle results

The load test results of the maximum reinforcement column are presented in Table 2.15. The modulus of elasticity E_c used to calculate the load of the strainmeters is the average modulus before the loading and unloading cycles and not the modulus

specific to the load step. The increase and decrease of the loads of each strainmeter through the loading and unloading cycles, called measured load, is compared to the load reported by the load cell in Figure 2.59. An ideal relationship between the strainmeter and the load cell would perfectly match at the 1:1 line. The loading and unloading cycle of loads less than 124,550 N shows greater deviation from the 1:1 ideal line than the large loads (Figures 2.60 and 2.61). During the cycle of loading and unloading loads in excess of 124,550 N, the range of loads recorded by the strainmeters was less than during the small load cycle.

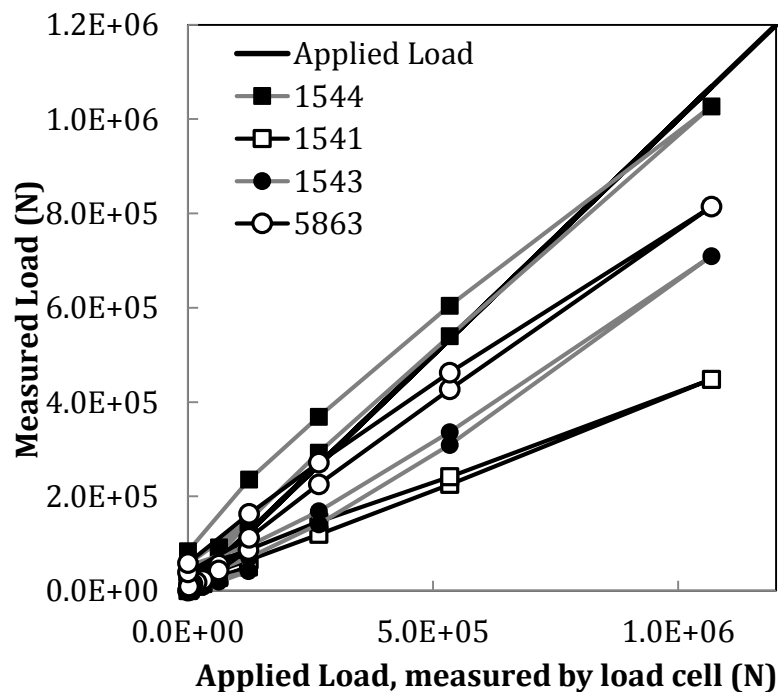


Figure 2.59 All compressive loads applied to the maximum reinforcement column

Table 2.15 Maximum reinforcement column load test results

Scheduled Load	Applied Load, Measured by Load Cell	Applied load measured by strainmeters*				Average Modulus of Elasticity
		Strainmeter				
		1541	1543	1544	5863	
<i>N</i>	<i>N</i>	<i>N</i>	<i>N</i>	<i>N</i>	<i>N</i>	<i>MPa</i>
0	0	0	0	0	0	36905
2224	2031	987	1268	3355	1192	36314
4448	4337	3532	1172	5364	2161	37331
8896	8571	6113	3451	11776	7842	NA ¹
17793	17330	9340	6345	24095	13693	37825
31138	30761	15150	10942	44829	24605	37957
62275	63066	30387	25024	91875	54884	38277
124550	123360	50210	41254	143892	86180	38519
62275	62890	27642	18972	76582	43111	38629
31138	30738	19950	8311	45251	22814	39286
17793	17762	17365	6113	30345	17449	38755
8896	8898	15531	5524	22405	14128	38726
4448	4513	14348	5695	18046	11308	38710
2224	2313	13419	6644	16678	9170	38684
0	0	18674	18750	55789	38503	NA ¹
124550	124550	65136	70659	149393	111788	37211
266893	266893	119416	140705	292817	225584	37659
533787	533787	225379	308950	539842	426949	37667
1067573	1067573	447992	709526	1027022	814105	37847
533787	533787	241608	336061	604362	462302	38360
266893	266893	146169	168222	368888	271342	38058
124550	124550	87538	95403	235393	162710	38371
0	0	39739	52691	83422	58195	NA ¹

NA¹ Ultrasonic wave velocity was not measured during the application of load.

* E_c used to calculate each strainmeter load is the E_c average perpendicular to the reinforcement calculated prior to loading. $E_c = 38055$ MPa

The load cycles follow separate loading and unloading paths. Figure 2.62 shows the variation between loading and unloading behaviors observed for loads in excess of 124,550 N. Each strainmeter recorded a greater load during unloading than during loading for the same actual, load cell measured, applied load. Strainmeters 1541, 1543, and 5863 under-predicted the load applied to the column during loading. The load was under-predicted during unloading by strainmeters 1543 and 5863. As unloading begins,

strainmeter 1541 under-predicts the applied load to the column, but once the load decreases several steps, the strainmeter over-predicts the applied load. Strainmeter 1544 over predicted the load during loading and unloading except at the maximum load, which was under-predicted.

The discrepancies between each of the strainmeters and the load cell may be explained by hysteresis. The change may be occurring in the concrete and steel, as indicated by the variation of the modulus of elasticity, or may be occurring in the load cell. The load recorded by the strainmeters may vary due to the imperfect contacts between the load distribution column and the instrumented column.

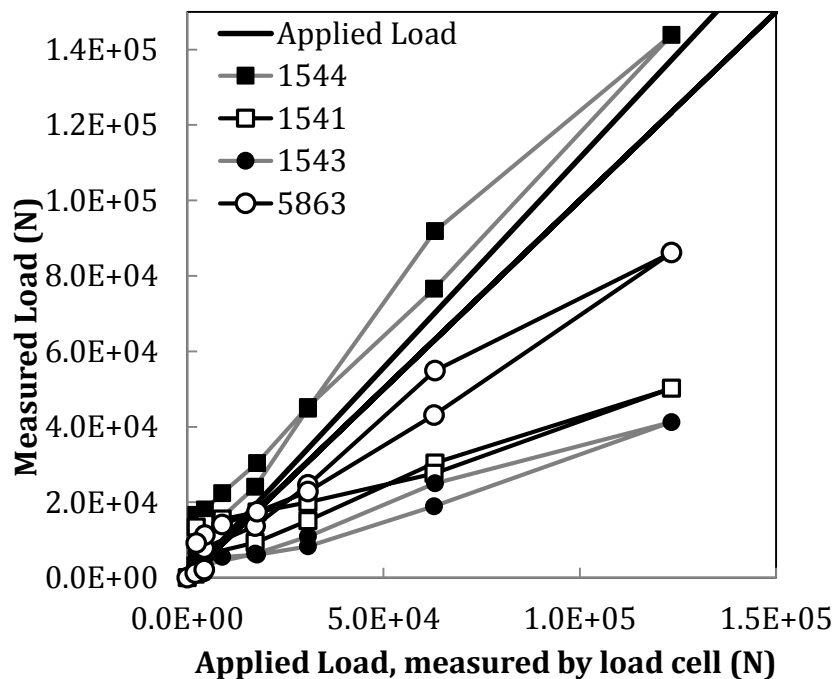


Figure 2.60 Small loads applied to the maximum reinforcement column

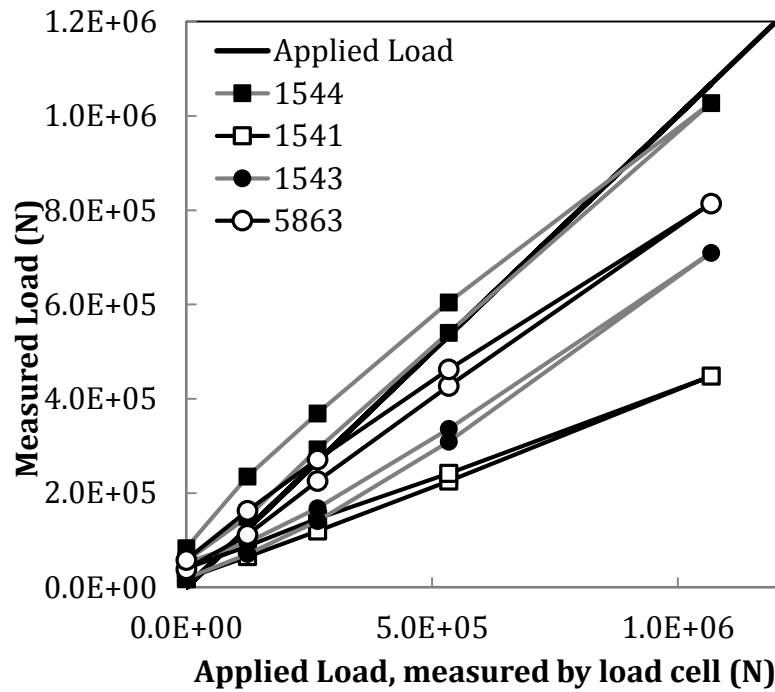


Figure 2.61 Large loads applied to the maximum reinforcement column

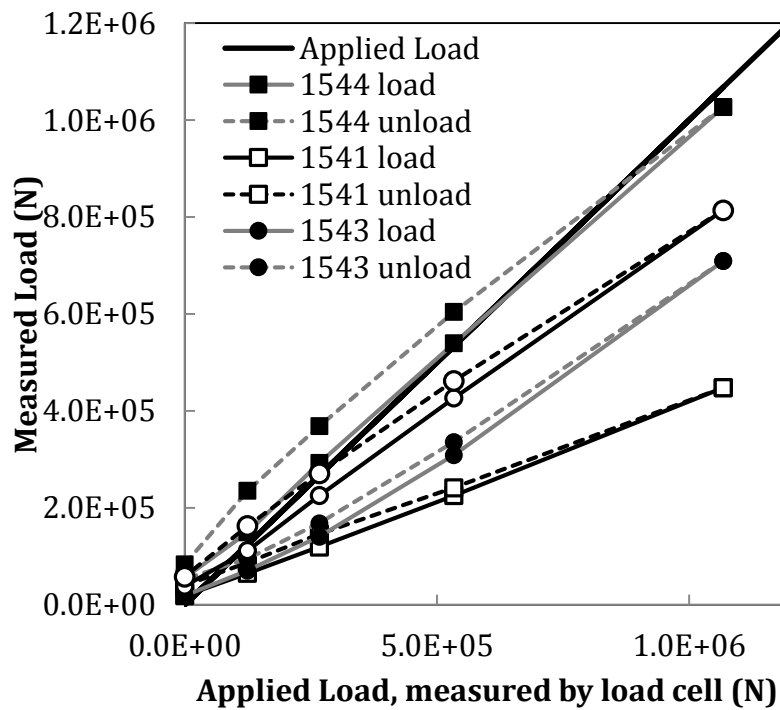


Figure 2.62 Loading and unloading the maximum reinforcement column

3. Wisconsin Structures

The design of transportation structures in Wisconsin must conform to the standards within the Wisconsin Department of Transportation Bridge Design Manual (WisDOT 2009). This document supplements and supersedes the Wisconsin Department of Transportation Standards (WisDOT 2008), the AASHTO LRFD Specifications, the ASTM specifications, and the American Welding Society (AWS) specifications.

Structural design depends on economic, aesthetic, construction, subsurface, geometric, and geographic considerations. Superstructures are classified by the location of the roadway: a through-structure has the roadway pass between structural components, while a deck structure usually supports the roadway from below. Superstructure types included in the WisDOT Bridge Manual (2009) are concrete slab, prestressed concrete girder, concrete box girder, concrete rigid frame, steel rolled sections, and timber longitudinally laminated decks.

3.1 Field research sites' locations

A total of three structures were instrumented to assess the load and settlement of transportation structures while three other structures were surveyed for deformation for a period of at least one winter season. Characteristics of the bridge structures and geotechnical reports were obtained from the construction documents. Four of the structures have bridge piers while three other structures have abutments wall. The structures were constructed between January 2010 and November 2010 and then between January 2013 and August 2014 (Highway 51 bridges in DeForest, WI). The structures were selected by the Wisconsin Department of Transportation and are located in the South area and Southeast area of Wisconsin (Figure 3.1).

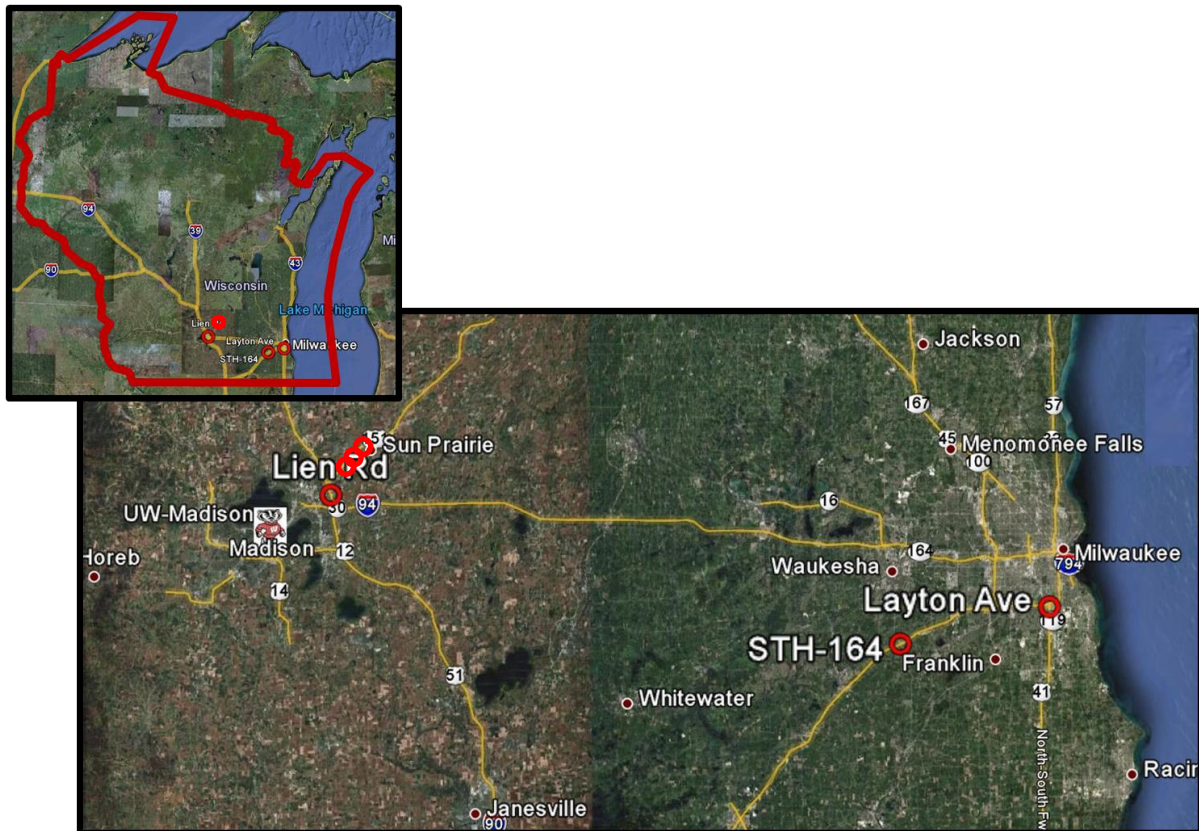


Figure 3.1 Location of the six research site locations in Southern Wisconsin.

3.2 Load Instrumented Bridges

Of the first three instrumented bridges (Layton Avenue, State Highway 164, and Lien Road Bridges), the Layton Avenue Bridge column was instrumented first, followed by a column in the State Highway 164 pier. Instrumentation was then installed at an abutment of State Highway 164, while instrumentation in a column of the Lien Road Bridge was the last to be installed. The design information and data for the three bridge columns and one abutment wall is summarized in Tables 3.1 and 3.2.

Subsurface exploration was conducted by private contractors on behalf of the Wisconsin DOT at each project location prior to design completion and construction. Information about the subsurface studies is presented in Table 3.3. Limited information was available about the geotechnical site exploration (mainly in the form of SPT results) and was presented in the structural plans. Without additional information or access to the geotechnical report, several assumptions have been made about the SPT procedures: a safety hammer was used, $C_h=1$; the sampler used did not require a liner or the required liner was in place correctly, $C_s=1$; the diameter of the borehole is between 66 mm and 115 mm, $C_d=1$ (AASHTO 2007, Salgado 2008, WisDOT 2008).

Table 3.1 Research site locations and design information provided by WisDOT

Research Site Name		Layton Avenue	State Highway 164 Pier	State Highway 164 Abutment	Lien Road
Structure Identification		B-40-0820	B-67-0325		B-13-541
WI State Project Number		1030-20-71	1090-23-71		1010-01-73
Research Site Location		Southeast WI	Southeast WI		South-central WI
Design					
Standards		AASHTO LRFD 2007	AASHTO LRFD 2007		AASHTO LRFD Design Specifications, 4th Edition
<i>Live Load</i>					
Design Loading		HL-93	HL-93		HL-93
WI Standard Permit Vehicle	kips	240	250		250
	kN	1068	1112		1112
Inventory Rating Factor		1.01	1.31		1.10
Operating Rating Factor		1.31	1.69		1.42
<i>Ultimate Design Stresses</i>					
Concrete Masonry: Superstructure (f _c)	psi	4000	4000		4000
	MPa	28	28		28
Concrete Masonry: Substructure (f _c)	psi	4000	3500		3500
	MPa	28	24		24
Structural Steel: ASTM A709 Grade 50 (f _y)	psi	50000			
	MPa	345			
Bar Steel Reinforcement (f _y)	psi	60000	60000		60000
	MPa	414	414		414
Steel Piling (f _y)	psi	50000			
	MPa	345			
Prestressed Girder: Concrete Masonry (f _c)	psi		8000		
	MPa		55		
Prestressed Girder: Strands Tensile Strength (f _s)	psi		270000		
	MPa		1860		

Table 3.2 Research site construction data provided by WisDOT

Research Site Name		Layton Avenue	State Highway 164 Pier	State Highway 164 Abutment	Lien Road
Structure Identification		B-40-0820	B-67-0325		B-13-541
WI State Project Number		1030-20-71	1090-23-71		1010-01-73
Research Site Location		Southeast WI	Southeast WI		South-central WI
Data					
Foundation: Abutments		Steel HP 12x53 Piling	Steel HP 10x42 Piling		Spread footings
Driving Resistance	tons/pile	215			275
	kg/pile	195000			249500
Estimated maximum pile lengths	feet	90			30
	m	27			9
Maximum design soil pressure	tons/ft ²		3		
	MPa		0.29		
Foundation: Piers		Spread footings	Spread footings		Steel HP 10x42 Piling
Driving Resistance	tons/pile				275
	kg/pile				249500
Estimated maximum pile lengths	feet				15
	m				5
Nominal bearing resistance	psf	1480			
	MPa	0.07			
Factored net bearing resistance	psf	7400			
	MPa	0.35			
Maximum design soil pressure	tsf		3		
	MPa		0.29		

Table 3.3 Subsurface exploration details for each research site included in construction documents

Research Site Name	Layton Avenue	State Highway 164 Pier	State Highway 164 Abutment	Lien Road
Structure Identification	B-40-0820	B-67-0325		B-13-541
WI State Project Number	1030-20-71	1090-23-71		1010-01-73
Research Site Location	Southeast WI	Southeast WI		South-central WI
Subsurface Exploration				
Soil Exploration Tests Performed	SPT	SPT		SPT, Unconfined Compression
Number of Soil Exploration Locations	8	10		12
Minimum Depth ¹ to Ground Water Table	ft	37.4	13.5	NR
	m	11.4	4.1	NR
Maximum Depth ¹ to Ground Water Table	ft	57.2	38.5	NR
	m	17.4	11.7	NR
Maximum Depth ¹ to Bedrock	ft	NR	35.0	20.6
	m	NR	10.7	6.3
Minimum Depth ¹ to Bedrock	ft	NR	60.0	32.1
	m	NR	18.3	9.8

NR: Not Recorded

¹Depths measured from elevation at the beginning of the boring

Layton Avenue Bridge

The first site to be instrumented was the Layton Avenue Bridge spanning Interstate Highway-94 in Milwaukee County, Wisconsin. The Wisconsin bridge identification number for this structure is B-40-820. The Layton Avenue Bridge construction is a component of the I-94 North-South corridor reconstruction project, and this project also included portions of I-43, US-41 and WIS-894. The Layton Avenue Bridge replaced an overpass structure on the same site.

A total of eight soil exploration locations were evaluated at the Layton Avenue Bridge prior to the design and construction of the new structure. The soil samples were collected by Split-spoon during Standard Penetration Test (SPT), and the bearing capacity of the soil was based on the resistance of the soil during the SPT. The traffic load, self-weight, snow load, wind load, and other forces transfer through to the supporting columns and into the soil. The loads induce tension and compression on the columns, but the anticipated loads and deflections are significantly greater in compression than tension (Structure B-40-820, 2009).

The bridge is supported by three piers and abutment walls at the east and west edges of the structure. The piers are numbered 1 to 3, with pier 1 located the furthest west, pier 2 central to the bridge, and pier 3 located the furthest east. Each pier is composed of 6 columns, numbered 1 to 6 from North to South direction. Sister bar stain meters were installed in pier 3, column 4 of the Layton Avenue Bridge. The average daily traffic (ADT) using Layton Avenue Bridge was 3,510 in 2003. The bridge has been designed for an anticipated increase in ADT to 6,940 in 2030. The vehicle speed used in the design is 65 km/hr (40 mi/hr).

The Layton Avenue Bridge has four spans separated by three piers. The spans' lengths are, from west to east, 38.6 m (126 ft, 6 in), 47.2 m (155 ft), 35 m (115 ft), and 38.6 m (126 ft, 6 in). The bridge deck width is 36 m (118 ft). Each of the three piers that support the Layton Avenue Bridge has six columns on six separate spread footing foundations. The footprint of each column's foundation is 4.6 m by 4.6 m (15 ft by 15 ft). The typical thickness of the footings is 0.9 m (3 ft). A mud mat was poured into the

excavation for the pier footings prior to construction of the reinforcement cage and formwork for the individual footings. The total footing area at each pier is 125.4 m² (1350 ft²). The columns supporting the Layton Avenue Bridge deck range in height from 6.44 m (21 ft, 1 ¾ in) to 7.85 m (25 ft, 9 in). Column 4 in pier 3 where the instruments were installed has a height of 7.75 m (25 ft, 5 in) above the footing, and a total height of 8.66 m (28 ft, 5 in). At the intersection of the column and the foundation the column measures 1.33 m by 0.9 m (4 ft 4.5 in by 3 ft).

State Highway 164 Bridge

The second and third sites to be instrumented were in the Interstate Highway 43 (I-43) bridge over State Highway 164 (STH-164). The site has two separate bridges, one for the south-bound vehicles and the other to carry the north-bound vehicles on I-43. The overpass structures are south of Waukesha, in Waukesha County, southeastern Wisconsin.

The instruments are located on the structure with the WisDOT identification number B-67-325; this bridge carries the south-bound traffic of the Interstate I-43. The instrumentation for the site identified as STH-164 Pier is located in the pier supports of the south-bound bridge, and the instrumentation of the abutment wall is identified as STH-164 Abutment. The north-bound lanes of I-43 are carried over STH-164 on structure B-67-324. The south-bound and north-bound structures are replacement construction for two overpass structures previously located on the site.

The bridge for south-bound traffic is supported by one pier and an abutment wall at the east and west edges of the structure. The pier is composed of 4 columns, numbered

1 to 4 in the North to South direction and the sister bar strainmeters were installed in column 3. Sister bar stain meters were also installed in the north abutment of the structure.

The ADT using the I-43 Bridge over STH-164 was 44,900 in 2010. The bridge has been designed for an anticipated increase in traffic volume of 55,600 in 2030. The vehicle speed used in the design is 112 km/hr (70 mi/hr). The ADT of STH-164 was 23,800 in 2010, and the projected ADT in 2030 is 31,400; the design speed for STH-164 is 80 km/hr (50 mi/hr) (Structure B-67-325 2009).

The I-43 Bridge has two spans, separated by a centrally located pier. The west span length is equal to the east span length, 27.7 m (91 ft). The pier supports a bridge deck that is 18.9 m (62 ft) wide. The pier includes 4 columns on separate spread footing foundations. The footprint of each foundation is 3.9 m by 4.6 m (13 ft by 15 ft). The typical thickness of the footings is 0.9 m (3 ft). A mud mat was poured into the excavation for the pier footings prior to the construction of the reinforcement cage and formwork for the individual footings. The total footing area at the pier is 72.46 m² (780 ft²). The columns supporting the I-43 bridge deck are 4.3 m (14 ft) in height from the top of the footing to girder supporting the deck. At the intersection of the column and the foundation the column measures 1.5 m by 0.9 m (5 ft by 3 ft) (Structure B-67-325 2009).

Lien Road Bridge

The fourth instrumented site was the Interstate Highway 39 (I-39) bridge over Lien Road in Madison, WI. This portion of interstate is also identified as I-90 and I-94. The site has two separate bridges, one to carry the east-bound traffic and the other to

carry the west-bound vehicles on I-39. The overpass structures are near the east side of Madison, in Dane County, south-central Wisconsin. The subsurface exploration of the Lien Road Bridge was conducted through 12 SPT boring locations.

The instruments are located on the structure with the WisDOT identification number B-13-541; this bridge carries the east-bound traffic of I-39. The instrumentation for the Lien Road Bridge is located in the column supports of the east-bound bridge pier. The west-bound lanes of I-39 are carried over the Lien Road Bridge on structure B-13-542. The east-bound and west-bound structures are replacement construction for two overpass structures previously located on the site. The east-bound bridge is supported by one pier and an abutment wall at the north and south edges of the structure. The pier is composed of 6 columns, numbered 1 to 6 from East to West direction. Sister bar stain meters were installed in column 3 of the Lien Road Bridge. The ADT using the I-39 Bridge over Lien Road was not included in the preliminary design. The bridge was designed for an anticipated traffic volume of 57,700 in 2030. The vehicle speed used in the design is 112 km/hr (70 mi/hr). The ADT of the Lien Road Bridge projected in 2030 is 14,700; the design speed for the Lien Road Bridge is 55 km/hr (35 mi/hr) (Structure B-13-541 2009).

Lien Road bridge has two spans separated by one pier. The spans are 15.24 m (50 ft) in length, and the I-39 bridge deck slab width is 27.78 m (91 ft 1.75 in). The bridge has six columns on six separate foundations. The 3.73 m by 3.73 m by 0.9 m (12 ft 3 in by 12 ft 3 in by 3 ft) concrete foundations are supported on HP 10x42 steel piling. The steel piling are embedded a minimum of 15.2 cm (6 in) into the bottom of the concrete base. A mud mat was poured into the excavation for the pier footings prior to the construction

of the rebar cage and formwork for the individual footings. The total footing area at each pier is 83.6 m² (900 ft²). The columns supporting the I-39 bridge deck are approximately 3.87 m (12 ft 8.5 in) in height. At the intersection of the column and the foundation the column measures 1.5 m by 1.2 m (5 ft by 4 ft). Column details are drawn from the structural pier plans (Structure B-13-541 2009).

3.3 Deformation Monitored Bridges

Three other bridges were surveyed for deformation from 2013 till 2015 to evaluate the response of the foundation and structures to both structural and environmental loads. The bridges were identified by WisDOT. The three bridges are located very close to each other (less than 5 miles apart) and undergo similar traffic and suffer similar environmental loads. While the bridges have similar dimensions, they are not identical. They also have differences in the type of foundation soils and the depth of foundation used.

Bridges on Highway 51 Deforest

These deep foundation bridges are located on United States Highway 51 (USH 51), northeast of Madison in Dane County, Wisconsin (Figure 3.2). The finished bridges are shown in Figure 3.3. Bridges built at this location go over the roads of Bear Tree, Windsor, and Vinburn. These bridges were open for traffic on June 23, 2013 (Bear Tree Bridge and Windsor Bridge); and on August 28, 2014 (Vinburn Bridge). The bridge over Bear Tree Road has the abutments being supported by H-piles 4.57 m (15 ft.) long, and the deck is 32.46 m (106.5 ft) long by 13.46 m (44.2 ft) wide. Subsurface exploration for this bridge

shows predominantly sandstone and gravel with a single clay layer 1.3 m thick under the north abutment.

At the bridge over Windsor Road the south and north abutments are being supported by H-piles 9.14 m (30 ft.) and 12.19 m (40 ft.) long respectively. The deck is 49.07 m long by 13.31 m wide and the abutments and three piers are supporting it. The piers themselves are being supported by H-piles 4.57 m (15 ft.) long under a square foundation of 2.74 m (8.1 ft.) per side. Also, the piers are 5.87 m (19.25 ft.) apart center-to-center, and are 4.8 m (15.74 ft.) long. Subsurface exploration for this bridge shows the presence of a clay and sandy clay layer ranging between 0.6 m (2 ft.) and 2.1 m (7 ft.) and overlying gravel and sandstone.

At the bridge over Vinburn Road the south and north abutments are being supported by H-piles 10.67 m (35 ft.) and 7.62 m (25 ft.) long respectively, and the deck is 33.99 m (111.5 ft.) long by 13.31 m (43.7 ft.) wide. Similar to the first two bridges the subsurface layers consist predominantly of gravel and sandstone, with sparse clay layers around 1 m (3.3 ft.) thick.

The traffic and loading conditions used for design, as well as the average annual and winter temperatures for the locations of the bridges, for all the studied bridges are summarized in Table 3.4. The temperature data was obtained from the Wisconsin State Climatology Office (<http://www.aos.wisc.edu/%7Eesco/clim-history/7cities/index.html>).

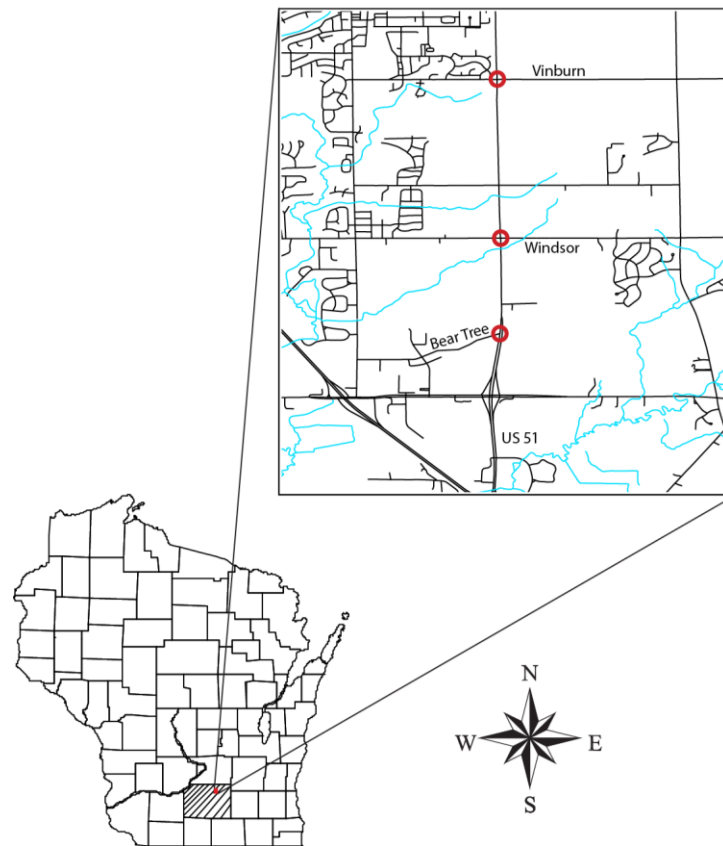


Figure 3.2 Detailed location of the deep foundation bridges on Highway 51. The red circle indicates the location of the bridges.

Deformations in all these three bridges were monitored using an expanded total station survey program. Conventional surveying techniques were implemented to monitor the deformation of the bridges. Total station, prism, and reflecting surveying targets (Figure 3.4) were implemented. The slope-distance, vertical and horizontal angles were measured using a total station with a precision of 3 mm (~ 0.01 ft). The surveying points on the deck, close to its edge, are approximately 0.5 m from the edge of the deck, and the middle one at the middle of each deck. The surveying points on the approaching road start between 1.8 m and 2.5 m from the edge of the deck, and are 5 m apart from each other. For all the bridges a reference point (i.e., REF in Figure 3.3) was

established. The reference point has a known elevation and it is considered to be fixed for the purpose of the analysis in this study. These bench marks were a nail on a power pole just inside the right of way for the Bear Tree Road and Vinburn Road bridges. For the Windsor Road bridge, the original power pole with the nail was removed during construction operations, so a new surveying monument was placed (on top of a concrete cylinder placed on a hole). In most of the cases the reference point was only visible from position one (i.e., POS 1 in Figure 3.4), thus all the surveying points visible from this location were shoot each time to guarantee a good tie to the reference point. The points that were not in sight from position one were then shoot from other positions (i.e., POS 2 in Figure 3.4). From the x, y, and z coordinates of each point their vertical and lateral deformations where calculated. The survey program included twelve target points on the bridge structure plus sixteen points on the approach road. The relative location of all the target points are presented in Figure 3.5.

Table 3.4 Design conditions and temperature averages for the studied bridges

Bridge	Deep foundation (USH51)
Traffic volume (daily)	28,800
Traffic speed (MPH/kph)	70/112
Design loading	HL-93
Average annual temperature (°C/°F)	8/46.4
Average winter temperature (°C/°F)	-6/21.2



Figure 3.3 Pictures of the finished bridges on USH51. Bridge over Bear Tree Road (Top). Bridge over Windsor Road (Middle). Bridge over Vinburn Road (Bottom).

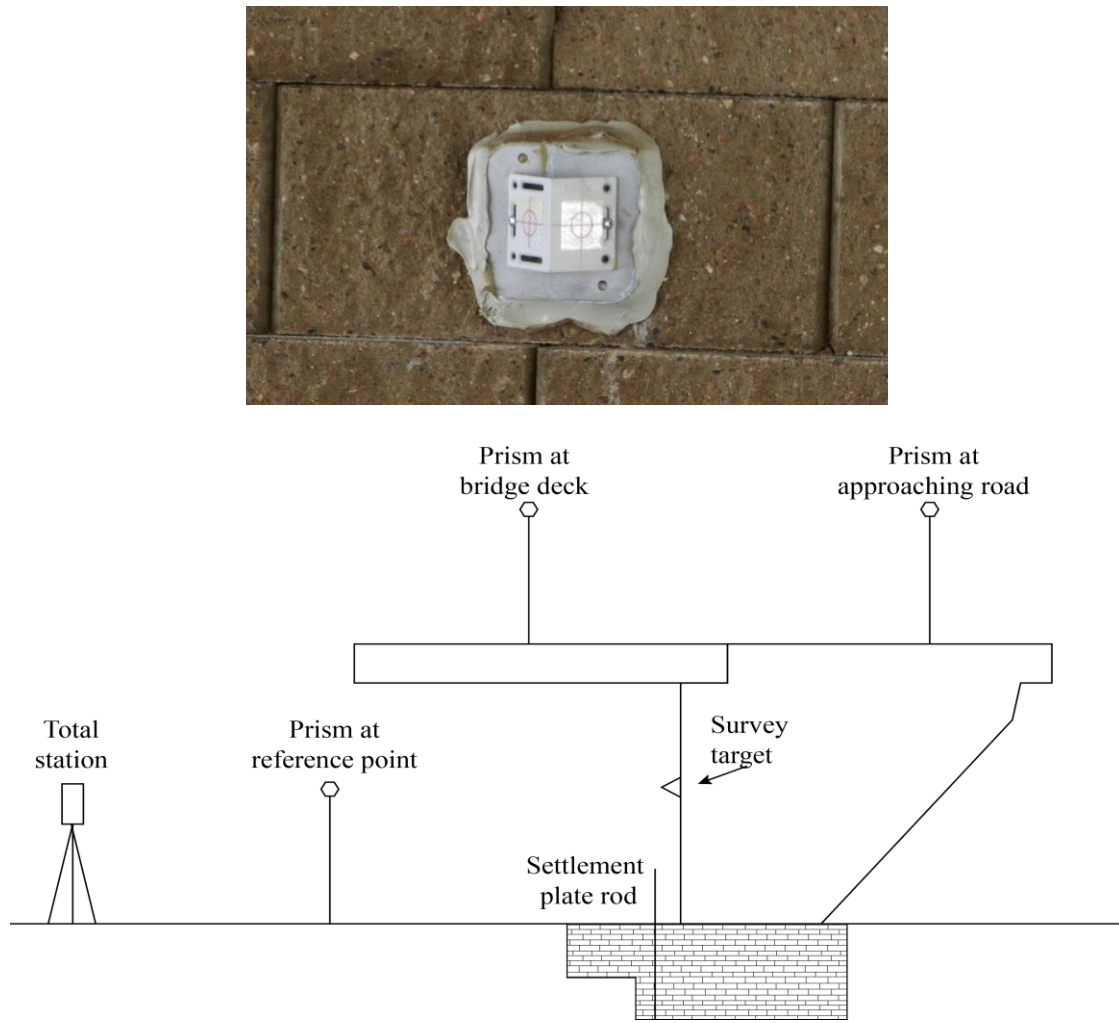


Figure 3.4 Surveying target and Surveying set up use to measure the deformation of the Highway 51 bridges.

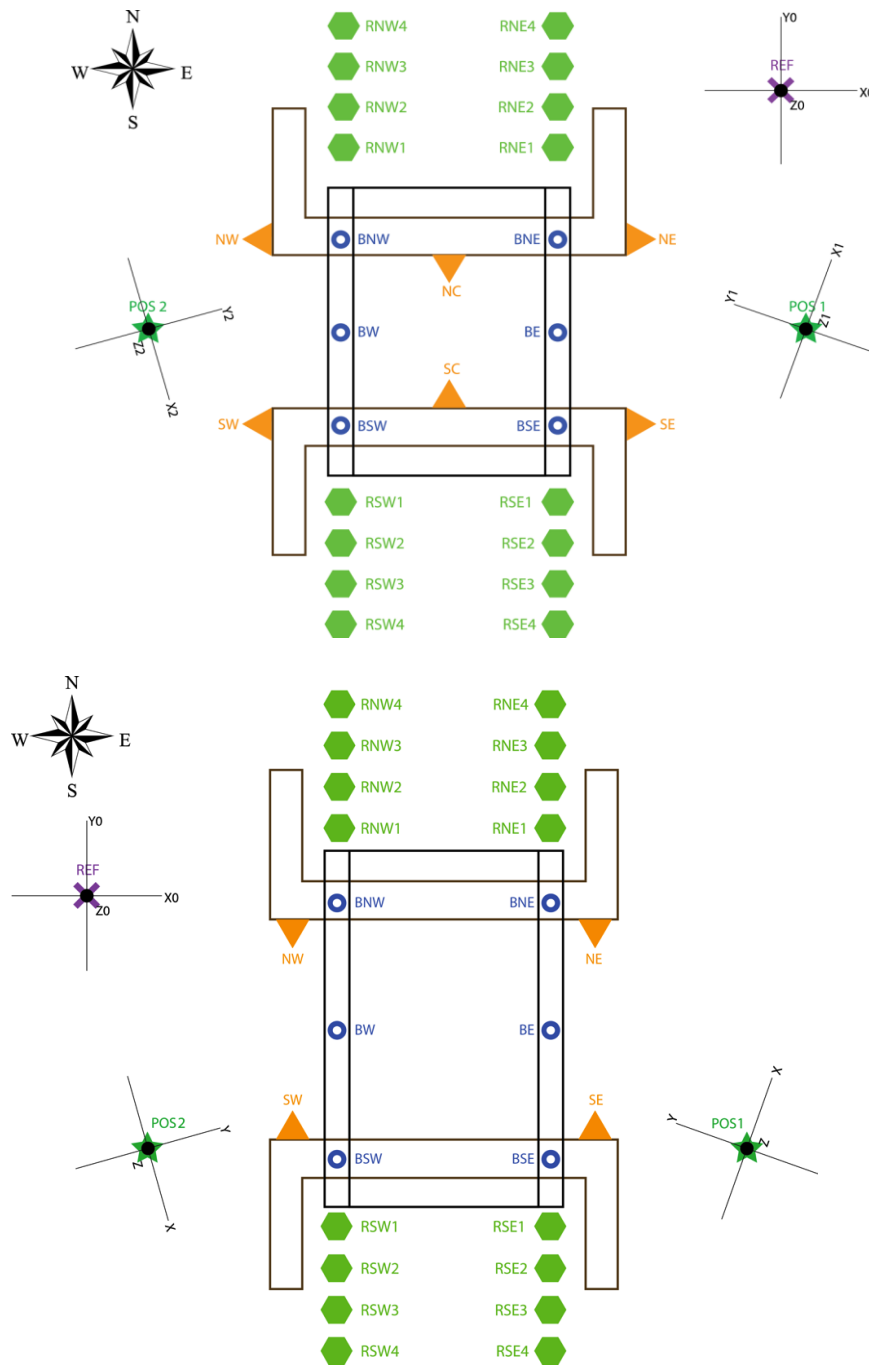


Figure 3.5: Location of the surveying points at Bear Tree Road and Windsor Road Bridges (top) and Vinburn Road Bridges (bottom).

3.4 Field research sites instrumentation installation

The field sites were instrumented between April and August 2010. Table 3.5 details the instrumentation location and identification. The naming convention used for the strainmeters is the last four digits of the manufacturer-assigned serial number.

Sensor installation occurred as the construction schedule progressed. Installation was rapid and required less than 2 hours for the rebar strainmeters to be connected to the structural reinforcement. Once the formwork was in place around the rebar, the location of the strainmeters were not discernible. Work proceeded without regard for the embedded strainmeters and the concrete was placed and vibrated according to typical practice.

Table 3.5 Research site instrumentation location and identification

Research Site Name	Layton Avenue	State Highway 164 Pier	State Highway 164 Abutment	Lien Road
Structure Identification	B-40-820	B-67-0325		B-13-541
Number of spans	4	2		2
Number of piers	3	1		1
Number of columns per pier	6	5		6
Maximum Span Length (m)	47	28		15
Data logger location	Pier 3, Column 4	Pier, Column 3	North Abutment	Pier, Column 3
Installed strainmeter serial number identification	4643 4804 4805 4806	6904 6905 6906 6907	6909 6910 6911 6912	6903 6908 4642 1540
Installation Date	4/1/2010	5/25/2010	6/4/2010	8/4/2010

The instrumented columns tested in the laboratory represented the extremes of reinforcement concentration that were encountered in the field (Table 3.6). The Layton Avenue Bridge contains the greatest percentage of reinforcement, and Lien Road Bridge contains the least percentage of reinforcement of all of the field sites.

Table 3.6 Comparison of reinforcement ratios in research sites to laboratory columns

		Minimum Reinforcement Laboratory Column	Maximum Reinforcement Laboratory Column	Layton Ave	STH-164 Pier	Lien Rd
Cross sectional area of column	cm ²	2787.09	2787.09	12193.52	13935.46	18580.61
Area of Steel	cm ²	5.16	169.03	491.61	196.65	244.64
Reinforcement Ratio	%	0.19%	6.06%	4.03%	1.41%	1.32%

Layton Avenue Bridge Instrumentation

Sister bar strainmeters were installed in the fourth column of pier 3 at the Layton Avenue Bridge. The strainmeters were spliced to the reinforcement where the reinforcement extending out of the foundation overlapped with the column reinforcement cage. Strainmeters were installed prior to the placement of the column reinforcement cage. Figure 3.6 provides the location of each strainmeter inside the column.

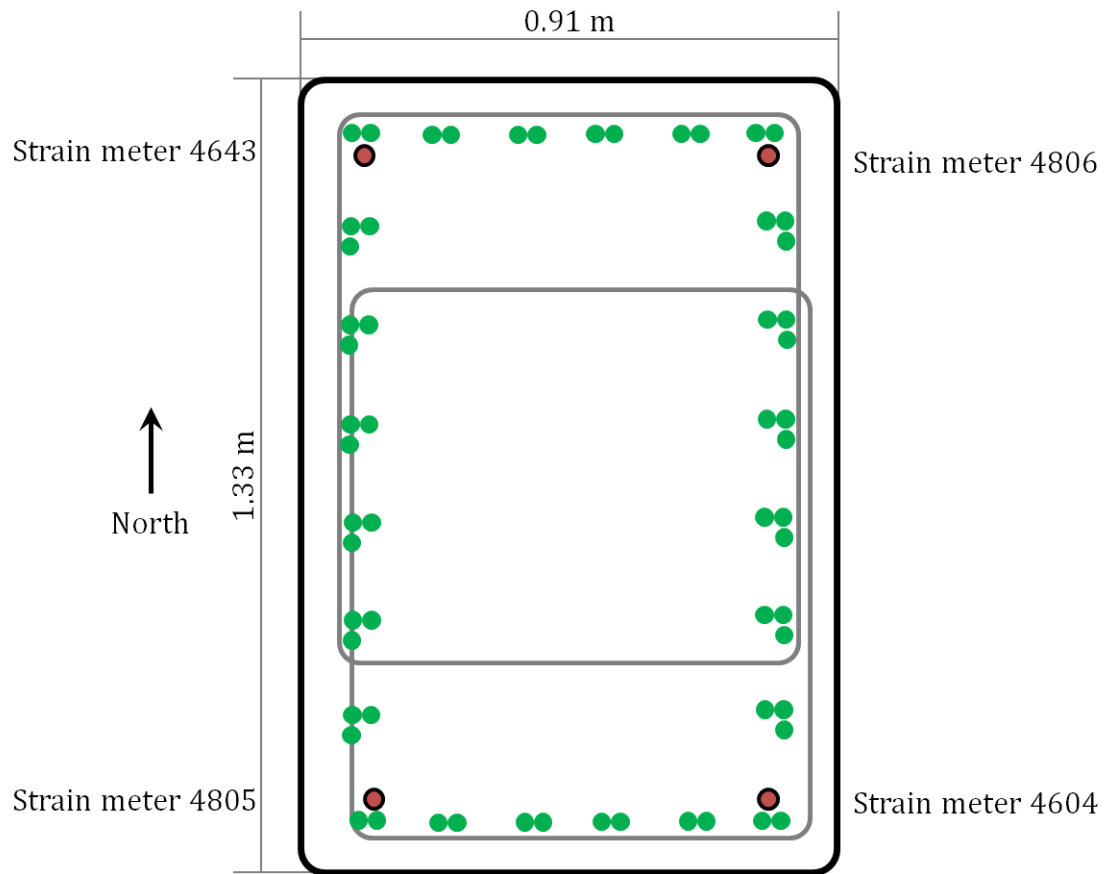


Figure 3.6 Cross section of instrumented column at the Layton Avenue Bridge, including strainmeter locations.

Ultrasonic waves were used to evaluate modulus of elasticity E_c of the instrumented column. The laboratory method developed to evaluate E_c was used at the Layton Avenue Bridge (Figure 3.7). The transmitter and receiver were moved along grid lines, separated by 10.16 cm. Several different paths were used to measure the wave velocity to reduce the influence of the reinforcement and consolidation differences in the cross section of the column (Figure 3.8). E_c was calculated when the column was 55 days old.



Figure 3.7 Ultrasonic wave transit time measurements through the column at the Layton Avenue Bridge.

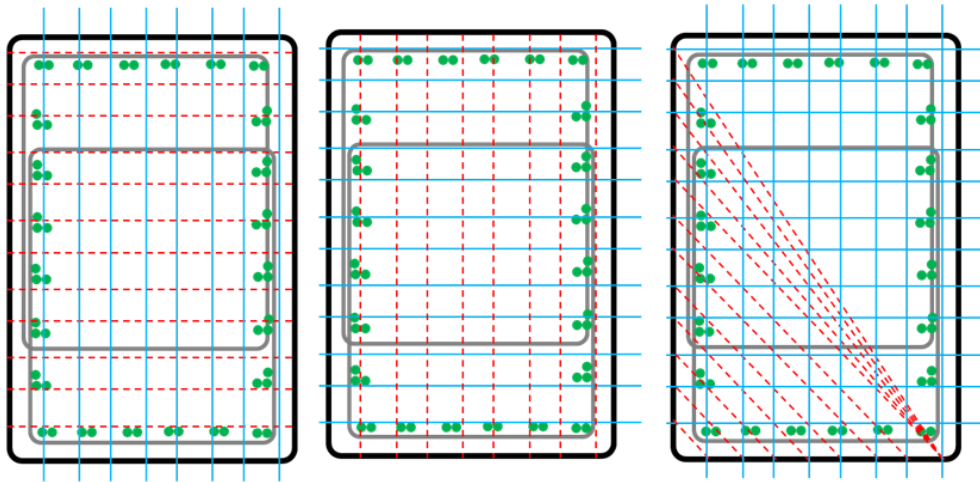


Figure 3.8 Ultrasonic wave paths used to determine modulus of elasticity at the Layton Avenue Bridge.

The fixed survey markers were not installed onto the column until the bridge was completed. The proximity of the column to an open interstate restricted the placement of the survey markers to three of the four sides of the column. Survey marker locations and the fixed points used to measure the settlement of the column are illustrated in Figure 3.9, a plan view of the bridge section where the instruments were installed. The instrumented column is outlined, and the level locations are approximate.

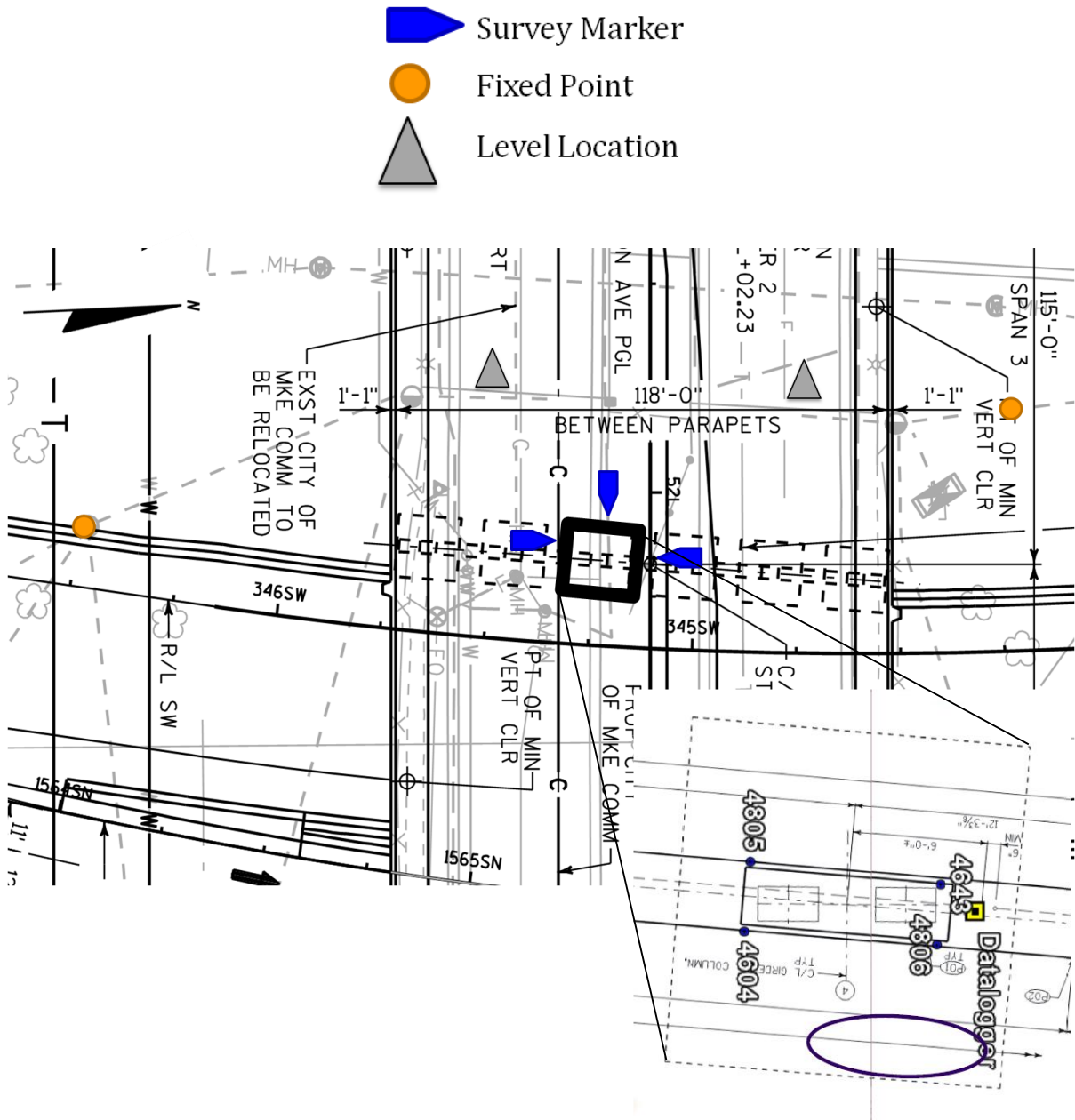


Figure 3.9 Plan view of survey locations at the Layton Avenue Bridge

State Highway 164 Bridge Instrumentation

Sister bar strainmeters were installed in the third column of the bridge pier and in the north abutment wall at STH-164. In the column, the strainmeters were spliced to

the reinforcement that extended out of the top of the foundation. Strainmeters were installed prior to the placement of concrete for the foundation. After the foundation was constructed, the column reinforcement cage was lowered into place around the strainmeters and extended foundation reinforcement. Figure 3.10 shows the location of each strainmeter inside the column.

Ultrasonic waves were used to evaluate the modulus of elasticity E_c of the instrumented column in the same method used in the laboratory. The transmitter and receiver were moved along grid lines separated by 10.16 cm. The influence of the reinforcement and consolidation differences in the cross section of the column was reduced by using several different paths to measure the wave velocity (Figure 3.11). The modulus of elasticity E_c was measured when the column was 77 days old.

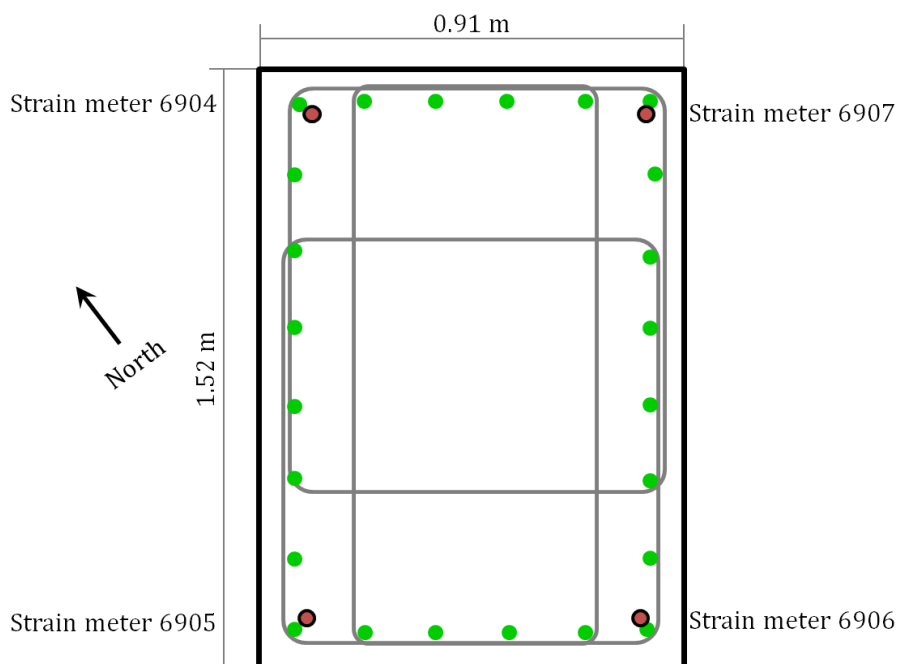


Figure 3.10 Cross section of instrumented column at the STH 164 Bridge Pier, including strainmeter locations

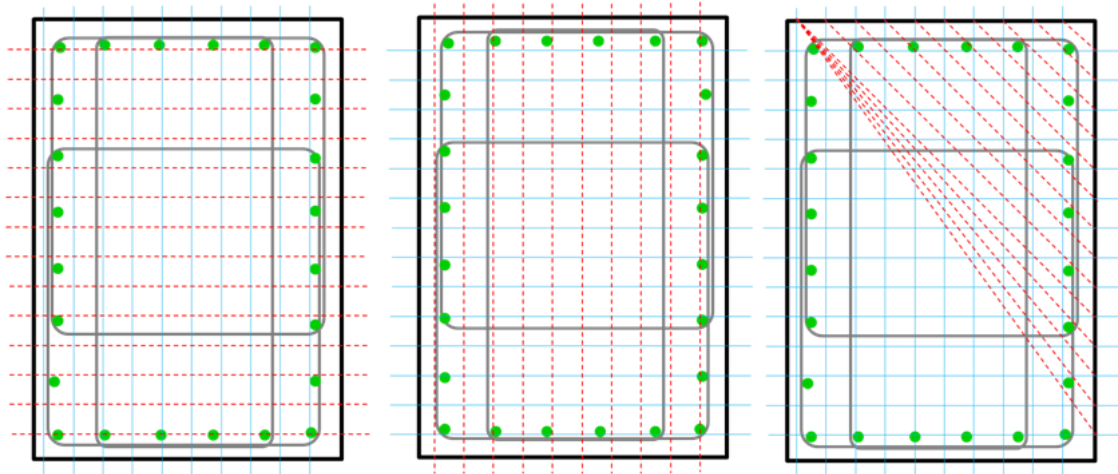


Figure 3.11 Ultrasonic wave paths used to determine modulus of elasticity E_c at the STH 164 Bridge Pier

The strainmeters were spliced to the reinforcement that extended from the top of the abutment foundation and were installed after the placement of the foundation's concrete. Figure 3.12 shows the location of each strainmeter inside the abutment, and measurements were taken from the west-most corner of the abutment. Two strainmeters were installed on each line of reinforcement. After the strainmeters were installed, the reinforcement for the abutment wall was built. The backfill of the abutment occurred before E_c could be measured through the structure.

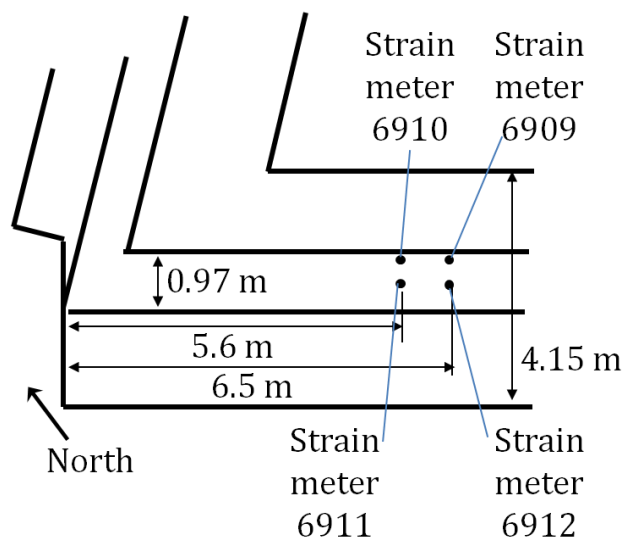


Figure 3.12 Cross section of STH-164 Abutment, including strainmeter locations

The STH-164 pier and abutment survey markers were installed once the bridge structure was completed but prior to the bridge deck opening to traffic. Three sides of the column were used for survey marker installation, and four survey markers were installed along the north abutment wall. The survey markers along the abutment were hung at the same elevation above the final grade of the road. Survey marker locations and fixed points are illustrated in a plan view of the bridge section where the strainmeters were installed (Figure 3.13). Figure 3.14 shows the location of the survey markers along the abutment wall, and the approximate level locations. The fixed points were the same for both the column and the abutment; the fixed points were manhole covers located outside the lanes of traffic.

-  Survey Marker
-  Fixed Point
-  Level Location

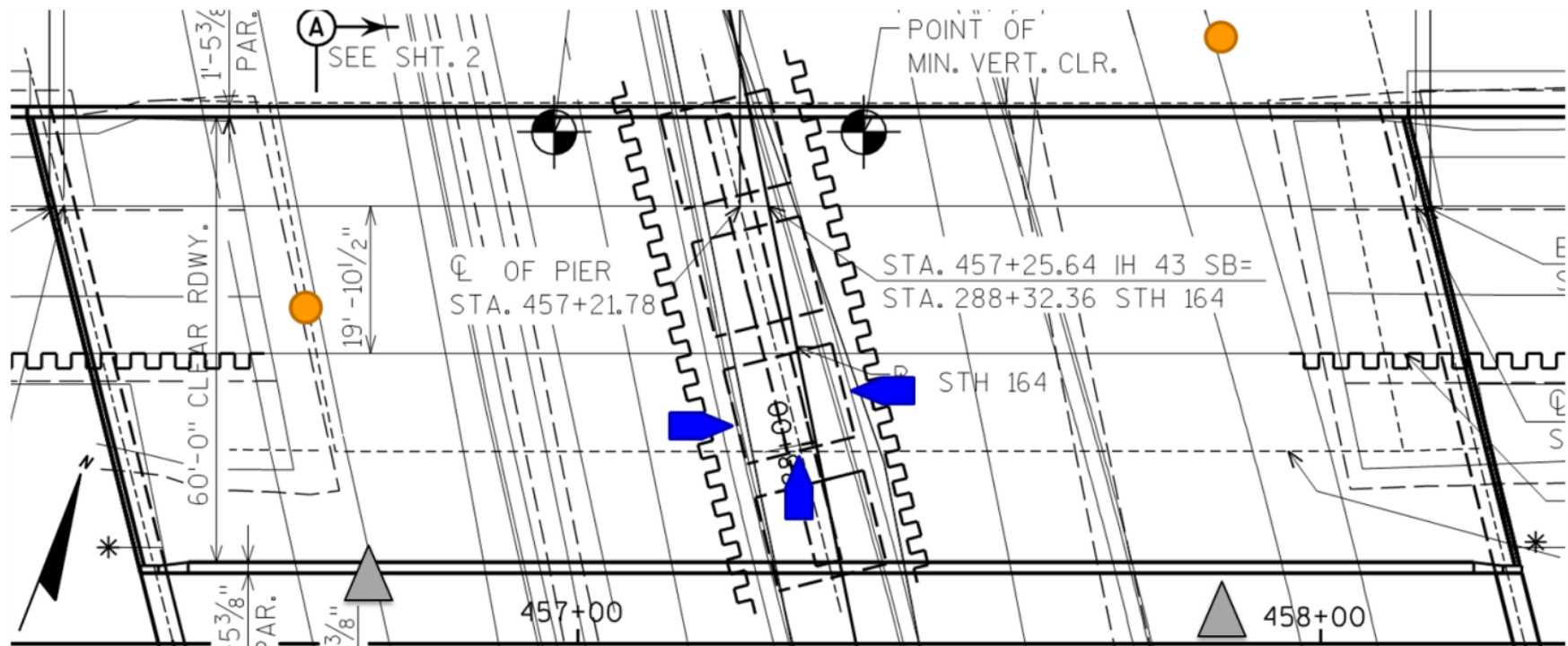


Figure 3.13 Plan view of survey locations at STH-164 Bridge Pier

Lien Road Bridge Instrumentation

Sister bar strainmeters were installed in the third column of the pier at the Lien Road Bridge. The strainmeters were spliced to the reinforcement that extended out of the top of the foundation where the column reinforcement overlaps with the reinforcement extending out of the foundation. Strainmeters were installed after the foundation concrete was placed and prior to the placement of the column reinforcement cage. Figure 3.15 provides the location of each strainmeter inside the column.

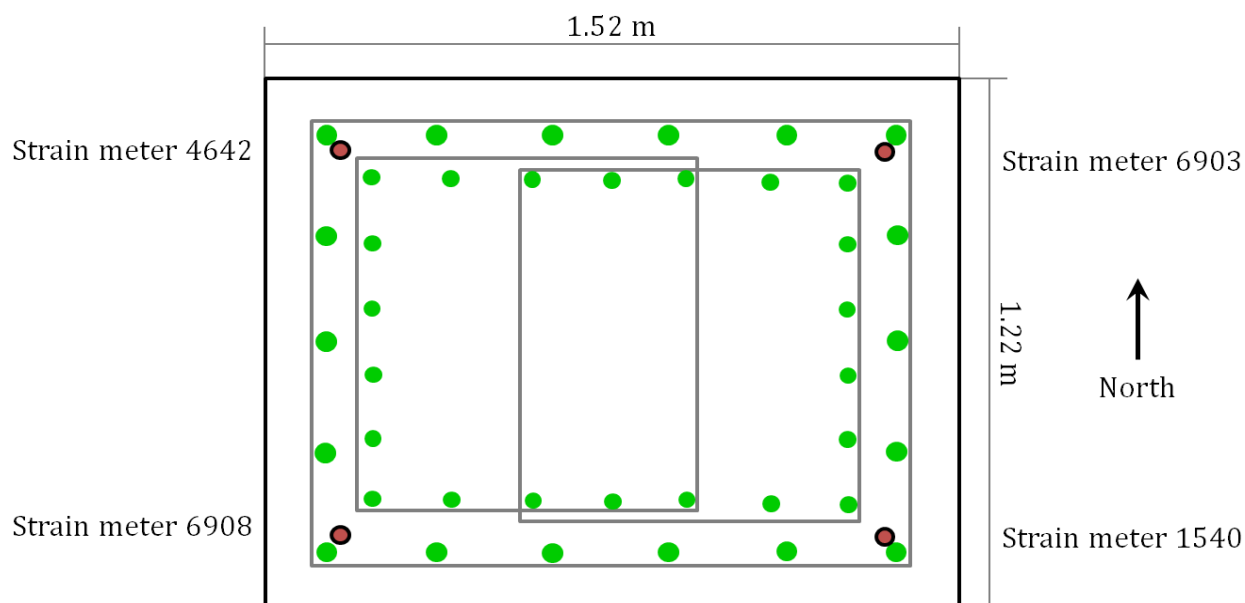


Figure 3.15 Cross section of the Lien Road Bridge column, including strainmeter locations

Ultrasonic waves were used to calculate the modulus of elasticity E_c of the Lien Road Bridge instrumented column. The method established to evaluate the E_c in the laboratory columns was used at this field site. The transmitter and receiver were moved to positions separated by 10.16 cm. The influence of reinforcement and variable concrete

consolidation was reduced by using several different paths were used to measure the wave velocity (Figure 3.16). E_c was measured when the column was 47 days old.

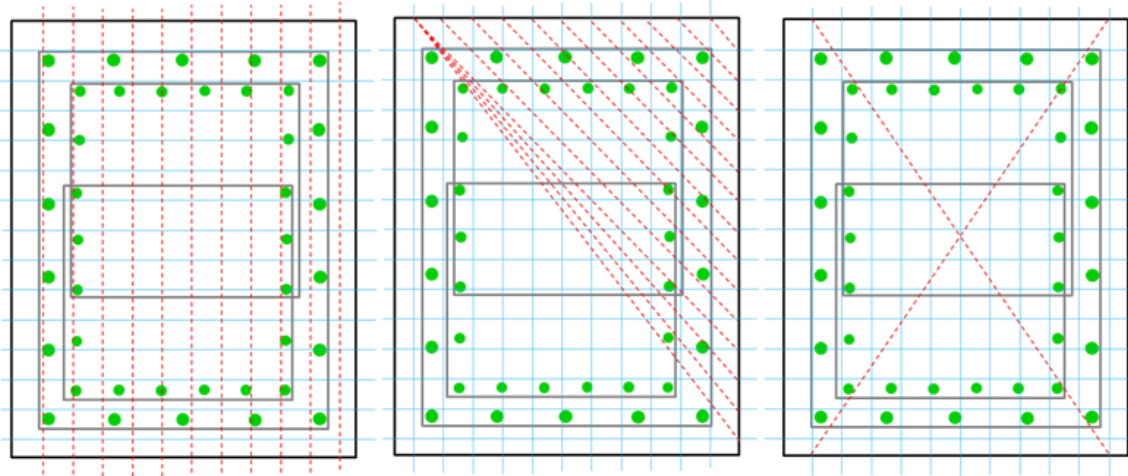


Figure 3.16 Ultrasonic wave paths used to determine modulus of elasticity at the Lien Road Bridge research site

The survey markers were not installed onto the Lien Road Bridge column until the bridge was completed and open to traffic. The steep incline west of the structure restricted the sight lines between the column and the fixed points that could be read by the level. Survey marker locations and the fixed points are illustrated in Figure 3.17, a plan view of the bridge section where the instruments were installed. The instrumented column is outlined and the level location is approximate.

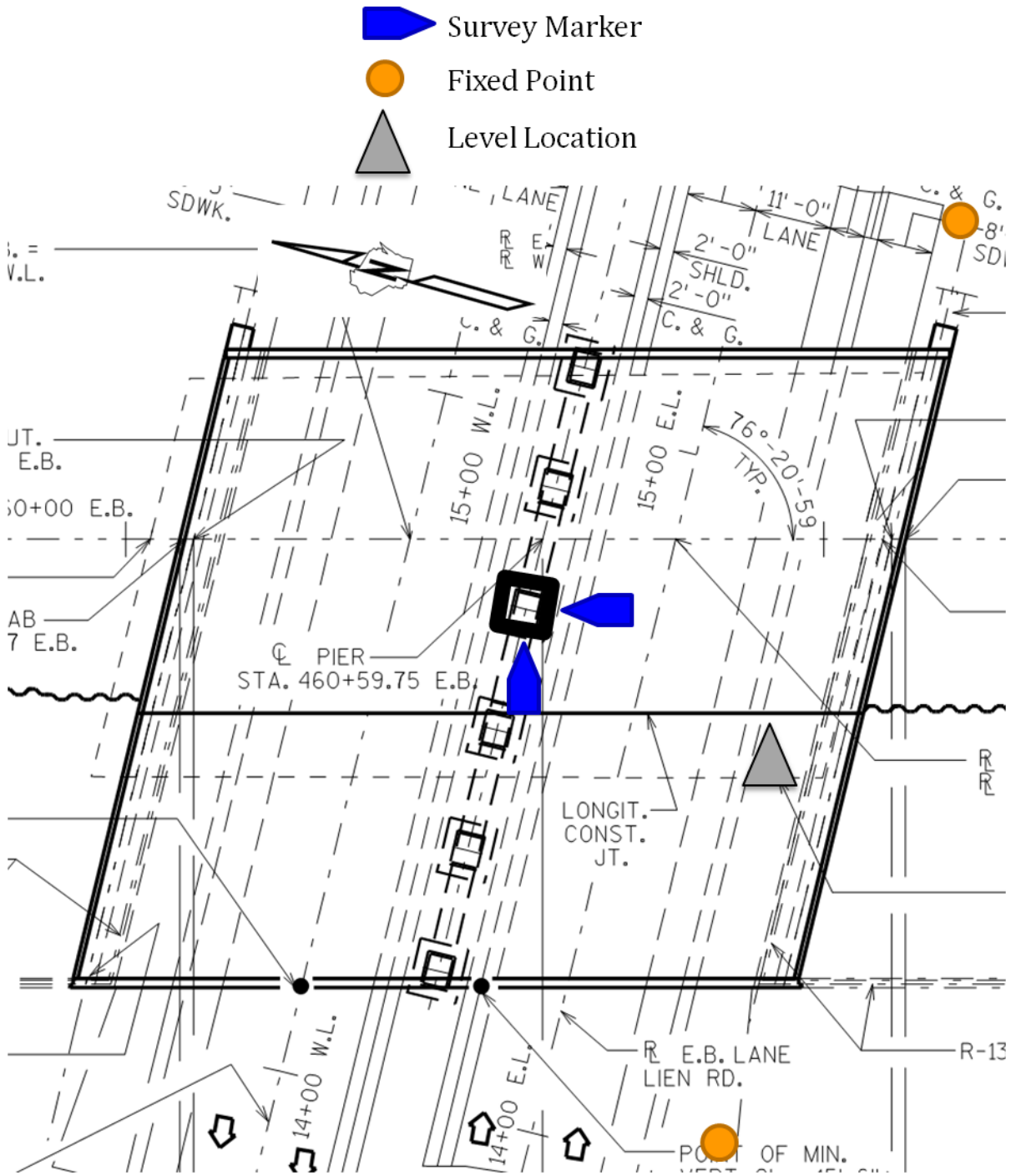


Figure 3.17 Plan view of survey locations at Lien Road Bridge.

3.5 Field research sites' modulus of elasticity

The modulus of elasticity E_c of each site was calculated using Equation 2.18. E_c values were expected to range between 35,000 MPa and 40,000 MPa based on laboratory testing. The distance between ultrasonic wave transmitter and receiver was constant, yet several different values for E_c were calculated for the STH-164 Pier. The variation of E_c may have resulted from either of two possibilities: (1) the poor contact between the column and ultrasonic wave transmitter and receiver, or (2) the variabilities in concrete consolidation that may lead to different stiffness along different concrete volumes. The distance between the transmitter and the receiver does not appear to influence the calculated E_c for the instrumented structures (Figure 3.18).

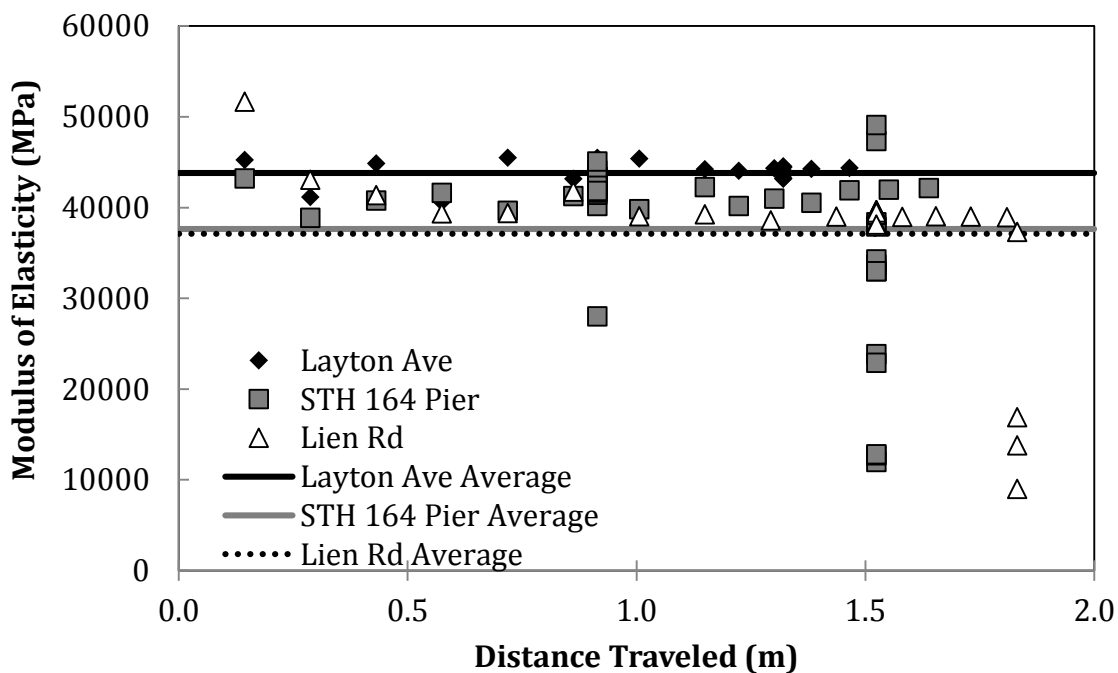


Figure 3.18 Modulus of elasticity calculated at each research site, compared to the travel distance of the ultrasonic waves

The recoded variation in the estimated modulus of elasticity E_c necessitated the removal of data points that were more than one standard deviation outside of E_c range for each site. The adjusted E_c value was then used to calculate the load within the columns based on the strainmeter readings (Table 3.7 and Figure 3.19).

Table 3.7 Modulus of elasticity E_c at each research site

	Average, All data points included	Standard Deviation	Average, Data within ± 1 Standard Deviation
	MPa	MPa	MPa
Layton Ave	43794	1297	43929
Lien Rd	37117	8698	39403
STH-164 Pier	37622	8882	40341
STH-164 Abutment ¹	39511	NA	41224

¹Data from Layton Ave, Lien Rd, and STH-164 Pier were averaged to calculate the modulus of elasticity of STH-164 Abutment.

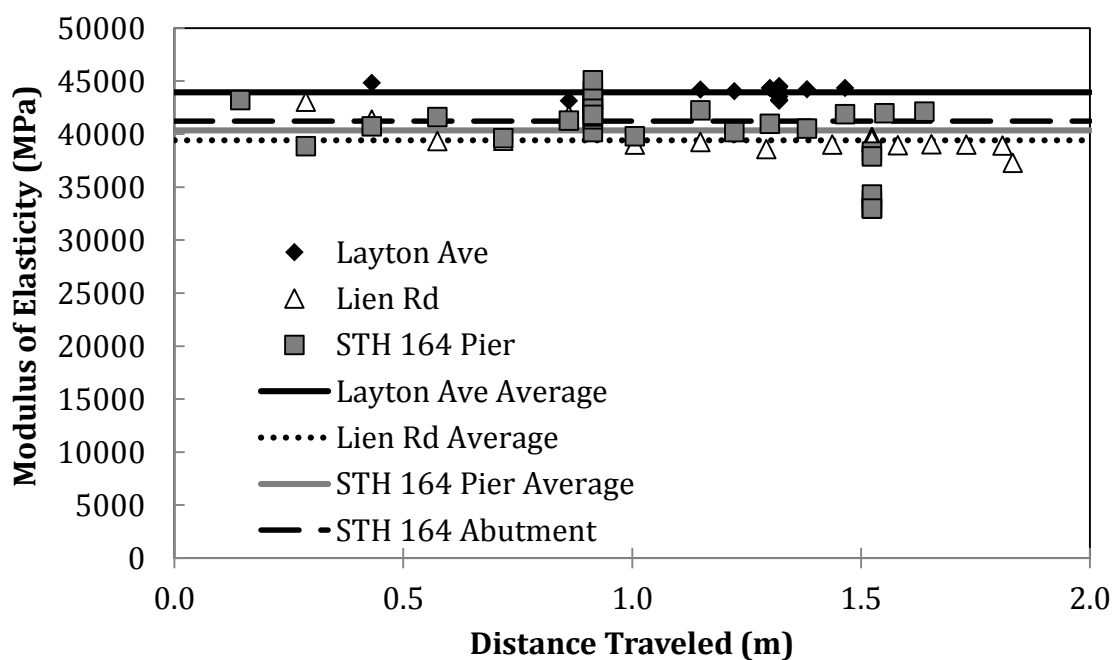


Figure 3.19 Modulus of elasticity calculated at each field site within one standard deviation

3.6 Field Research Sites' Complications

Each instrumented site had challenges that interfered with collection of the load and settlement data. Due to these challenges important construction events were missed when recording the load changes in the structure and movement of the structure. The settlement was expected to be greatest during construction, however the delay of establishing the survey baseline limited the settlement that could be observed and may have resulted in missing the most significant settlement. Site specific complications that interfered with data collection are presented with the interpreted data.

The surveying system used a level and fixed points of elevation and was fast to install but difficult to maintain. An unforeseen complication was the loss of the fixed points during and after construction was completed. Without fixed reference points to establish the elevations of survey markers, the foundation movement could not be properly measured. Base line readings were repeated with new fixed points once construction was complete and the fixed points could reliably be established, but the previous survey data were not usable and the deformations caused during construction were missed.

An accurate construction schedule to plan for the strainmeter installation and significant construction events was not available for the research sites. The planned construction activities were not communicated with the researchers, and the researchers' time at the construction sites was not efficient as contractors and researchers have in many cases different and conflicting priorities. Without a construction schedule, the time of load application and the magnitude of the loads could

not be properly estimated. The result was a limited understanding of the correlation between construction activities and the load and survey data.

Safety concerns and limited budget restricted access to the construction sites and eliminated the opportunity to observe ongoing construction activity on a regular and long-term basis. Access to the construction sites was hampered by poor communication and the data loggers were not installed permanently at the sites until the construction was nearly complete, resulting in an incomplete record of structural loading.

The cables connecting each strainmeter to the data logger were frequently damaged during construction. In most cases, the damage did not fully sever the cable and the insulation of the wires could be quickly and easily repaired. However, several cables required splicing and water-tight connections. For this reasons, cables were required to undergo inspection at each site visit.

Access to the data logger remained difficult after construction was completed at each instrumented structure. The proximity of the data loggers to open transportation routes was a safety concern while downloading the information stored in the data logger and making measurements of settlement. Secured data loggers discourage theft and vandalism, and also decrease accessibility for the researchers. The data logger tied to the instrumented column at the Layton Avenue Bridge structure was moved once construction at that site is concluded. The Lien Road Bridge is an unsecured area with significant pedestrian and vehicular traffic which prevented permanent installation of the data logger until an appropriate protective case was in place.

Concerned citizens several times contacted local authorities about the data logger at STH-164 Abutment, STH-164 Pier, and Lien Rd. Researchers have been questioned by law enforcement while accessing STH-164 Pier, STH-164 Abutment, and the Lien Road Bridge project sites. Bright colors on the data logger container and WisDOT emblems attached to the containers with contact information have the frequency of concerned calls to law enforcement.

The rate of battery use of the data loggers varies with season. Battery replacements were more frequent in the cold months than during the warmer months of year. As the rate of battery depletion is not constant during the life of the battery, and the loss of voltage accelerates as the battery becomes more depleted, the visit to sites required constant changes to reduce the number of times the data logger ceased to function.

3.7 Layton Avenue Bridge Results

Settlement results

The Layton Avenue Bridge was the project site that presented the most inconsistent fixed points for movement measurement. The initial level survey data were not usable once the fixed points were destroyed during later construction, and the process of taking baseline measurements has been performed twice at this structure. There are no conclusive data of the settlement at this column location.

Load results

The Layton Avenue Bridge structure was the first to be instrumented. The strain data collection was successful until the site experienced drainage issues, and a data logger was submerged for more than 24 hours. Strain measurements taken by the data logger were not recoverable. The lost data spanned a 137 day period during the end of 2010 and the beginning of 2011. A new data logger was installed and successfully recorded strainmeter outputs. The constants for calculation of load were obtained from the calibration information provided by the manufacturer of the strainmeters and the ultrasonic wave velocity testing performed at the structure (Table 3.8).

Table 3.8 Layton Avenue Bridge structural load calculation input information

	Channel	1	2	3	4
Sensor ID Number	ID	4643	4804	4805	4806
Gage Factor	GF	0.348	0.349	0.348	0.351
Gage Offset	GO	0	0	0	0
Zero Reading	ZR	6761	6905	7037	7048
Temperature at Zero Reading	T0	21.2	21.2	21.4	21.3

Structural Dimensions	Units	Variable	Footing	Column
Area	m ²	A	20.903	1.219
Length	m	L	4.572	1.334
Width	m	B	4.572	0.914
Height	m	H	0.914	7.747
L/B	m/m	L/B	1.000	1.458
Influence Factor	m/m	I	5.538	6.617
Rectangular area coefficient	m/m	C	0.944	0.932

Material Properties				
Coefficient of Expansion, Steel	ppm/°C	K _{steel}	12.2	12.2
Coefficient of Expansion, Steel and Concrete	ppm/°C	K _{composite}	2.2	2.2
Elastic Modulus of Concrete	MPa	E _{50,c}	43929	43929
Elastic Modulus of Soil	MPa	E _{soil}	100	100
Poisson's ratio	unitless	ν	0.25	0.25

Load experienced by the instrumented column is plotted versus time in Figure 3.20. The increase in load at the beginning of structural monitoring resulted from the ongoing construction at the site. Strainmeter number 4806 stopped reporting strainmeter measurements 33 days after installation, although the thermistor embedded with the strainmeter continued to function.

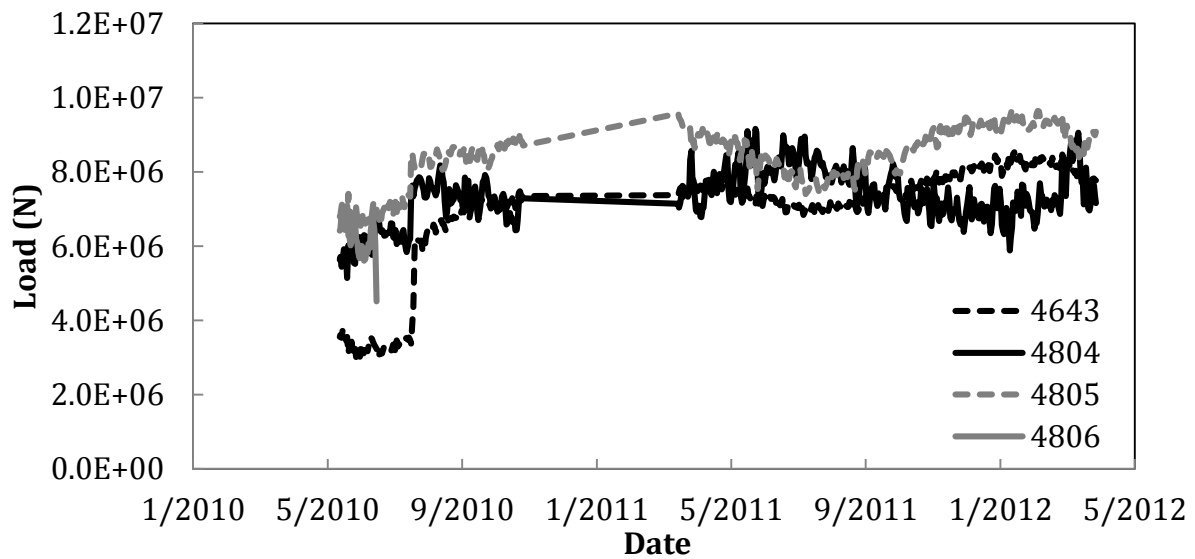


Figure 3.20 Load experienced by the Layton Avenue bridge structure over time

The behavior of strainmeters 4643 and 4805 is similar. These strainmeters are located on the west face of the column. The opposite behavioral trend of strainmeter 4804 suggests that there is differential loading of the column. This effect may be explained by the differences in heating and cooling of the column depending on the location of the sun. To investigate this further, a statistical analysis was performed on the data collected May to December 2010.

Statistical Analysis

A statistical analysis by Il-Youp Kwat examined the data collected at the Layton Avenue Bridge between May and December, 2010. The data points were determined to not be independent. The correlation factor changes with the temperature. The correlation exists in the temperature data and was addressed in the statistical model by linking the temperature difference between each data point. The strain measurements

were determined to be independent. The analysis demonstrated that the battery voltage did not affect the measurement of strain by the strainmeter. The time elapsed between measurements does not have a direct influence on the statistical model or the data validity.

The times of the strain measurements were examined for trends; the maximum loads in the 24 hour period were recorded between 1400 and 1600 local time. The time delay between peak temperatures recorded by the thermistor inside the column and the temperature sensor within the data logger varied though the data set. The temperature recorded by the data logger precedes the temperature recorded by the thermistor at the strainmeter by 15 to 60 minutes. If a peak temperature was recorded by the data logger at 1400, then the peak temperature would be recorded by the strainmeter thermistor between 1415 and 1500. The median and mode of the predicted time delay was 60 minutes. The average time delay of temperature was 48 minutes.

3.8 State Highway 164 Bridge Results

Settlement results

The fixed points used in the first settlement survey to determine a baseline for the settlement measure at the pier and abutment of STH-164 were not accessible after construction. The post-construction fixed points were manhole covers. No conclusive measurements of settlements were possible for the pier (Table 3.9) or the abutment (Table 3.10). The calculated settlement at a survey marker should be the same regardless of the fixed point to which the survey marker is compared. When the movement of a survey marker was calculated using the eastern fixed point manhole, the survey markers' elevations are increasing. When the western fixed point is used with the same survey markers, the calculated movement is in the downward direction. This suggests that the points assumed to be fixed were moving independently and at different rates of each other.

Table 3.9 STH-164 Pier settlement results along with the location of reference point, level, and marker on the bridge. Their locations are presented in Figure 3.13. (Negative values indicate settlements).

 Level	 Fixed Point	 Survey Marker	Settlement
Location	Location	Location	<i>mm</i>
East	West	East	-5.2
East	East	East	14.4
East	West	South	-6.9
East	East	South	12.7
West	East	South	4.0
West	West	South	-2.0
West	West	West	-0.3
West	East	West	5.7

Table 3.10 STH-164 Abutment settlement results along with the location of reference point, level, and marker on the bridge. Their locations are presented in Figure 3.14. (Negative values indicate settlements).

 Level	 Fixed Point	 Survey Marker	Settlement
Location	Location	Location	<i>mm</i>
West	West	North-most	-49.2
West	West	North of center	-48.9
West	West	Center	-49.9
West	West	South-Most	-44.2
East	East	North-most	17.3
East	East	North of center	17.6
East	East	Center	15.5
East	East	South-Most	20.3

Load results

STH-164 Pier strain measurement data were collected reliably. The constants input into the calculation of load were obtained from the calibration information provided by the manufacturer of the strainmeters and the testing performed at the structure to determine (Table 3.11). The north abutment of STH-164 was instrumented after strainmeters were installed at the pier. Construction site accessibility prevented the data logger from being connected permanently at the time of abutment strainmeter installation. Table 3.12 details the constants used when calculating the load experienced by the abutment.

Table 3.11 STH-164 Bridge Pier structural load calculation input information

	Channel	1	2	3	4
Sensor ID Number	ID	6904	6905	6906	6907
Gage Factor	GF	0.345	0.352	0.35	0.344
Gage Offset	GO	0	0	0	0
Zero Reading	ZR	6892	7094	7117	6988
Temperature at Zero Reading	T0	21.1	20.8	20.8	21.1

Structural Dimensions	Units	Variable	Footing	Column
Area	m ²	A	18.116	1.394
Length	m	L	4.572	1.524
Width	m	B	3.962	0.914
Height	m	H	0.914	4.267
L/B	m/m	L/B	1.154	1.667
Influence Factor	m/m	I	5.939	7.012
Rectangular area coefficient	m/m	C	0.940	0.926

Material Properties				
Coefficient of Expansion, Steel	ppm/°C	K _{steel}	12.2	12.2
Coefficient of Expansion, Steel and Concrete	ppm/°C	K _{composite}	2.2	2.2
Elastic Modulus of Concrete	MPa	E _{50,c}	40341	40341
Elastic Modulus of Soil	MPa	E _{soil}	100	100
Poisson's ratio	unitless	v	0.25	0.25

Table 3.12 STH-164 Bridge abutment structural load calculation input information

	Channel	1	2	3	4
Sensor ID Number	ID	6909	6910	6911	6912
Gage Factor	GF	0.349	0.35	0.34	0.35
Gage Offset	GO	0	0	0	0
Zero Reading	ZR	6951	6878	7047	7038
Temperature at Zero Reading	T0	20.8	20.8	20.9	20.8

Structural Dimensions	Units	Variable	Footing	Column
Area	m ²	A	49.332	12.181
Length	m	L	11.989	11.989
Width	m	B	4.115	1.016
Height	m	H	0.914	5.664
L/B	m/m	L/B	2.914	11.800
Influence Factor	m/m	I	8.709	13.075
Rectangular area coefficient	m/m	C	0.893	0.703

Material Properties				
Coefficient of Expansion, Steel	ppm/°C	K _{steel}	12.2	12.2
Coefficient of Expansion, Steel and Concrete	ppm/°C	K _{composite}	2.2	2.2
Elastic Modulus of Concrete	MPa	E _{50,c}	41224	41224
Elastic Modulus of Soil	MPa	E _{soil}	100	100
Poisson's ratio	unitless	ν	0.25	0.25

Load experienced by the instrumented STH-164 Pier column is plotted versus time in Figure 3.21. The increase in load at the beginning of the monitoring process resulted from the ongoing construction at the site (from the beginning of monitoring until the end of October 2011). After that, the load throughout the column appears to be relatively uniform and constant. However from October 2011 until the end of the observation period, the measured load goes through cycles of valleys and peaks with a periodicity of about 1.5 year but with overall increase in loads. At the beginning of 2012, the loads measured by the different strainmeters diverges and yields the largest range

between the sensors. The increase in response of sensors over time may have been the result of the strainmeters' response deterioration or due to internal stressed caused by the continuing curing of the concrete. While each sensor's appear to mirror the increase and decrease by the other sensors in the column, sensor 6905 appears to drift away and the measure load value drops. Poor prediction of the battery life caused the data logger at STH-164 Pier to stop recording in March and October 2011 until the power source was replaced.

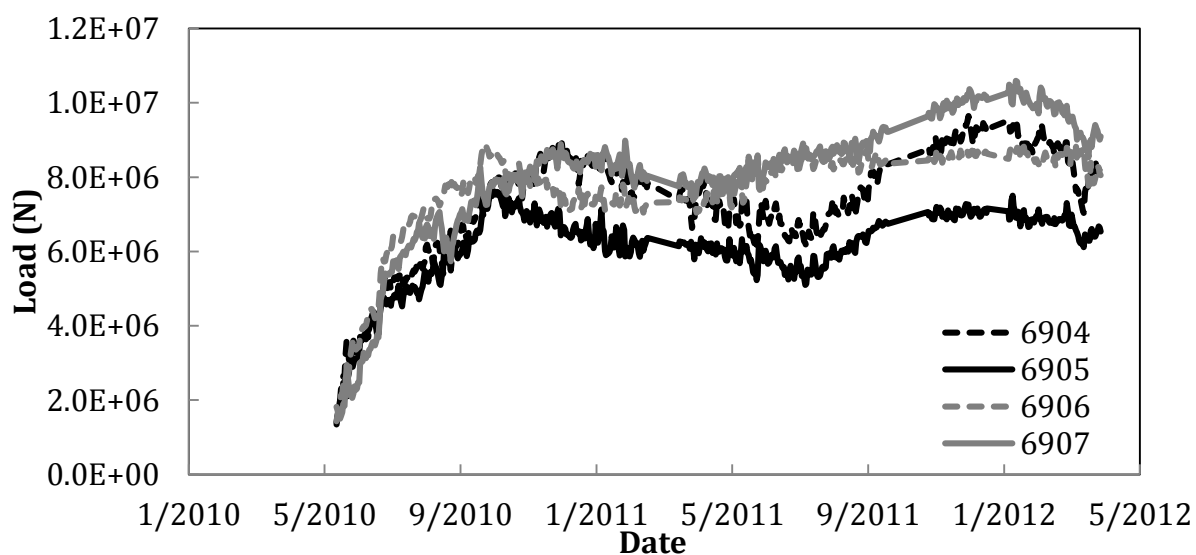


Figure 3.21 Load sensed by the STH 164 Bridge pier over time

The load measured in the STH 164 Bridge Abutment appears influenced significantly by the location of the sister bar strain gage (Figure 3.22). The two strainmeters that are located nearest the exposed face of the abutment wall, 6911 and 6912, show very similar loading trends and load amounts. Sensor 6910 is located nearest the backfill and experienced loads approximately $6.0 \cdot 10^7$ N less than the other sensors. Construction activities severed the cable between strainmeter 6909 and the data logger

and regrettably the cable was not accessible for repair. The difference in the response between strainmeter may indicate the effect of the eccentric loads caused by the horizontal forces (i.e., earth pressures against the abutment wall) acting along the vertical self-weight and service loads. Note that the response of strainmeter 6911 and 6912 are 180 degree out of phase with respect to the response of the strainmeter 6910. Also that the responses seen after October 2010 in the abutment closely follow the response of the strainmeters 6904 and 6905 in the column of the STH 164 bridge (Figure 3.21).

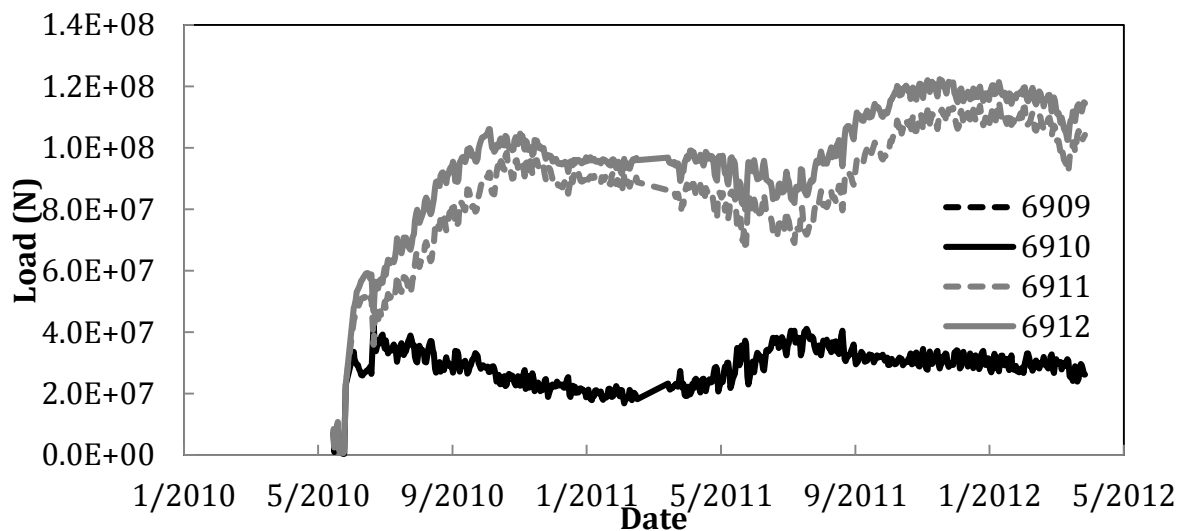


Figure 3.22 Load experienced by the STH 164 Bridge abutment over time

3.9 Lien Road Bridge Results

Settlement results

Settlement measurements at the Lien Road Bridge did not begin until after the structure was completed and open for service. The movement of the instrumented column at the Lien Road Bridge appears to be occurring as a tilt of the structure and thus a tilting of the foundation footing (Table 3.13). The delays in establishing a baseline survey prevent a definitive conclusion about the movements of survey markers relative to the position of the structure during construction.

Table 3.13 Lien Road Bridge settlement results. (Negative values indicate settlements).

 Level	 Fixed Point	 Survey Marker	Settlement
Location	Location	Location	<i>mm</i>
Center	East	East	7.7
Center	West	West	-2.0

Load results

The Lien Road Bridge structure was the last to be instrumented. The data collection from the strainmeters was frequently interrupted while the site was under construction. The construction site had experienced thefts of equipment over night, so the data logger had to be installed at the beginning of each day and removed at the end of the work day. A semi-truck collided with the west edge of the bridge deck, north of the instrumented column while the bridge was under construction. After the collision, the data logger was removed from the site until the integrity of the structure was confirmed.

The constants input into the calculation of load were obtained from the calibration information provided by the manufacturer of the strainmeters and the testing performed at the structure (Table 3.14).

Table 3.14 the Lien Road Bridge structural load calculation input information

	Channel	1	2	3	4
Sensor ID Number	ID	6903	6908	4642	1540
Gage Factor	GF	0.349	0.35	0.341	0.346
Gage Offset	GO	0	0	0	0
Zero Reading	ZR	7006	7077	6873	7125
Temperature at Zero Reading	T0	20.8	20.8	21.3	21.7

Structural Dimensions	Units	Variable	Footing	Column
Area	m ²	A	13.941	1.858
Length	M	L	3.734	1.524
Width	M	B	3.734	1.219
Height	M	H	0.914	3.874
L/B	m/m	L/B	1.000	1.250
Influence Factor	m/m	I	5.538	6.168
rectangular area coefficient	m/m	C	0.944	0.937

Material Properties

Coefficient of Expansion, Steel	ppm/°C	K _{steel}	12.2	12.2
Coefficient of Expansion, Steel and Concrete	ppm/°C	K _{composite}	2.2	2.2
Elastic Modulus of Concrete	MPa	E _{50,c}	39403	39403
Elastic Modulus of Soil	MPa	E _{soil}	100	100
Poisson's ratio	unitless	ν	0.25	0.25

Load experienced by the instrumented column is plotted versus time Figure 3.23. The initial increase in load correlated with loads being added to the structure as construction progressed. The data logger was returned to the bridge site in early 2011. Shortly

following the reinstallation, the data logger was reported as a 'suspicious package' to law enforcement and was again removed. Researchers collaborated with WisDOT to create a solution that would allow the data logger to remain at the Lien Road Bridge location without causing additional alarm. The data logger was reinstalled once a protective, clearly labeled container was allowed to be placed at the column. The data logger has remained at the site; the final section of missing data resulted from a programming error while the data were downloading.

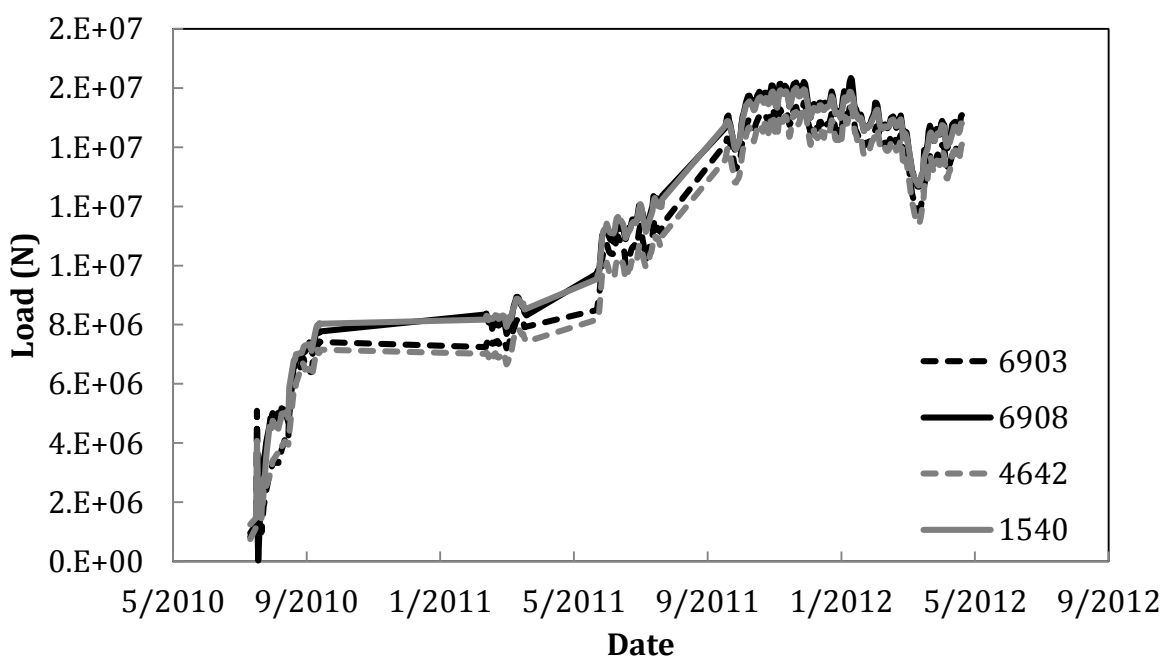


Figure 3.23 Load experienced by the the Lien Road Bridge column over time

The loads measured at the beginning of instrumentation are less than the loads experienced by the Lien Road Bridge in spring 2012, but repeated interruptions to the data collection prevent conclusions about the rate of loading increase. The load

experienced at each sensor is approximately equal and the increase and decrease of the load in each sensor matches the increase and decrease of the other sensors. There does not appear to be a difference between the sensors based on their relative locations within the column.

3.10 Highway 51 Bridges - Deformation Results

While the first three structures were instrumented to document the response of the abutment and columns founded to construction and service loads, the monitoring of deformations of the structures were limited due to problems with the establishment of bench marks and monitoring points. Furthermore, due to limited number of measurements only vertical settlements were documented and the quality of these results were suspected due to the problems coordinating with contractors, establishing target points, and setting fixed points within the construction area. In an attempt to improve these measurements, the three bridges along the Highway 51 were monitored to assess both the vertical and horizontal deformations of the bridges during operation. Monitoring points were established on the abutment, deck, and approach roads of all three bridges while fixed points were located close to the right of way boundaries. These three bridges were located along a 6.5 km (4.5 mi.) stretch of road on WI Highway 51 (Figure 3.2). While these bridges are not identical (i.e., different sizes, spans, and deep foundation depths), they are exposed to similar traffic loads, environmental conditions (temperature and rain), and there were open to traffic within a year of each other.

Bear Tree Road Bridge

This bridge is founded onto small 3-m (10-ft) H-piles into a variable foundation soils with several layers heterogeneous distributions top soils, silt, sand and gravelly sand and bedrock at 4.7 m (15.5 ft) below grade level. The results subsurface exploration borings are show in Figure 3.24. Please note that the in situ testing includes mainly SPT results that are used mostly to determine strength parameters in soils. While the use of

SPT values for the design of foundation systems is common in transportation design practice, SPT results have limited use the in modelling of geotechnical structure responses.

The results from the monitoring are shown in Figures 3.25 to 3.30, a summary of the results is also presented in Tables 3.15 to 3.17. Figure 3.25 shows the vertical deformation of the abutment walls, showing a clear downward trend, with in maximum deformation of less than -1.9 cm. To compare, a simple estimation of elastic settlement for a single end bearing pile, and assuming homogeneous conditions, can be performed:

$$s_e = \frac{Q_a}{rE_s} \left(\frac{1-v^2}{2} \right) \quad 3.1$$

where Q_a is the allowable load, r is the radius of the pile, E_s is the soil's elastic modulus, and v is the soil's Poisson's ratio. Using a load of 320 kN, a radius of 0.13 m, a soil's elastic modulus of 60 MPa, and a Poisson's ratio of 0.3, the estimated settlement of a single pile is 1.87 cm, which provides an order of magnitude to the measured vertical deformations.

Figure 3.26 shows the vertical deformation of the deck, while Figures 3.27 and 3.28 show the vertical deformation for the north and south approaching roadways respectively. The deformations for these sections show similar trends. In general, the last reading shows an upward movement, which could be due to soil expansion or relaxation of the over consolidated soils of the area.

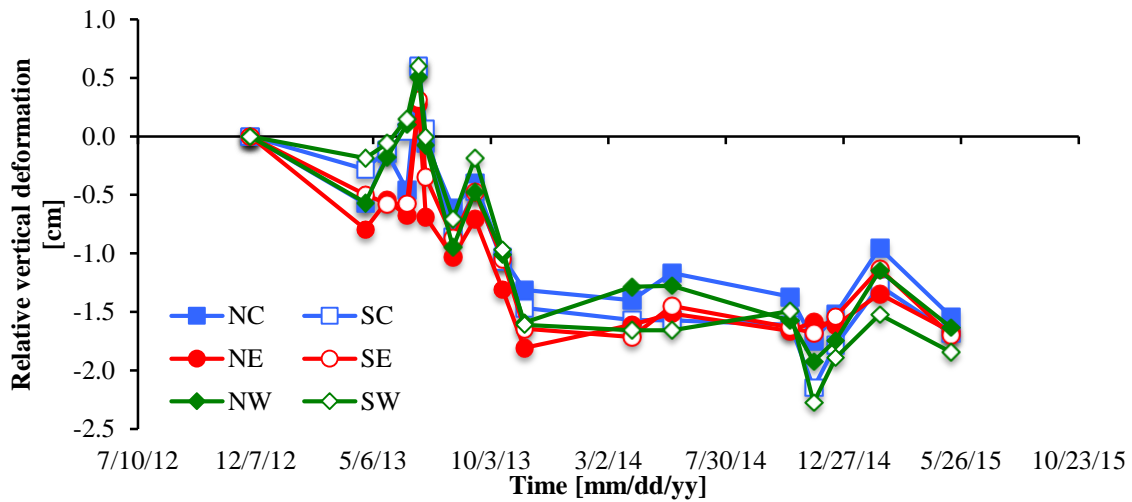


Figure 3.25 Relative vertical deformation on the abutment walls. Positive values correspond to upward movement.

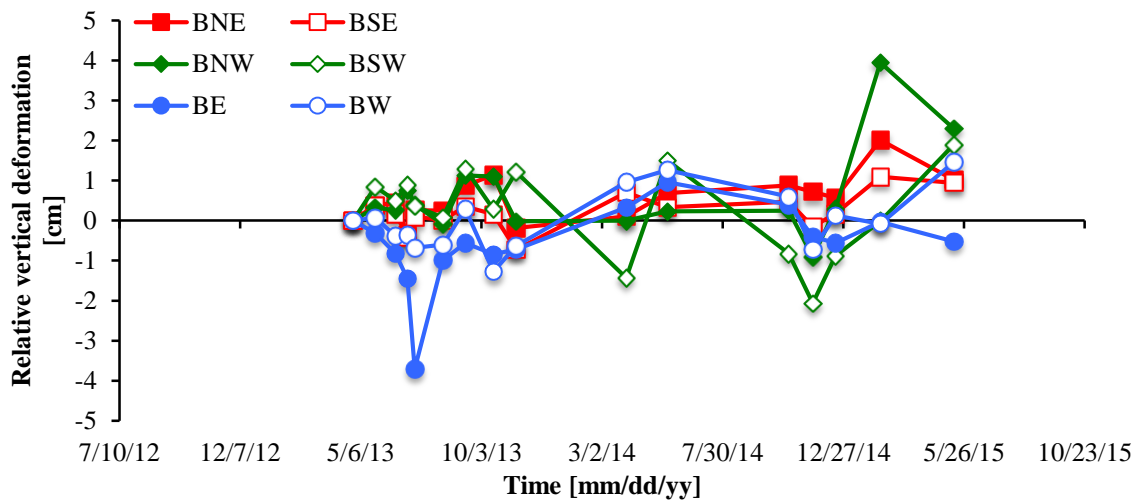


Figure 3.26 Relative vertical deformation on the bridge deck. Positive values correspond to upward movement.

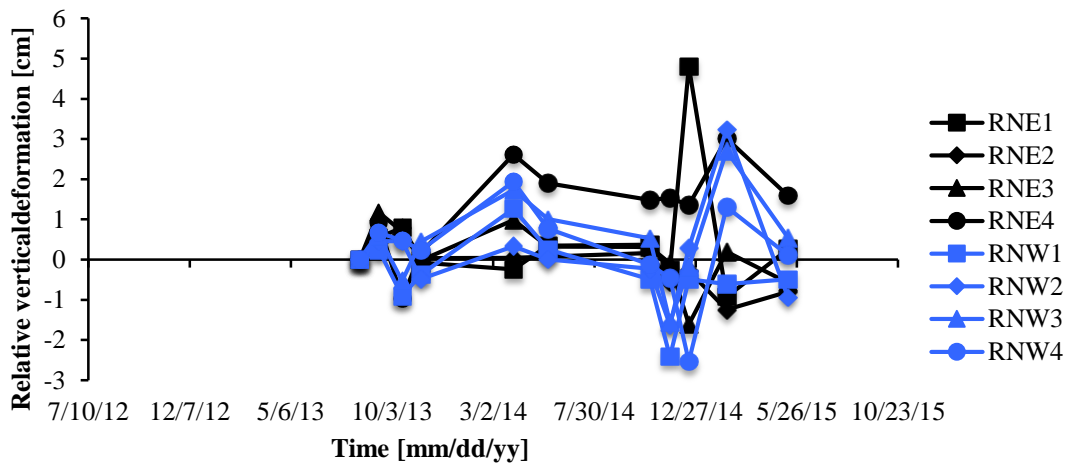


Figure 3.27 Relative vertical deformation on the north approaching road. Positive values correspond to upward movement.

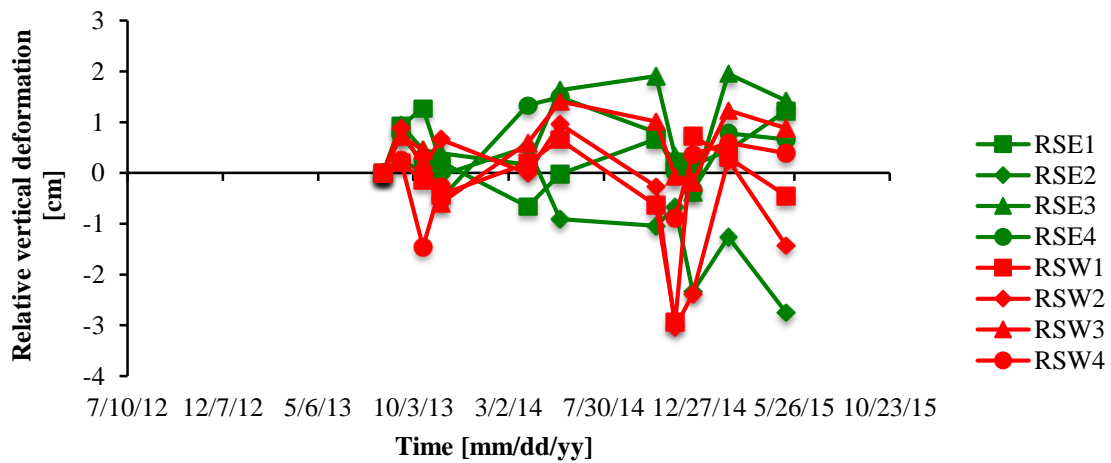


Figure 3.28 Relative vertical deformation on the south approaching road. Positive values correspond to upward movement.

Table 3.15 Summary of relative vertical deformations for the Highway 51 Bridge over Bear Tree Road. Positive values indicate upward movement.

Surveying point/section	Relative vertical deformations [cm]			
	NW	NE	SE	SW
Abutment wall	-1.63	-1.67	-1.70	-1.84
Deck	2.30	1.02	0.94	1.89
Road1	-0.49	0.26	1.23	-0.45
Road2	-0.94	-0.80	-2.75	-1.43
Road3	0.54	-0.58	1.42	0.88
Road4	0.11	1.59	0.66	0.39

Table 3.16 Summary of relative lateral deformations on the abutment wall with respect to the reference point.

Surveying point/section	Relative lateral deformations [cm]			
	NC	NE	SC	SE
Abutment wall	1.95	2.72	0.11	0.08

Table 3.17 Summary of relative lateral deformations on the abutment wall with respect to the NC surveying point.

Surveying point/section	Relative lateral deformations [cm]				
	NE	SE	NW	SW	SC
Abutment wall	-1.00	-1.19	0.11	-2.41	-1.32

The lateral deformation of the abutment walls is shown in Figures 3.29 and 3.30. The lateral deformation shows that NC and NE points have moved away from the reference point, which would correspond to an outward movement of the wall at these points. The SC and SE points show barely any movement with respect to the reference point, indicating little lateral deformation. The NW and SW points are calculated with respect to the NC point, as these points are not visible when shooting the reference point. Both of the points show an outward movement.

In general the behavior of the lateral deformations could be attributed to the change in temperature and resulting contraction and expansion of the backfill soil, as well as the load applied by the traffic, resulting in a net outward movement of the points on the abutment walls.

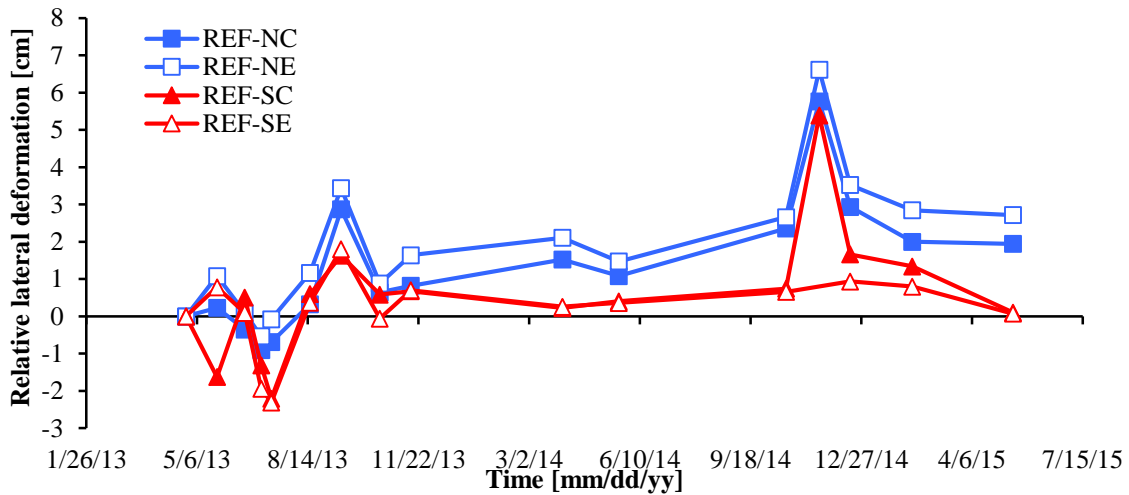


Figure 3.29 Relative lateral deformation on the abutment wall with respect to the reference point.

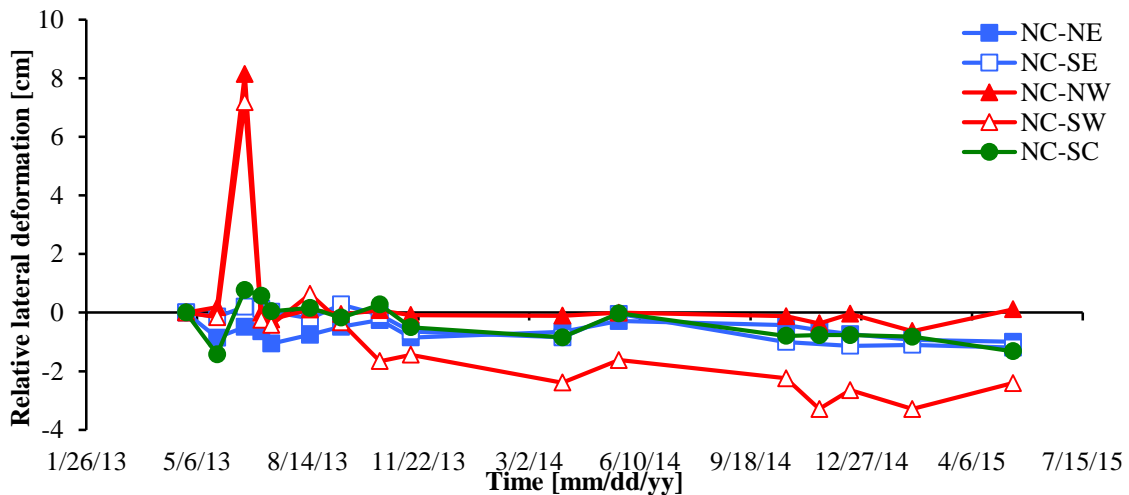


Figure 3.30 Relative lateral deformation on the abutment wall with respect to the NC surveying point.

In order to assess the quality of the data, relative measurements of the different points of the structures were plotted against each other and compared against environmental conditions: rain and temperatures. The results are presented in Figures 3.31 to 3.35. These figures summarize the complexity of the results. While there seems to be a trend between neighboring measurements: (do not consider outliers as they typically fall in the very cold days), the correlation with environmental forces is not as clear.

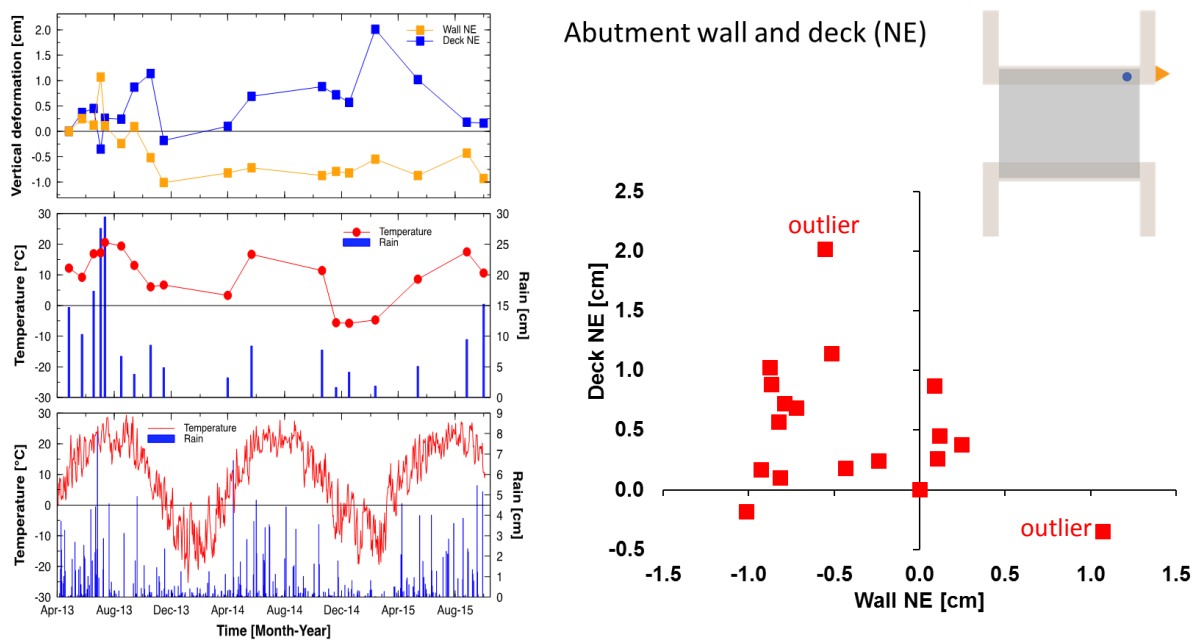


Figure 3.31: Bear Tree Road Bridge. Comparison of relative settlement of NE abutment wall and deck versus temperature (at the time of measurement and daily average) and rain fall (one month cumulative and daily total).

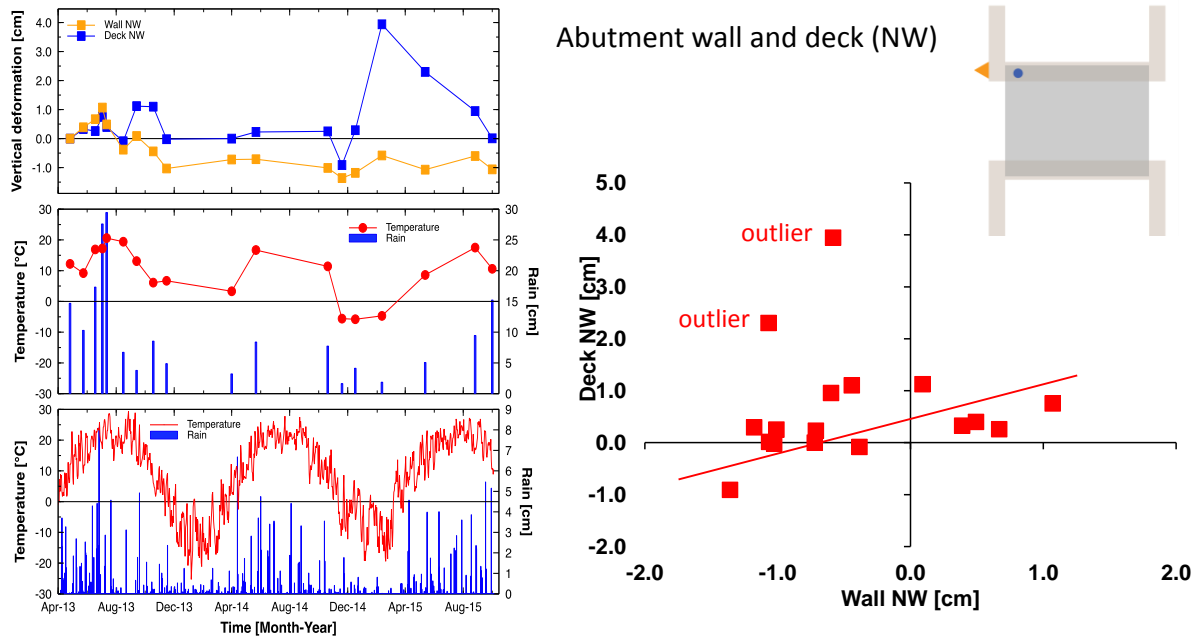


Figure 3.32: Bear Tree Road Bridge. Comparison of relative settlement of NW abutment wall and deck versus temperature (at the time of measurement and daily average) and rain fall (one month cumulative and daily total).

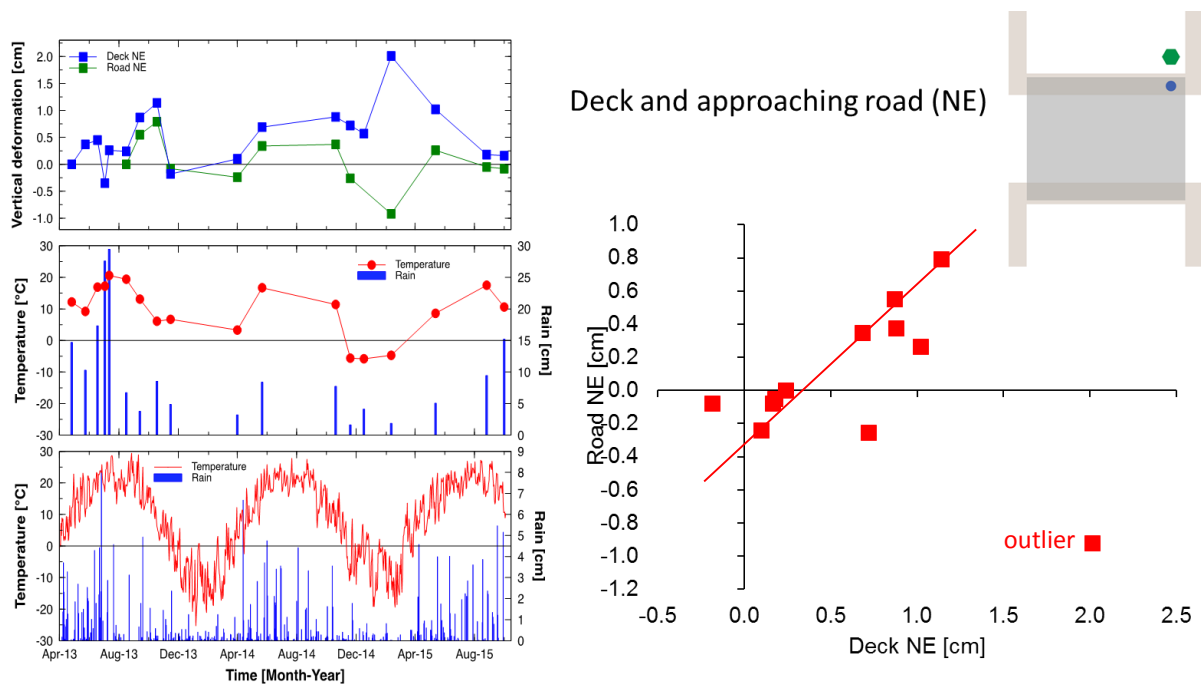


Figure 3.33: Bear Tree Road Bridge. Comparison of relative settlement of NE deck and approaching road versus temperature (at the time of measurement and daily average) and rain fall (one month cumulative and daily total).

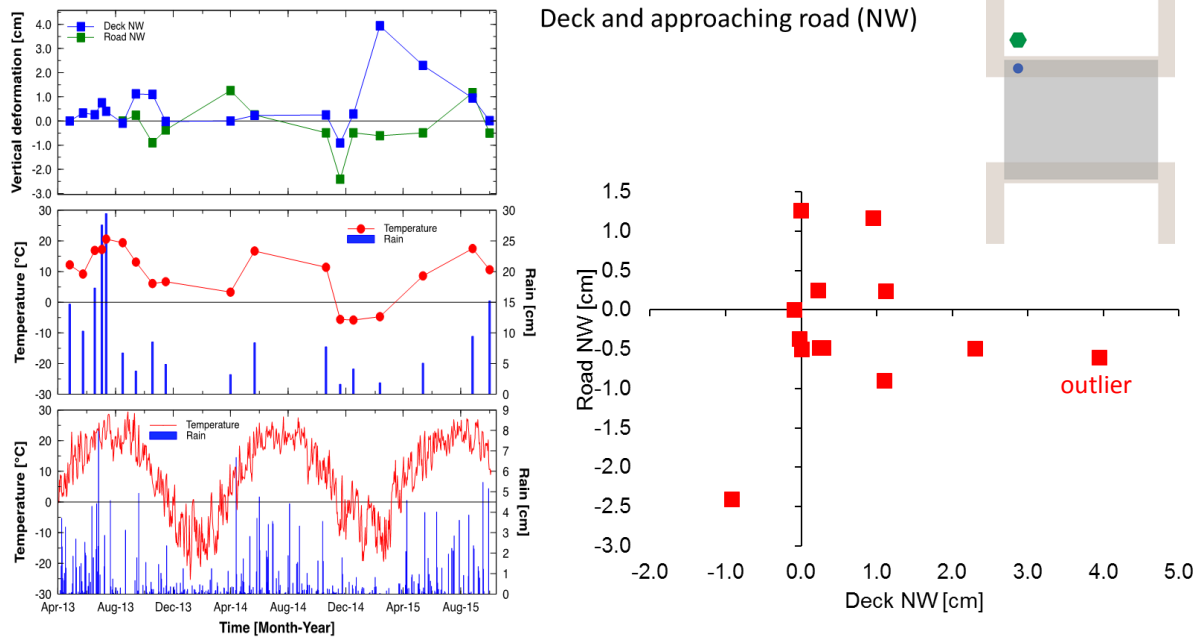


Figure 3.34: Bear Tree Road Bridge. Comparison of relative settlement of NW deck and approaching road versus temperature (at the time of measurement and daily average) and rain fall (one month cumulative and daily total).

Windsor Road Bridge

Figure 3.35 summarizes the results of the geotechnical investigation performed on the foundation soil at the site of the foundation bridge. The figure also document the designed depth of the H-piles supporting the abutments (12.2 m and 15.24 m / 40 ft. and 50 ft. deep) and center columns (6.1 m / 20 ft. deep). The boring show very heterogeneous foundation soils with layers of top soil, sandy clay, sand, gravelly sand and gravel. All these soils overlay sandstone at the site (but the boring BOR-6 on the south-west). For all soils, SPT values are presented along with unconfined compression strength results for the sandy clay soils (The SPT results for clayey soils should be considered suspect at best and should not be used for modeling or design).

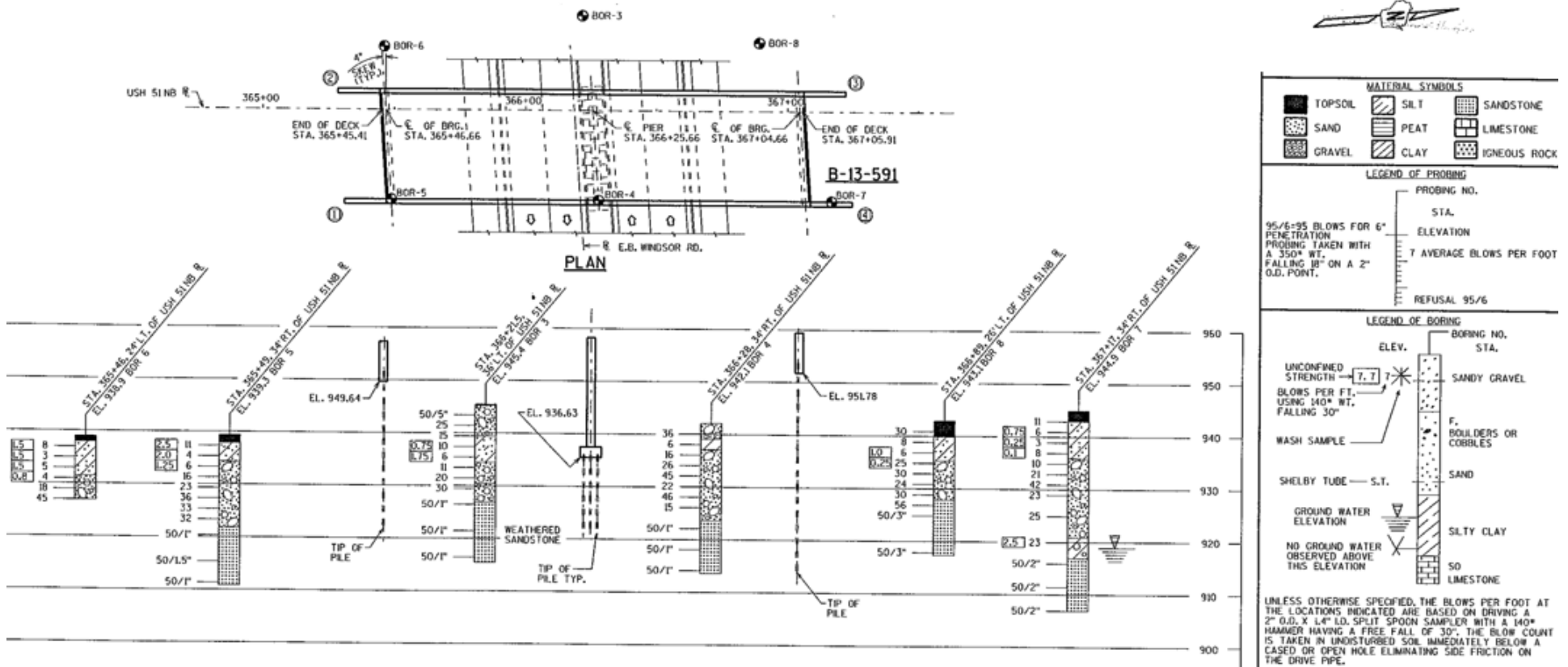


Figure 3.35 Subsurface exploration data for the bridge over Windsor Road.

The displacement results from the monitoring are shown in Figures 3.36 to 3.41 and a summary of the results is presented in Tables 3.18 to 3.19. All of the sections show very similar deformation trends. A similar estimation for the settlement (Equation 3.1), like as shown before, can be performed for this bridge, with the difference that the piles for this bridge reach to the sandstone bedrock, which is a much stiffer material than the sand and gravel bearing layers for the other two bridges and therefore should constrain the measured foundation settlements. The upward and downward deformations shown by all the sections could be caused in part by the expansion and contraction of the soil as temperature changes due to a relaxation of the overconsolidated soils in the area.

Table 3.18 Summary of relative vertical deformations for the Windsor road bridge. Positive values indicate upward movement.

Surveying point/section	Relative vertical deformations [cm]			
	NW	NE	SE	SW
Abutment wall	1.65	1.49	3.18	1.22
Deck	0.77	0.09	-0.55	0.58
Road1	-0.30	0.40	0.56	-0.52
Road2	-0.66	-1.21	-1.03	-3.16
Road3	0.33	-0.50	-2.52	-5.89
Road4	0.58	0.07	-1.68	-1.18

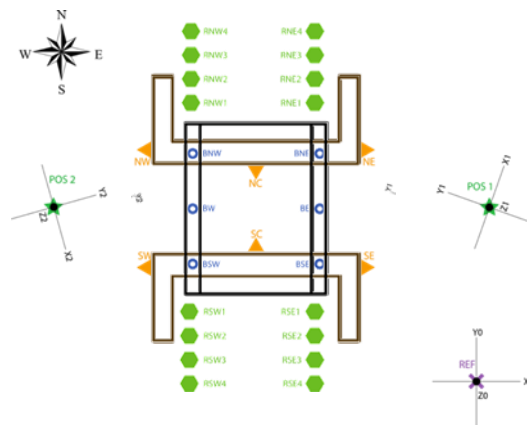


Table 3.19 Summary of relative lateral deformations on the abutment wall with respect to the reference point.

Surveying point/section	Relative lateral deformations [cm]			
	NC	NE	SC	SE
Abutment wall	0.32	0.65	-0.73	-1.48

Table 3.20 Summary of relative lateral deformations on the abutment wall with respect to the NC surveying point.

Surveying point/section	Relative lateral deformations [cm]				
	NE	SE	NW	SW	SC
Abutment wall	-0.05	-1.77	0.04	-2.66	-0.87

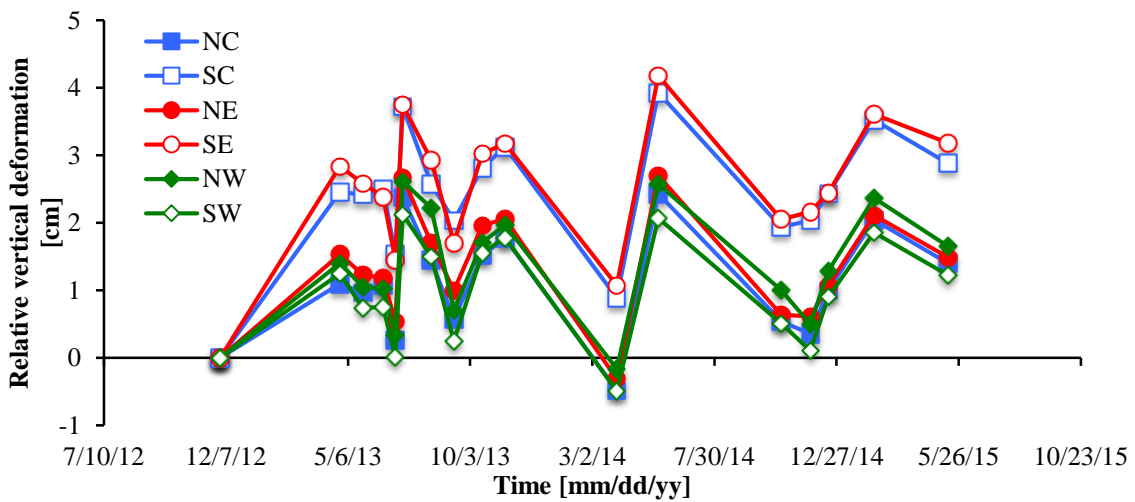


Figure 3.36 Relative vertical deformation on the abutment walls. Positive values correspond to upward movement.

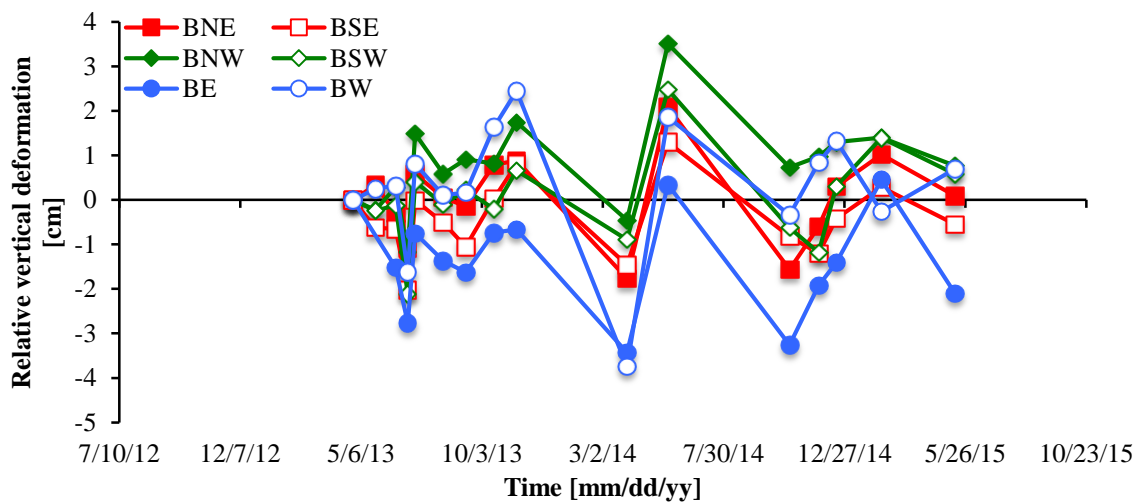


Figure 3.37 Relative vertical deformation on the bridge deck. Positive values correspond to upward movement.

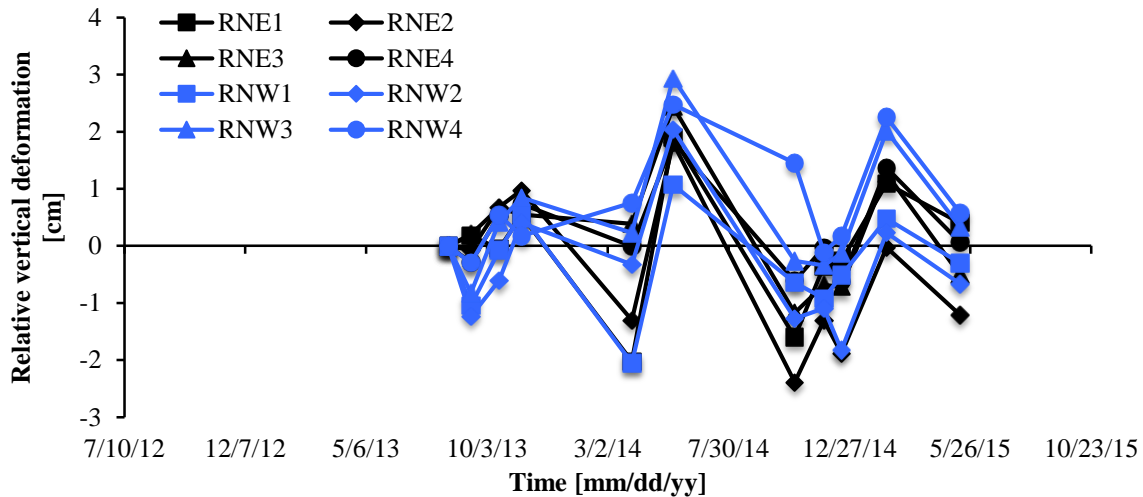


Figure 3.38 Relative vertical deformation on the north approaching road. Positive values correspond to upward movement.

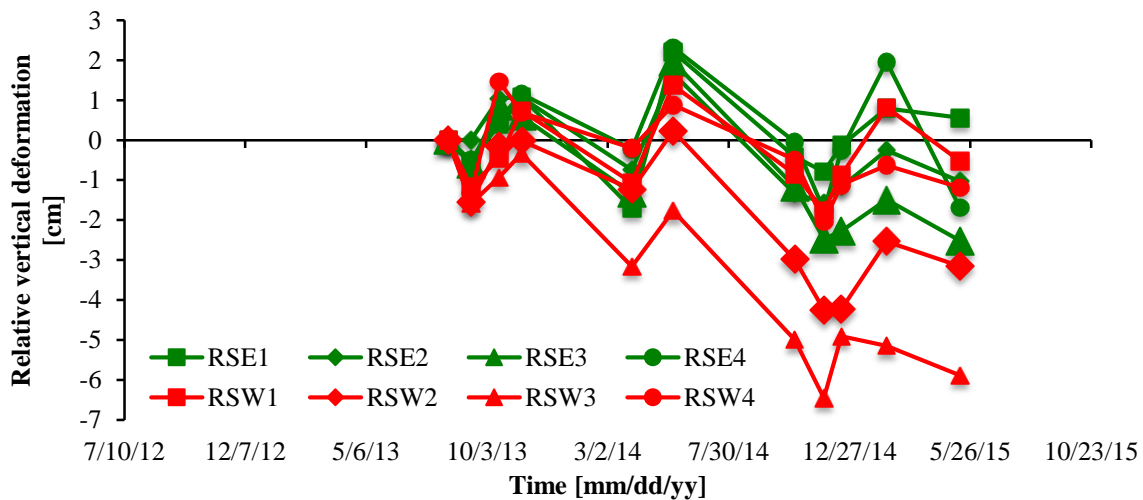


Figure 3.39 Relative vertical deformation on the south approaching road. Positive values correspond to upward movement.

The lateral deformations of the abutment walls are shown in Figures 3.39 and 3.40. The lateral deformation shows that NC and NE points have moved away from the reference point, while the SC and SE points show a shortening of the distance between

them and the reference point, all of which would correspond to an outward movement of the wall at these points. The NW and SW points are calculated with respect to the NC point, as these points are not visible when shooting the reference point. Both of the points show an outward movement, as the NW is moving away from the NC and the SW is moving closer to the NC.

Similar to the Bear Tree Road Bridge, the behavior of the lateral deformations could, in part, be attributed to the change in temperature and resulting contraction and expansion of the backfill soil, as well as the load applied by the traffic and potential changes in the moisture of the embankment and foundation soils, resulting in a net outward movement of the points on the abutment walls.

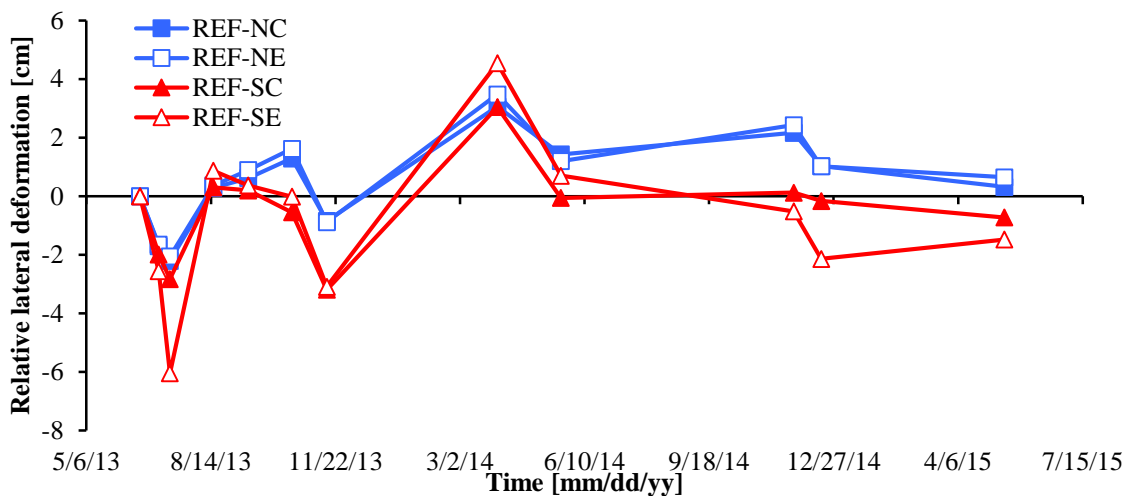


Figure 3.40 Relative lateral deformation on the abutment wall with respect to the reference point.

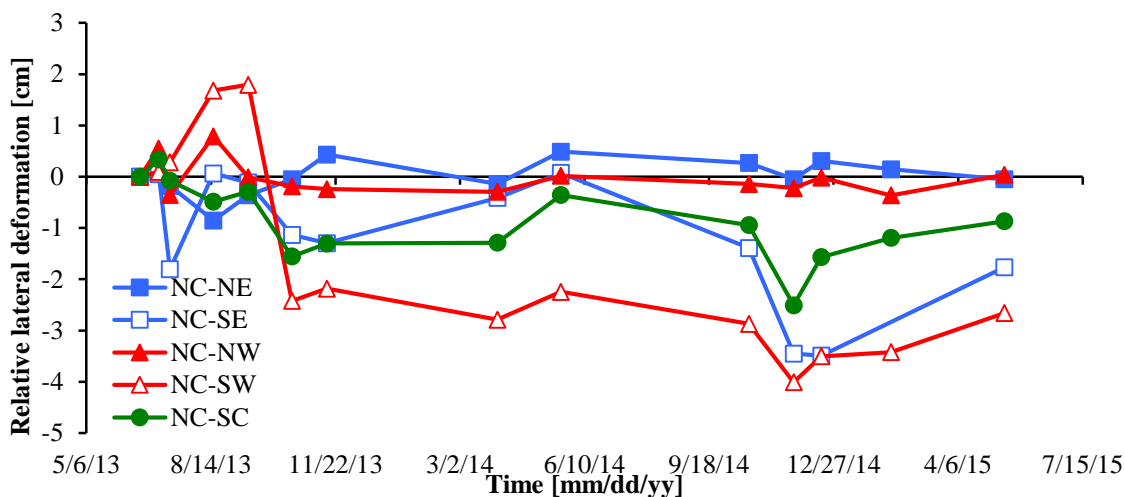


Figure 3.41 Relative lateral deformation on the abutment wall with respect to the NC surveying point.

To further evaluate the potential effect of environmental loads and to assess the relative quality of the measurement data, results were presented versus temperature and precipitation, and versus neighboring measuring points. Figures 3.42 to 3.45 present these data. The concept presented here is that due to compatibility of deformations, neighboring points across different structural elements should follow similar trends deformation trends. If the results are not correlated, there would be a gap in the structure or the measurement would be incorrect. For this bridge the displacement results are much more consistent than the results from the Bear Tree Road Bridge. For example there are no outlier data points and the trends in the data tend to follow the ambient temperature fairly closely. These data seem to support the hypothesis that bridges deforms due to environmental loads.

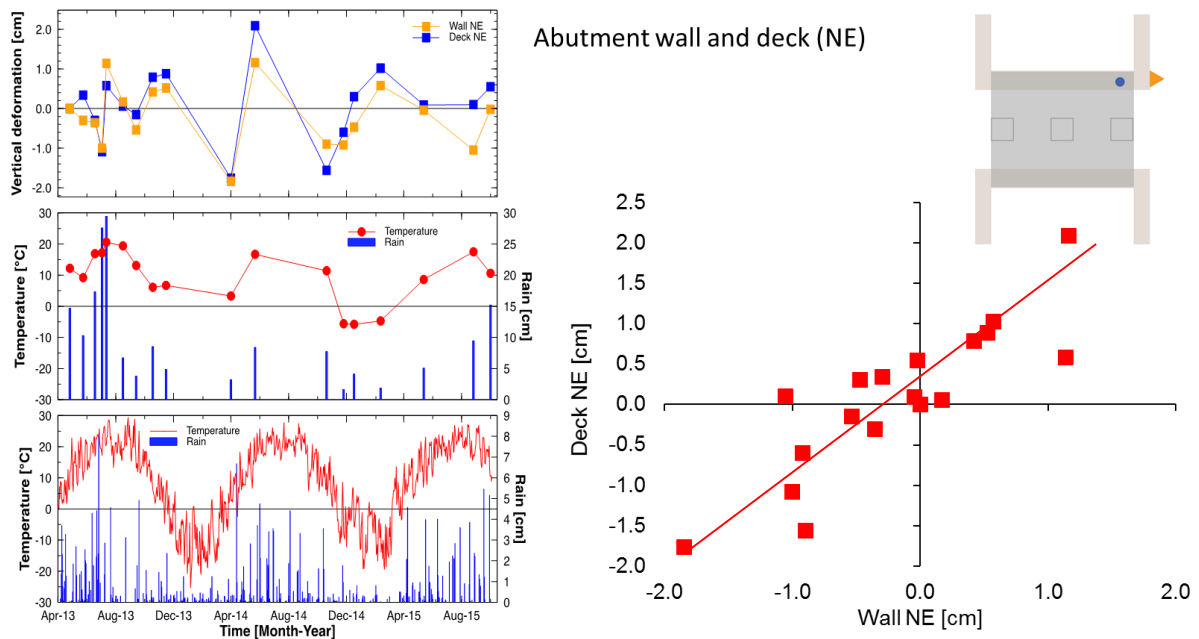


Figure 3.42: Windsor Road Bridge. Comparison of relative settlement of NE abutment wall and deck versus temperature (at the time of measurement and daily average) and rain fall (one month cumulative and daily total).

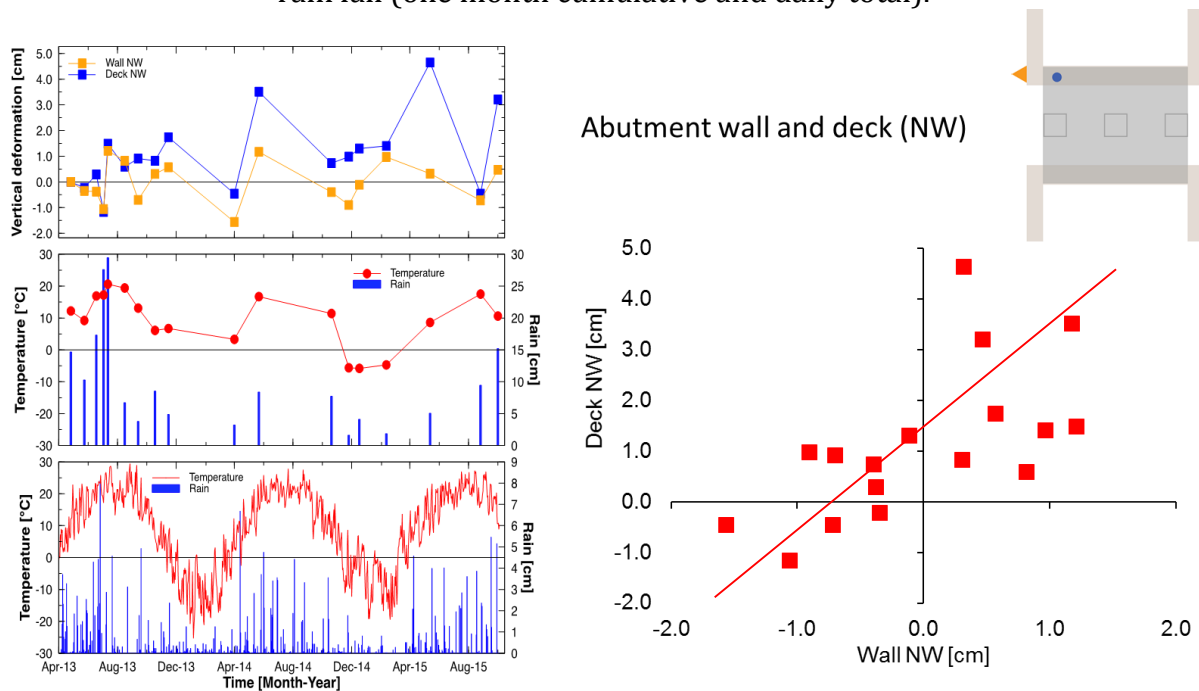
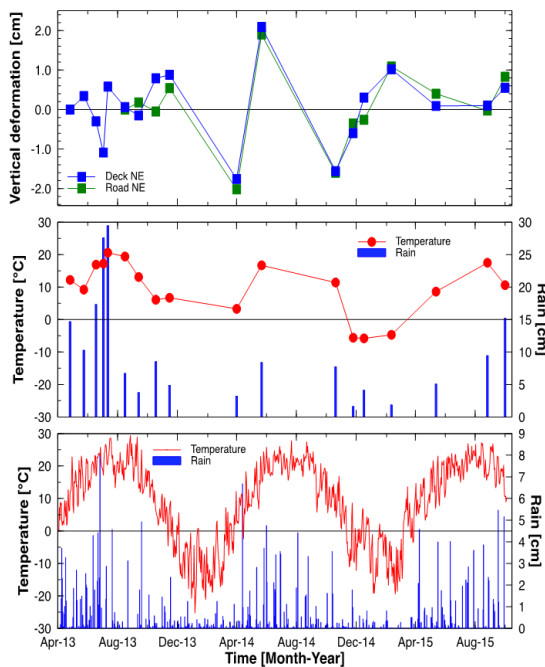


Figure 3.43: Windsor Road Bridge. Comparison of relative settlement of NW abutment wall and deck versus temperature (at the time of measurement and daily average) and rain fall (one month cumulative and daily total).



Deck and approaching road (NE)

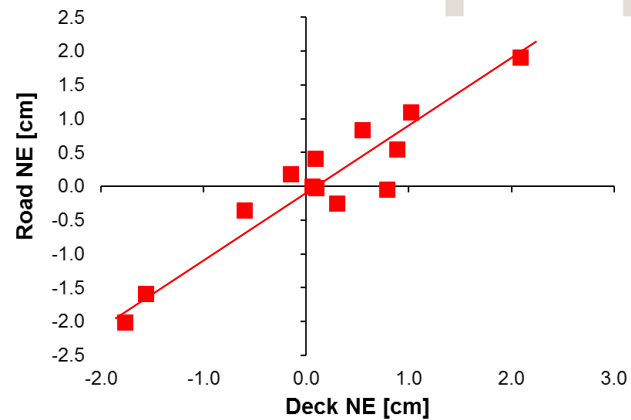
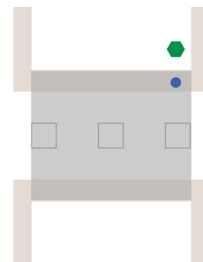
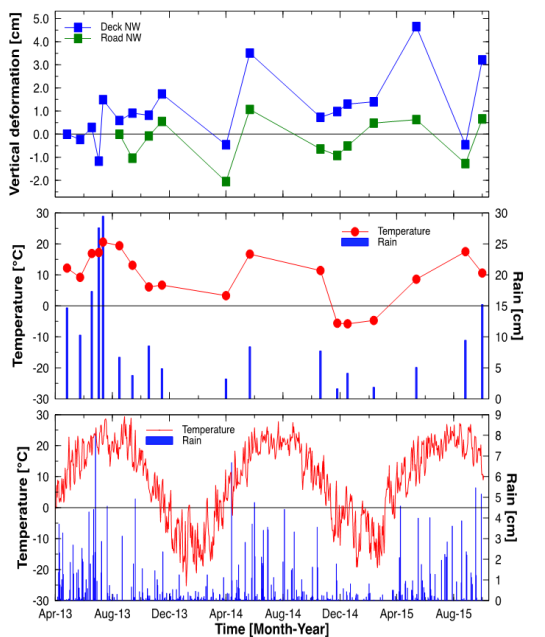


Figure 3.44: Windsor Road Bridge. Comparison of relative settlement of NE deck and road approach versus temperature (at the time of measurement and daily average) and rain fall (one month cumulative and daily total).



Deck and approaching road (NW)

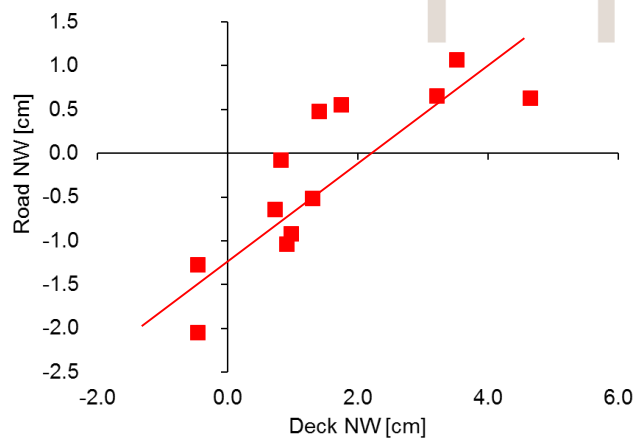
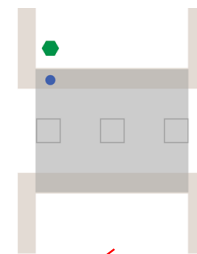


Figure 3.45: Windsor Road Bridge. Comparison of relative settlement of NW deck and road approach versus temperature (at the time of measurement and daily average) and rain fall (one month cumulative and daily total).

Vinburn Road Bridge

The subsurface exploration results for the bridge structure over the Vinburn Road are shown in Figure 3.46. The foundation soils at this site appear to be more homogeneous than the soils at the other two bridge structures on Highway 51. The two soil explorations show top soils, a pocketed silt, and a gravel layer as thick 12.2 m (40 ft.) at the deepest boring. Weathered sandstone was found at a depth of 12.2 m (40 ft.) at the south most boring. The abutment of this bridges are founded on H-piles with approximately design depths of 7.6 and 10.7 m (25 and 35 ft.). The strength of the foundation soil was documented with SPT numbers (unconfined compression strength values were also given to pocket of silts in the foundation soil). No direct measurements of stiffness were provided.

The results from the monitoring are shown in Figures 3.47 to 3.50, a summary of the results is presented in Tables 3.21 to 3.23, and in general the different sections trend has been to settle over time. Given that the subsurface conditions are similar to the ones found under the Bear Tree Road Bridge (predominately made of sand and gravel layers), the estimation of settlement shown before could apply for this bridge as well, which would explain the observed deformations. These deformations could also be affected by the contraction and expansion of the underlying soils as the ambient temperature changes.

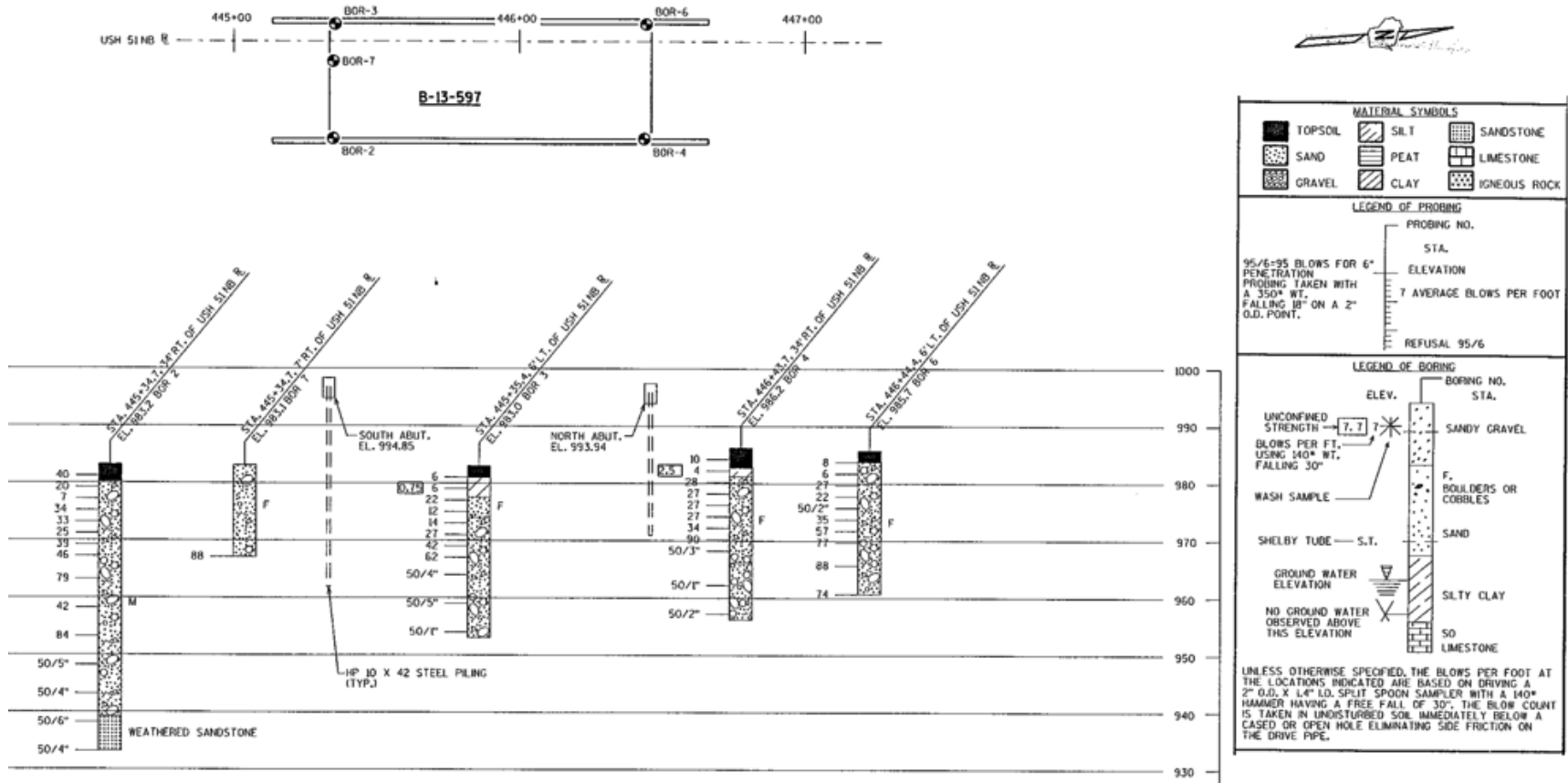


Figure 3.46: Subsurface exploration data for the bridge over Vinburn Road.

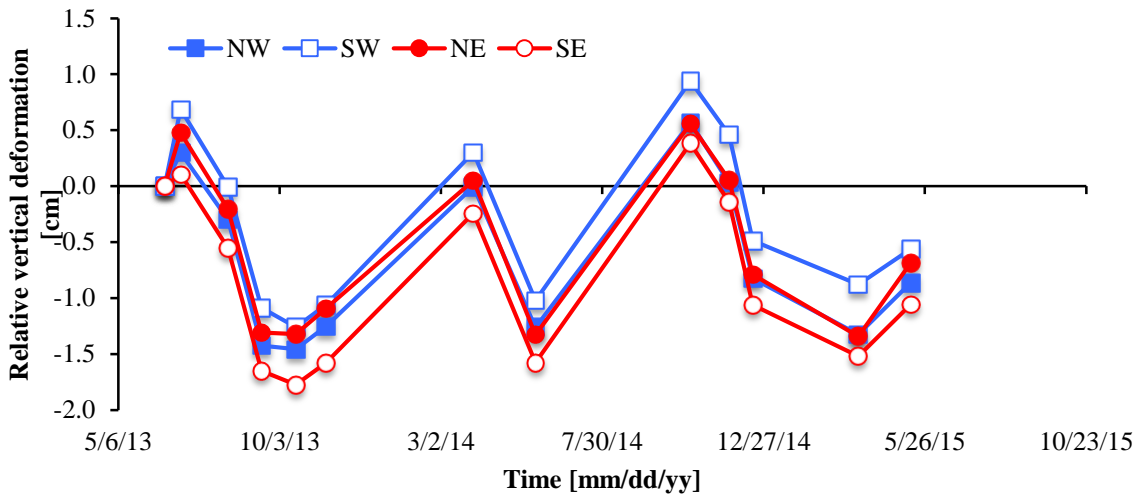


Figure 3.47: Relative vertical deformation on the abutment walls. Positive values correspond to upward movement.

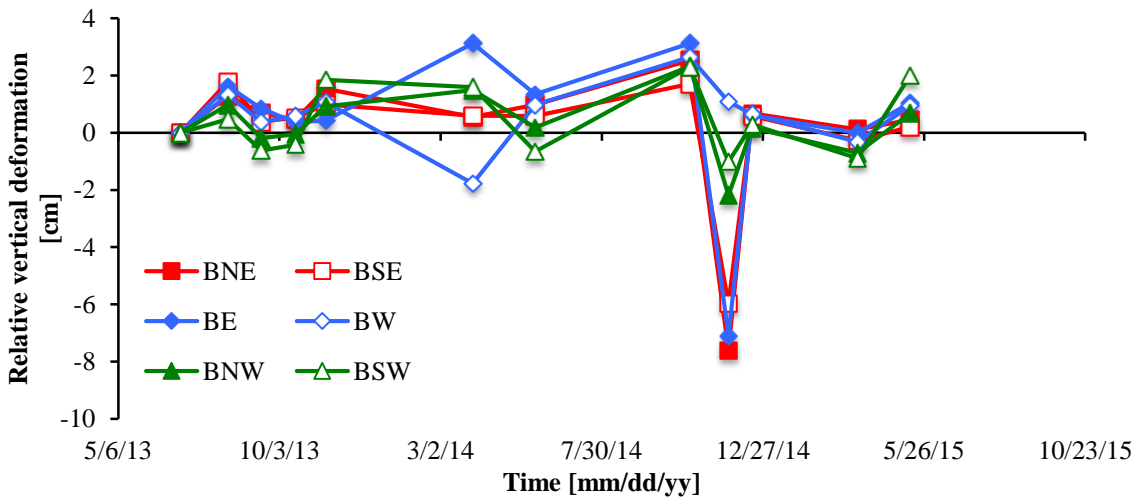


Figure 3.48: Relative vertical deformation on the bridge deck. Positive values correspond to upward movement.

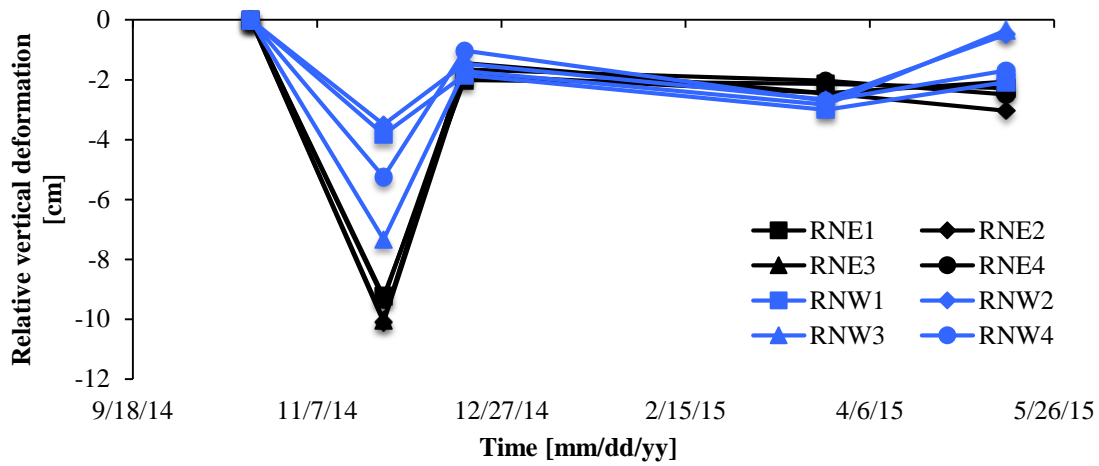


Figure 3.49: Relative vertical deformation on the north approaching road. Positive values correspond to upward movement.

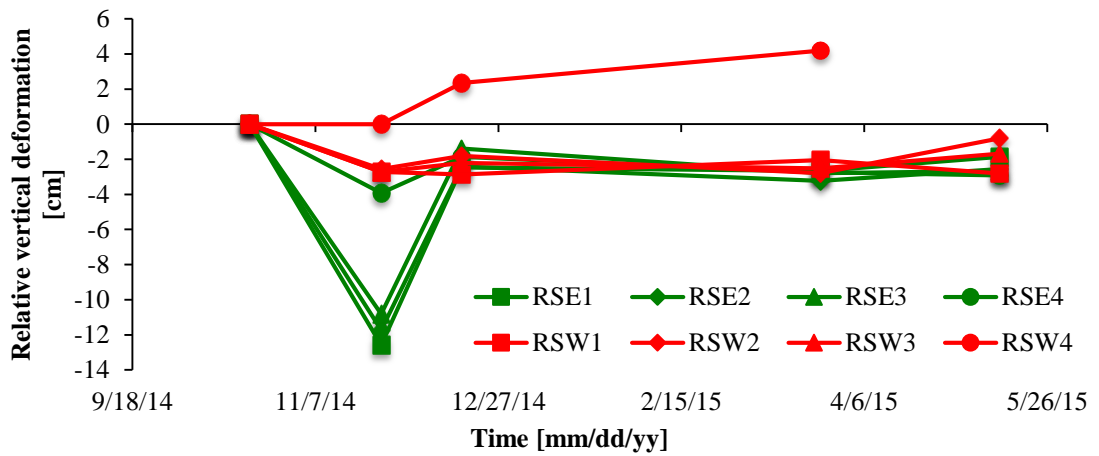


Figure 3.50: Relative vertical deformation on the south approaching road. Positive values correspond to upward movement.

Table 3.21 Summary of relative vertical deformations for the Vinburn Road Bridge. Positive values indicate upward movement.

Surveying point/section	Relative vertical deformations [cm]			
	NW	NE	SE	SW
Abutment wall	-0.86	-0.68	-1.06	-0.56
Deck	0.68	0.45	0.20	2.00
Road1	-2.08	-2.28	-1.86	-2.81
Road2	-0.48	-3.03	-2.55	-0.80
Road3	-0.34	-2.07	-2.66	-1.68
Road4	-1.69	-2.49	-2.92	4.19

Table 3.22 Summary of relative lateral deformations on the abutment wall with respect to the reference point.

Surveying point/section	Relative lateral deformations [cm]			
	NW	NE	SW	SE
Abutment wall	10.35	8.24	10.77	8.84

Table 3.23 Summary of relative lateral deformations on the abutment wall with respect to the NC surveying point.

Surveying point/section	Relative lateral deformations [cm]		
	NE	SW	SE
Abutment wall	-1.80	-5.16	-4.72

The lateral deformation measurements of the abutment walls is shown in Figures 3.50 and 3.51. The lateral deformation shows that all of the points have moved away from the reference point, which indicate an Eastward motion as the reference point is to the West of the bridge. When compared the movement of the NE, SW and SE points with respect to the NW point, the deformations show an outward movement of the SW and SE points and an inward deformation for the NE point, which could correspond to the presence of a soft spot or small void in the backfill area near this point.

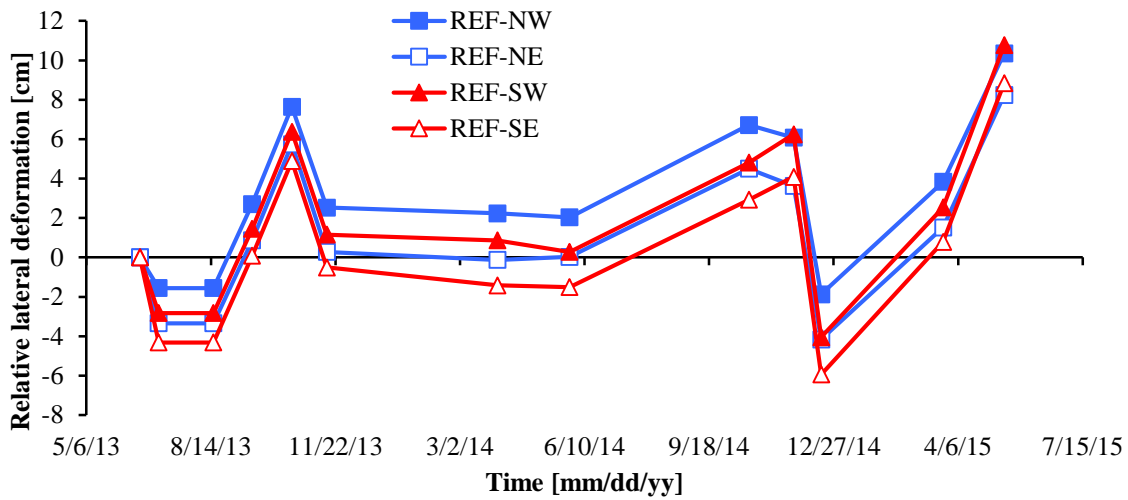


Figure 3.51: Relative lateral deformation on the abutment wall with respect to the reference point.

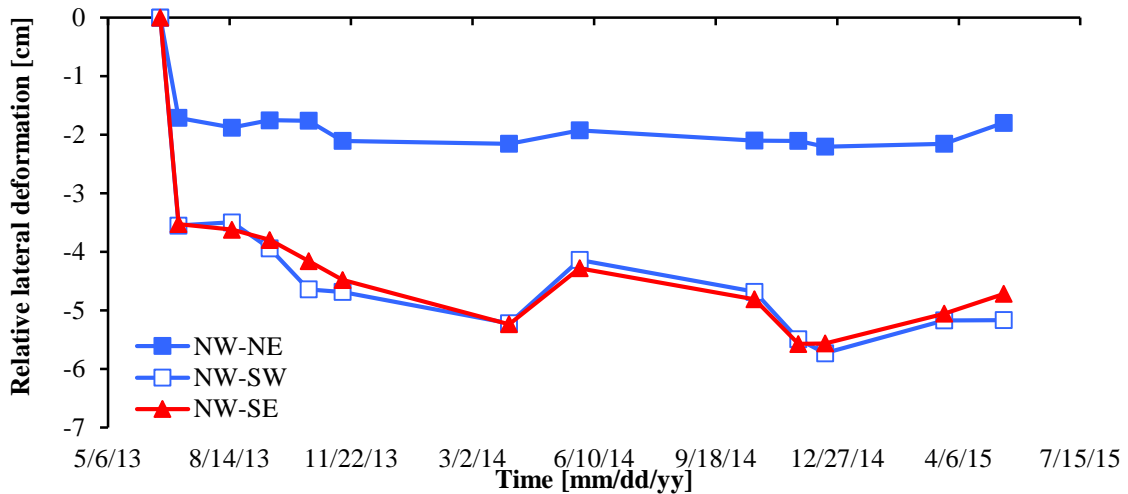


Figure 3.52: Relative lateral deformation on the abutment wall with respect to the NC surveying point.

Similar to the other two bridges, the behavior of the lateral deformations could be, in part, attributed to the change in temperature and resulting contraction and expansion of the backfill soil, as well as the load applied by the traffic. Also, an error on the measurements could be influencing the larger magnitude of these deformations when

compared to the other two bridges, as these magnitudes are thought to be quite large (> 8 cm). As reported by Civjan et al. (2013) and researchers, the lateral deformation of abutments could be attributed to temperature changes, with as mentioned before could be an explanation for the movements for all the three bridges.

Finally, Figures 3.53 through 3.56 present a comparison of the field data between different neighboring points of different structural elements versus temperature and precipitation. These data series are smaller than the data series of other bridges but they still show a definite trend with temperature, although there is a time delay. That would be expected as there is a diffusion time required for the heat to leave or enter the foundation soil and embankment structure.

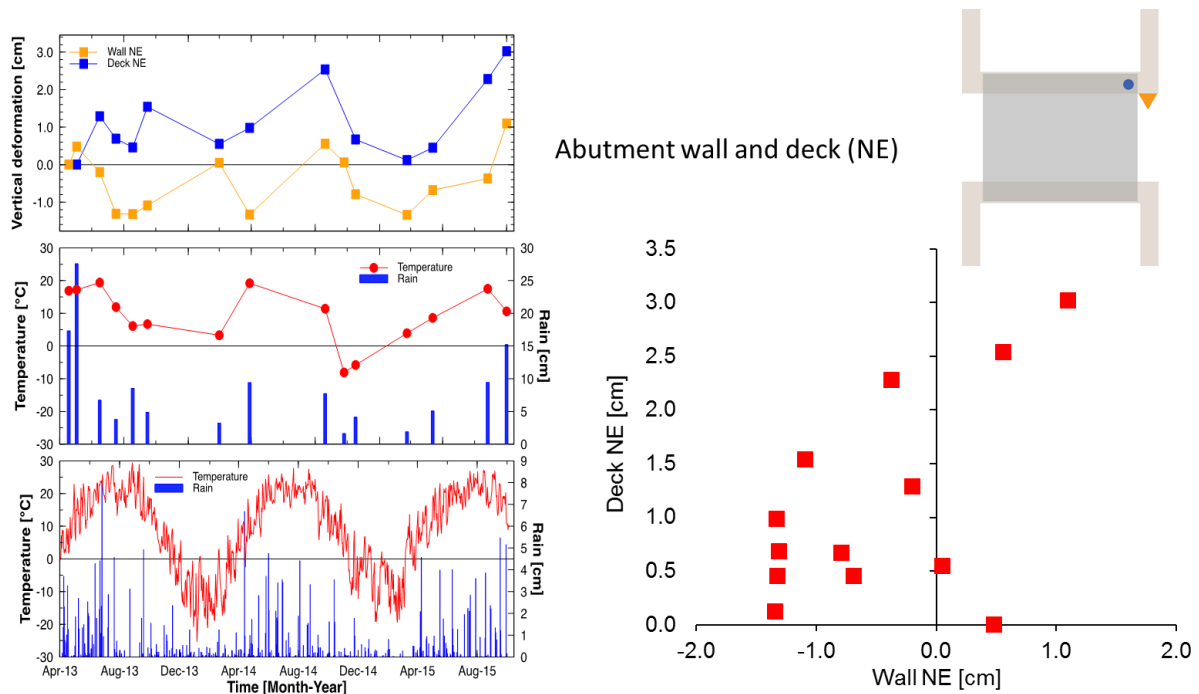
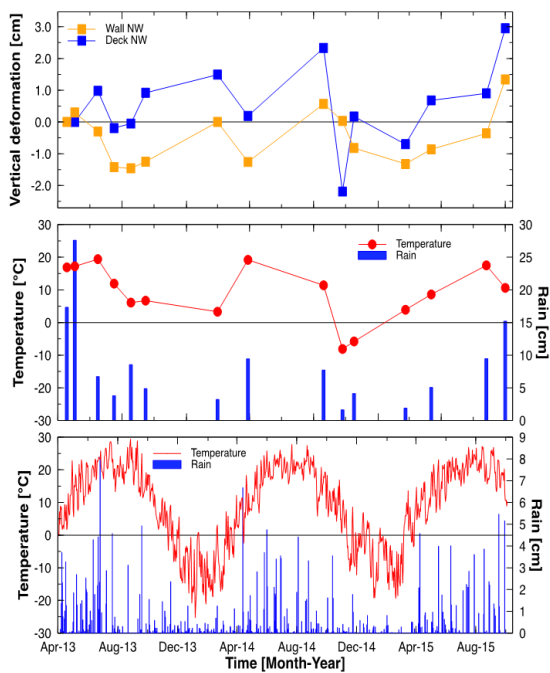


Figure 3.53: Vinburn Road Bridge. Comparison of relative settlement of NE abutment wall and deck versus temperature (at the time of measurement and daily average) and rain fall (one month cumulative and daily total).



Abutment wall and deck (NW)

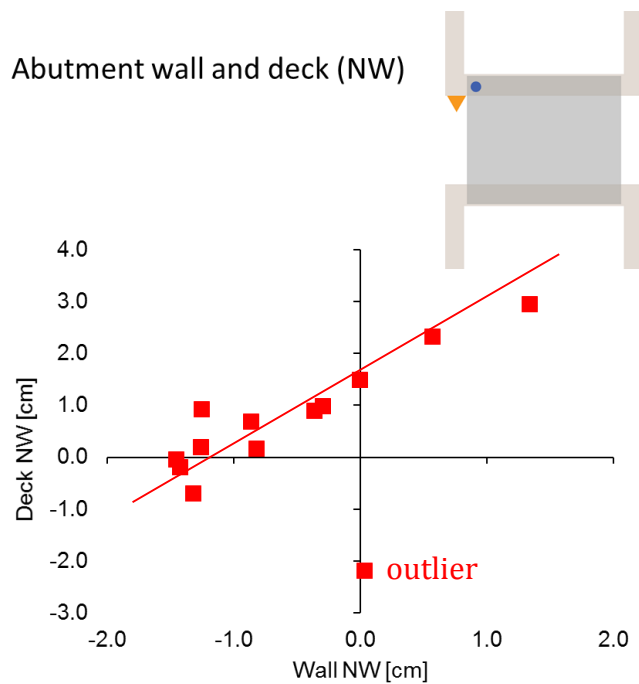
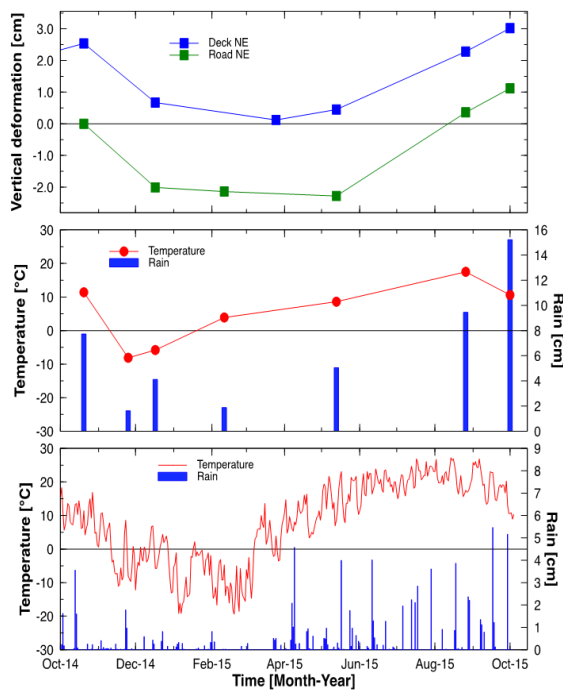


Figure 3.54: Vinburn Road Bridge. Comparison of relative settlement of NW abutment wall and deck versus temperature (at the time of measurement and daily average) and rain fall (one month cumulative and daily total).



Deck and approaching road (NE)

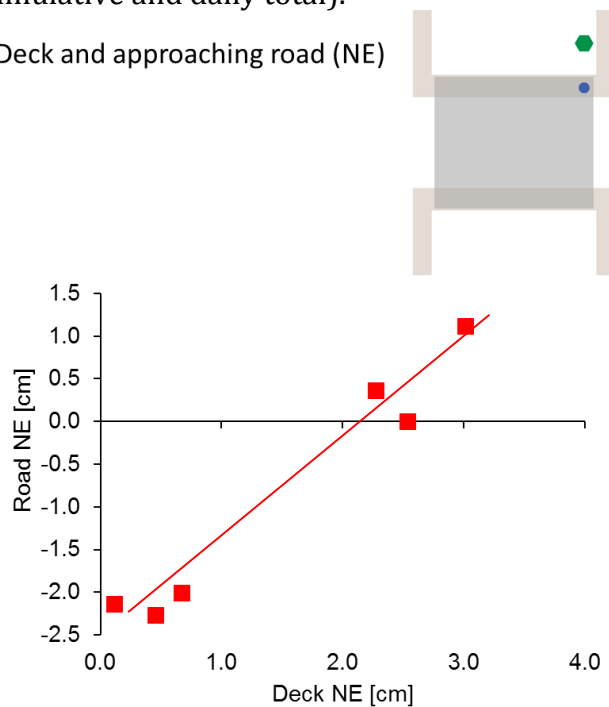


Figure 3.55: Vinburn Road Bridge. Comparison of relative settlement of NE deck and approach road versus temperature (at the time of measurement and daily average) and rain fall (one month cumulative and daily total).

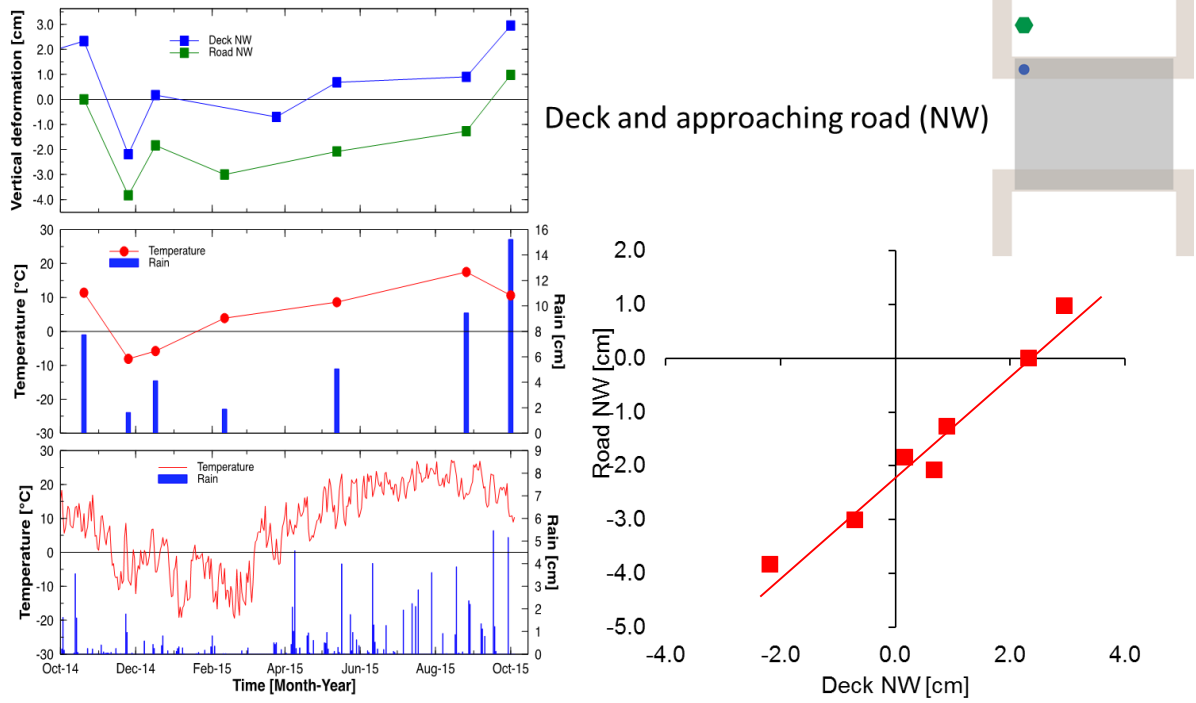


Figure 3.56: Vinburn Road Bridge. Comparison of relative settlement of NW deck and approach road versus temperature (at the time of measurement and daily average) and rain fall (one month cumulative and daily total).

4 Conclusions and Recommendations

WisDOT engineers use the AASHTO Design Code for the design of foundations for transportation structures. This code is based on the Load and Resistance Factor Design (LRFD) method and it specifies that in addition to satisfying the requirements of global stability, the AASHTO Design Code also requires that the structure must fulfill horizontal and vertical serviceability displacement requirements. The problem is that the prediction of foundation vertical and horizontal displacements is inexact and is subjected to assumptions. Prediction of deformation is also highly dependent of the quality of the models (elastic, non-linear, plastic, etc.) and input model parameters (simple SPT results vs. laboratory testing of undisturbed samples). Systematic studies of foundation settlement predications have shown that the profession does a poor job predicting settlements, even in the simplest of the cases. A better understanding of the relationship between the loads a structure applies to the foundation soil and the interaction of the foundation with the subsurface may increase the accuracy and reduce the over-engineering of engineering designs. The original intent of this research program was to combine loads, displacements, and geotechnical data to improve foundation settlement estimates.

We instrumented and monitored several bridges in Southern Wisconsin and collected load and settlement data during and after construction of bridges. We assessed options to rapidly and accurately measure the forces acting within different elements of bridge structures and to assess horizontal and vertical movements. We settled on developing inexpensive methodologies to measure loads bridges apply to the

foundations and monitor their displacement over time after service loads were applied. Options for the monitoring of the structures were evaluated and tested. Methods to install, use, and maintain the deployed instruments were developed. A program was developed to report collected data in a usable form, and preliminary analysis of the structural loads and movements was completed.

The first three bridges were fitted with load strain gauges into the concrete structure to monitor the load carried to the foundations. Results show that while most loads and deformations occurs during construction, the effect of service load is minimum (Figures 3.20, 3.21, 3.22). One bridge showed an increase in load over time (Figure 3.23) but it appears that that was caused by the sequence of construction and by the forces generated by the embankment over the abutment of the bridge. Settlements measurements in these bridges were marred by problems in establishing base lines and by poor coordination with contractors.

The deformations in bridges along Highway 51 provided an opportunity to measure the response of similar structures under similar service loads and environmental conditions (e.g., traffic, temperature, precipitation). These bridges show significant relative movements of up to 5 cm (2 in.), indicating the importance of the environmental effects on the structured. It should be emphasized that the foundation soils were not expected to present considerable consolidation deformations. Most of the foundation soils were either gravels or sands and the few clayey and silty soils were likely to be over consolidated. Furthermore, dead loads did not influence these observations as measurements started around the time the structures were open to traffic.

High quality geotechnical information corresponding with the displacement and load data for each structure was not available. The subsurface information available for each project site was that which was included in the construction documents. The geotechnical investigation only included strength responses of soils: SPT results for all borings and soils, and unconfined compression test results for clays and silts. The problem with these data is the relationship for deformation cannot be fully developed. Therefore, an analysis of the predicted and actual settlement could not be reliably completed nor would it be transferrable to other design situations.

Furthermore, due to the heavy use of SPT data it is recommended that design engineers should also consider using reliability data (e.g., Table 2.3) to both decide and collect higher quality foundation data. That is, if SPT data are used for design and analysis, the strength factors should be reduced by a factor greater than two to accommodate for the variability of the results. Also the model parameters used in settlement calculations would corrected as well as there is a potential for even much greater errors associated to correlation and other uncertainties. Without reliability information, the results of sophisticated numerical model are at best suspect. For those reasons, it is recommended that WisDOT designers should consider in their cost analysis the potential of using more sophisticated field investigation tools and laboratory testing programs. The cost of a greater investment in the early part of the design may reduce the overall cost of the project.

These recommendations, in general, are not new, they were already presented by Lutteneger and de Grout (1995): "... (1) lack of a complete site investigation to provide

sufficient test results on the nature and variability of granular deposits at a particular site; and (2) the use of simplistic, empirical and generally outdated methods of analysis which tend to give erratic results which are not of a sufficiently general nature and generally do not recognize the important factors contributing to the deformation characteristics of granular soils under foundation stresses imposed by shallow foundations.” That is, both the testing program and the method of analyses must be improved.

References

- AASHTO (2007). AASHTO LRDF Bridge Design Specifications, Fourth Edition. American Association of State Highway and Transportation Officials, Washington, D.C.
- AASHTO (2008). Guide Specifications for Highway Construction. American Association of State Highway and Transportation Officials, Washington, D.C.
- Al-Omaishi, N., Tadros, M.K., and Seguirant, S.J. (2009). "Elasticity modulus, shrinkage, and creep of high-strength concrete as adopted by AASHTO." *Precast/Prestressed Concrete Institute Journal*, 54, no. 3, 44-63. PCI Journal, Chicago.
- Ashford, S.A., and Juirnarongrit, T. (2003). "Evaluation of pile diameter effect on initial modulus of subgrade reaction." *J. of Geotech. and Geoenv. Eng.*, 129(3), 234-242.
- ASTM Standard C125. (2011). "Standard terminology relating to concrete and concrete aggregates."
- ASTM Standard C183. (2010). "Standard test method for density (unit weight), yield, and air content (gravimetric) of concrete."
- ASTM Standard C192. (2007). "Standard practice for making and curing concrete test specimens in the laboratory."
- ASTM Standard C215. (2008). "Standard test method for fundamental transverse, longitudinal, and torsional resonant frequencies of concrete specimens."
- ASTM Standard C31. (2010). "Standard practice for making and curing concrete test specimens in the field." ASTM International, West Conshohocken, PA.
- ASTM Standard C39. (2011). "Standard test methods for compressive strength of cylindrical concrete specimens."
- ASTM Standard C469. (2010). "Standard test method for static modulus of Elasticity and Poisson's Ratio of Concrete in Compression."
- ASTM Standard C597. (2009). "Standard test method for pulse velocity through concrete."
- ASTM Standard C617. (2011). "Standard practice for capping cylindrical concrete specimens."
- ASTM Standard C684. (2003). "Standard test method for making, accelerated curing, and testing concrete compression test specimens."
- ASTM Standard C823. (2007). "Standard practice for examination and sampling of hardened concrete in constructions."
- Atkinson, J.H. (2000). "Non-linear soil stiffness in routine design." *Géotechnique* 50, No. 5, 487-508.
- Banerjee, P.K. (1978). "Analysis of axially and laterally loaded pile groups." *Developments in Soil Mechanics*, Applied Science Publishers, London, 317-346.
- Beck, W.K and Harrison, P.J. (2009). "Load tests on small diameter augered cast-in-place piles through fill." *Contemporary Topics in Deep Foundations; Selected Papers from the 2009 International Foundation Congress and Equipment Expo*, March 15-19, 2009. No. 185, 430-437. American Society of Civil Engineers, Reston, Virginia, USA.
- Bentler, J.G., Hoppe, M.J.L., and Dasenbrock D.D. (2009). "Analysis and QA/QC performance monitoring of a spread footing bridge foundation during

- construction loading." Annual Conference of the Minnesota Geotechnical Society Conference Paper.
- Briaud, J.-L. and Gibbens, R. (1999). "Behaviors of five large spread footings in sand." *Journal of Geotechnical and Geoenvironmental Engineering*, 125, no. 9, 787-797. ASCE, Reston, VA.
- Brown J.L., Sivakumar, V., McKinley, J.D., Harmon, N., and McDonald, K. (2009). "The miniature wireless data-logger for pressure measurements in geotechnical applications." *Geotechnique* 59, no. 2, 141-146.
- Bryson, L.S., Barnes, A., and Lutz, T. (2008). "Deformations determined from wireless MEMS accelerometers." TRB 2009 Annual Meeting CD-ROM. Transportation Research Board 88th Annual Meeting, Transportation Research Board of the National Academies, Washington D.C.
- Budhu, M. (2007). *Foundations and Earth Retaining Structures*. John Wiley & Sons. 483 pages.
- Cai, C.S., Shahawy, M.A., and El-Saad, A. (1999). "Comparison of bridge load rating based on analytical and field testing methods." *Proceedings of SPIE conference on nondestructive evaluation of bridges and highways, Volume 3*. The International Society for Optical Engineering, 3587, 127-136. SPIE, Bellingham, WA.
- Caliendo, J.A., Anderson, L.R., Winward, R.F., Dapp, S., and Musser, S.C. (1996). "Instrumentation for laterally loaded model piles." *Transportation Research Record: Journal of the Transportation Research Board* 1548, 67-73. Transportation Research Board of the National Academies, Washington D.C.
- Civjan, S.A., Kalayci, E., Quinn, B.H., Breña, S.F., and Allen, C.A. (2013). "Observed integral abutment bridge substructure response." *Engineering Structures*, 56, 1177-1191.
- Coduto, D.P., Kitch, W.A, and Yeeung, M.R. (2016). *Foundation Design – Principles and Practices*. Pearson. Boston, MA. 960 pages.
- CrossBow Catalogue. (2007). URL: <http://www.moog-crossbow.com/products/inertial-products/>
- Day, R.W. (2010). *Foundation Engineering Handbook*. 2nd Edition. McGraw-Hill. New York.
- DeJong, J.T., Howey, D.S., Civjan, S.A., Brena, S.F., Butler, D.S., Crovo, D.S., Hourani, N., and Connors, P. (2004). "The influence of daily and annual thermal variations on integral abutment bridge performance." *Geotechnical Engineering for Transportation Projects, Geotechnical Special Publication no. 126*, 496-505.
- Domalik, D.E., Shura, J.F., and Linzell, D.G. (2005). "Design and field monitoring of horizontally curved steel plate girder bridge." *Transportation Research Record: Journal of the Transportation Research Board* 1928, 83-91. Transportation Research Board of the National Academies, Washington D.C.
- Ensoft Inc. (2015). *Software for Complex Geotechnical and Structural Engineering Challenges*. URL: <http://www.ensoftinc.com/> [Accessed on July 30, 2015].
- Fasana, A., Garibaldi, L., Giorcelli, E., Marchesiello, S., and Ruzzene, M. (1999). "Comparison between three identification techniques of a road bridge dynamic test." *Proceedings of SPIE conference on nondestructive evaluation of bridges and*

- highways, Volume 3. The International Society for Optical Engineering. SPIE, Bellingham, WA.
- Fasl, J., Romage, M., Helwig, T., Herman, R., and Frank, K. (2009). "Field measurements on steel girder bridge with skewed supports utilizing lean-on bracing." Don't Mess with Structural Engineers: Expanding our role. Proceedings of the 2009 Structures Congress, April 30-May 2 2009, 125-134. ASCE, Reston, VA.
- FHWA (2001). "Load and Resistance Factor Design (LRFD) for Highway Bridge Substructures". Publication No. FHWA HI-98-032. Federal Highway Administration. US Department of Transportation. Washington, DC. 592 pages.
- Gajan, S., and Kutter, B.L. (2009). "Effects of moment-to-shear ratio on combined cyclic load-displacement behaviors for shallow foundations from centrifuge experiments." *Journal of Geotechnical and Geoenvironmental Engineering*, 135, no. 8, 1044-1055. ASCE, Reston, VA.
- Galan, A. (1990). Combined ultrasound methods of concrete testing. *Developments in civil engineering*, 34. Institute of construction and architecture, Slovak Academy of Sciences, Bratislava, Czechoslovakia. Translation of: *Kombinované metódy skúšania betónu*. Translation by Jarmila Perlakiová. Elsevier Science Publishers, New York.
- Geokon Model 4911. (2009). Model 4911A/4911 VW rebar strainmeters. Geokon, Inc., Lebanon, NH.
- Geokon Model LC-2x4. (2007). Model LC-2x4 four channel VW datalogger. Geokon, Inc. Lebanon, NH.
- Geokon Splicing Instructions. (2009). Cable Splicing. Geokon, Inc., Lebanon, NH.
- Greenwood R.J. and Hrrrick, G.W. (1990). "Instrumentation for highway works-obtaining value for money." *Geotechnical instrumentation in practice: Purpose, performance and interpretation; Geotechnical instrumentation in civil engineering projects conference proceedings*, April 3-5, 1989. Thomas Telford, London.
- Grosse, C.U. and Reinhardt, H.W. (2001). "Fresh concrete monitored by ultrasound methods." *Otto Graf Journal*, 12, 157-168.
- Herrero, T.V., Rutz, F.R., and Rens, K.L. (2008). "Wind pressure and strain measurements on bridges. II: Strain transducer development." *Journal of Performance of Constructed Facilities*, 22, no. 1, 12-23.
- Huang, J., Shield, C., and French, C. (2005). "Time-dependent behavior of a concrete integral abutment bridge." *Transportation Research Record: Journal of the Transportation Research Board* 11S, 299-309. Transportation Research Board of the National Academies, Washington D.C.
- Inaudi, D., Vurpillot, S., Glisic, B., Kronenberg, P., and Lloret, S. (1999). "Long-term monitoring of a concrete bridge with 100+ fiber optic long-gauge sensors." *Proceedings of SPIE conference on nondestructive evaluation of bridges and highways, Volume 3. The International Society for Optical Engineering*, 3587, 50-59. SPIE, Bellingham WA.
- Lawver, A., French, C., and Shield, C. (2000). "Field performance of integral abutment bridge." *Transportation Research Record: Journal of the Transportation Research*

- Board 1740, 108-177. Transportation Research Board of the National Academies, Washington D.C.
- Lehane, B.M., Doherty, J.P., and Schneider, J.A. (2008). "Settlement prediction for footings on sand." *Deformation Characteristics of Geomaterials*. Edited by. S.E Burns, P.W. Mayne, and J.C. Santamarina. Proceedings of Pre-Failure Deformation Characteristics of Geomaterials. Atlanta, GA. 133-150.
- Liu, S.C. (2008). "Sensors, smart structures technology and steel structures." *Smart Structures and Systems* 4, no. 5, 517-530.
- Long, J.H., Hendrix, J., and Jaromin, D. (2009). "Comparison of five different methods for determining pile bearing capacities." Wisconsin Highway Research Program #0092-07-04.
- Lyndon, A., Price, G., Wardle, I.F., and Varey, L.S. (1989). "The effect of pile loading on subsequent lateral behavior." *Piling and Deep Foundations; Proceedings of the International Conference on Piling and Deep Foundations*, 377-382.
- Lutenegger, A. and DeGroot, D. (1995). "Settlement of Shallow Foundations in Granular Soils". Report of Research Conducted for Massachusetts Highway Department of Transportation Research Project. Contract #6332, Task Order #4.
- Mayne, P.W., and Poulos, H.G. (1999). "Approximate displacement influence factors for elastic shallow foundations." *Journal of Geotechnical and Geoenvironmental Engineering*, 125, no. 6, 453-460. ASCE, Reston, VA.
- Mayne, P.W., and Poulos, H.G. (1999). "Approximate displacement influence factors for elastic shallow foundations." *J. of Geotech. and Geoenv. Eng.*, 125(6), 453-460.
- McManus, K. J., N. Burdon, R. R., and Anonymous. (2001). "Lateral resistance of shallow foundations." *New Zealand Society for Earthquake Engineering Technical Conference and Conference Technical Papers*, March 23-25, 2001. New Zealand Society for Earthquake Engineering, Upper Hutt, New Zealand.
- Mirza, S.A., Hatzinikolas, M., and MacGregor, J.G. (1979). "Statistical descriptions of strength in concrete." *Journal of the Structural Division of the American Society of Civil Engineers*, 105, no. ST6, 1021-1037. ASCE, Reston, VA.
- Ohtsu, M., Yoshiara, T., Uchida, M., Saeki, H., and Iwata, S. (2003). "Estimation of concrete properties by elastic-wave method." *International Symposium Nondestructive Testing in Civil Engineering*. NTD-2003.
- Ooi, P.S.K., Lin, X., and Hamada, H.S. (2010). "Numerical study of an integral abutment bridge supported on drilled shafts." *Journal of Bridge Engineering*, 15, no. 1, 19-31. ASCE, Reston, VA.
- Osouli, A., Hashash, Y.M.A., and Song, H. (2010). "Interplay between field measurements and soil behavior for capturing supported excavation response." *Journal of Geotechnical and Geoenvironmental Engineering*, 136, no. 1, 69-84. ASCE, Reston, VA.
- Pascale, G. and Di Leo, A. (1984). "Assessment of elastic modulus of concrete and its influence on structural design." *Cement and Concrete Research*, 14, 705-716. Pergamon Press, Ltd.
- Popovics, S., Komlos, K., and Popovics, J. (1995). "Comparison of DIN/ISO 8047 (Entwurf) to seven standards on determination of ultrasonic pulse velocity in concrete."

- International Symposium Nondestructive Testing in Civil Engineering. NDT-1997, 2, no. 4.
- Poulos, H.G. (1987). "From theory to practice in pile design." Transactions of the Australian Geomechanics Society, 1-31.
- Poulos, H.G. (1989). "Pile behaviour: theory and application." *Géotechnique*, 39(3), 363-416.
- Randolph, M.F., and Wroth, C.P. (1979). "A simple approach to pile design and the evaluation of pile tests." Behavior of Deep Foundations, ASTM STP 670, 484-499.
- Raychowdhury, P. and Hutchinson, T. (2008). "Nonlinear material models for Winkler-based shallow foundation response evaluation." Geocongress-2008, Characterization, Monitoring, and Modeling of Geosystems: Proceedings of Sessions of Geocongress 2008; Geotechnical Special Publication no. 179, 686-693. ASCE, Reston, VA.
- Reinhardt, H.W., Grosse, C., Weiler, B., Bohnert, J., and Windisch, N. (1996). "P-wave propagation in setting and hardening concrete." Annual Journal of Research and Testing Materials. Materialprüfungsanstalt Universität Stuttgart, 7, 181-189.
- Robertson, P.K., Davies, M.P., and Campanella, R.G. (1989). "Design of laterally loaded driven piles using the flat dilatometer." *Geotech. Test. J.*, 12(1), 30-38.
- Rutz, F.R. and Rens, K.L. (2008). "Wind pressure and strain measurements on bridges. I: Instrumentation/data collection system." *Journal of Performance of Constructed Facilities*, 22, no. 1, 2-11. ASCE, Reston, VA.
- Salgado, R. (2008). *The Engineering of Foundations*. McGraw-Hill Companies, Inc., New York.
- Sandford, T.C., Davids, W.G., Hartt, S.L., and Delano, J.G. (2006). "Construction-induced stresses in H-piles supporting an integral abutment bridge." *Transportation Research Record: Journal of the Transportation Research Board* 1975, 39-48. Transportation Research Board of the National Academies, Washington D.C.
- Sargand, S.M., and Hazen, G.A. (1999). Field and laboratory performance evaluation of spread footings. Ohio Department of Transportation and Federal Highway Administration. FHWA/OH-98/017. Ohio Department of Transportation, Columbus, OH.
- Sargand, S.M., and Khoury, I.S. (1999). "Sensor installation in rigid pavement." *Experimental Techniques*, May-June. 25-27.
- Sargand, S.M., Masada, T., and Abdalla, B. (2003). "Evaluation of cone penetration test-based settlement prediction methods for shallow foundations on cohesionless soils at highway bridge construction sites." *Journal of Geotechnical and Geoenvironmental Engineering*, 129, no. 10, 900-908. ASCE, Reston, VA.
- Schmertmann, J.H. (1970). "Static cone to compute static settlements over sand." *Journal of Soil Mechanics Foundation Division*, 96, SM3, 1011-1043.
- Schneider, J.A., Fahey, M., and Lehane, B.M. (2008). "Characterization of an unsaturated sand deposit using in situ testing." Proceedings of the 3rd International Conference on Site Characterization. Taipei, Taiwan. 633-638.

- Silvestri, V. (2000). "Performance of shallow foundations on clay deposits in Montréal Island." *Canadian Geotechnical Journal*, 37, no. 1, 218-237. National Research Council Canada.
- Structure B-13-541. August 24, 2009. "East Bound Lane IH-39 over Lien Road."
- Structure B-40-820. October 19, 2009. "Layton Avenue over IH-94."
- Structure B-67-325. December 17, 2009. "IH-43 South bound over State Highway 164."
- Sweet and Mathews. (1989). "Advantages of a new data logging systems in the field of instrumentation." *Geotechnical instrumentation in practice: Purpose, performance and interpretation; Geotechnical instrumentation in civil engineering projects conference proceedings*, April 3-5, 1989. 607-616. Thomas Telford, London.
- Tan, C.K. and Duncan, J.M. (1991). Settlement of footing on sand - accuracy and reliability. *Proceedings of the Geotechnical Engineering Congress 1991*. GSP 27, Reston, VA
- Take, W.A., White, D.J., Bowers, K.H., and Moss, N. (2005). "Remote real-time monitoring of tunneling-induced settlement using image analysis." *Proceedings of the Fifth International Symposium on Geotechnical Aspects of Underground Construction in Soft Ground*, 771-777.
- Tia, M., Liu, Y., and Brown, D. (2005). Modulus of Elasticity, Creep and Shrinkage of Concrete Final Report. Florida Department of Transportation. U.F. Project No. 49104504973-12. Florida Department of Transportation, Tallahassee, FL.
- Wang, C.K., Salmon, C.G., and Pincheira, J.A. (2007). Reinforced concrete design. Seventh edition. John Wiley and Sons, Inc. New Jersey.
- Wisconsin Department of Transportation. (2010). Construction and materials manual. URL: <ftp://ftp.dot.wi.gov/dtsd/rdwy-stds/DCC/CMM%20April%202010/2010%20April%20CMM.pdf> [Accessed on August 1, 2015].
- Wisconsin Department of Transportation. (2014). WisDOT Bridge Manual. URL: <http://wisconsindot.gov/dtsdManuals/strct/manuals/bridge/ch-all.pdf> [Accessed on August 1, 2015].



WHRP

Wisconsin Highway Research Program
University of Wisconsin – Madison
1415 Engineering Drive
Madison, WI 53706
<http://wisdotresearch.wi.gov/whrp>